THESIS

This is to certify that the

dissertation entitled

THEORY OF THE ELASTIC AND VIBRATIONAL

PROPERTIES OF CENTRAL FORCE RANDOM NETWORKS

presented by

Edward Joseph Garboczi

has been accepted towards fulfillment
of the requirements for

Ph.D. degree in Physics

M. F. Thorpe
Major professor
M. F. Thorpe

Date February 20, 1985

0-12771

THEORY OF THE ELASTIC AND VIBRATIONAL PROPERTIES OF CENTRAL FORCE RANDOM NETWORKS

By

Edward Joseph Garboczi

A DISSERTATION

Submitted to
Michigan State University
in partial fulfillment of the requirements
for the degree of

DOCTOR OF PHILOSOPHY

Department of Physics and Astronomy

1985

ABSTRACT

THEORY OF THE ELASTIC AND
VIBRATIONAL PROPERTIES OF
CENTRAL FORCE RANDOM NETWORKS

By

Edward Joseph Garboczi

Central force random networks which are generated by randomly removing bonds on a lattice are simple models with which to study the rigidity transition where the elastic moduli of a system go to zero as a function of decreasing mean connectivity. A simple constraint counting argument gives a prediction for the critical threshold p^*, called the rigidity threshold, and $f(p)$, the fraction of zero frequency modes, where p is the fraction of bonds present. Chapter 1 presents evidence from three different networks that shows these predictions to be in excellent agreement with numerical simulations. Also it is shown that the elastic moduli for nearest neighbor central forces scale linearly with p, in excellent agreement with a simple effective medium theory. Chapter 2 demonstrates how this coherent potential approximation based effective medium theory also gives a quite good description of the entire vibrational density of states for

these same networks. Chapter 3 extends the ideas of Chapter 1 to systems with first and second neighbor central force bonds. Evidence is presented from both numerical simulation and effective medium theory that a fixed point exists--the ratio of C_{11}/C_{44} always converges to a constant along a given track in phase space independent of its starting value before removing bonds. The dependence of this critical value along the rigid-floppy boundary in phase space is derived under effective medium theory. It is demonstrated that f for this system depends only on the total number of first and second neighbor bonds present and not on the details of the phase space track. It is shown how these results can be extended to systems with central forces of arbitrary range.

ACKNOWLEDGEMENTS

First of all I would like to thank my advisor Professor M.F. Thorpe for all of his careful patient guidance over the last five years. His knowledge of solid state physics and his approach to research have been a real inspiration to me. I would also like to express my appreciation to Professor J. Bass for a year of carefully taught solid state lectures, to Professor S.D. Mahanti for a year of invaluable statistical mechanics lectures and many helpful conversations, to Professor W.W. Repko for not a few helpful conversations about computational and mathematical topics, and to all three of the above for serving on my guidance committee. I gratefully acknowledge Dr. J. Parkinson's many contributions of ideas and advice to the work described in Chapter 1.

H. He, Dr. D. Heys, Dr. D. Sahu, and Dr. J.M. Thomsen have been good friends and the source of much help throughout my graduate career.

Many thanks are due to my son Joshua, whose birth inspired me to work very hard, and who kindly allowed me to convert his changing table back into a desk at night in order to write this thesis. I would like also to express my gratitude to my dear wife Alice for all her patience,

encouragement, and assistance over these last four and one half years.

And finally, my gratitude and praise go to the Lord God, the infinite-personal Creator of the universe, Who with His incredible skill has made it such a delight to study His marvellously intricate creation.

TABLE OF CONTENTS

LIST OF TABLES

LIST OF FIGURES

Chapter 1. Rigidity Percolation on Central Force Elastic Networks

Section 1.1. Introduction and Definition of Problem

It is widely believed that the structure of amorphous solids whose bonding is primarily covalent is well described by some form of covalent random network (Zallen 1983). A good example is amorphous germanium (a-Ge). Crystalline germanium (c-Ge) has the diamond structure, where each atom is tetrahedrally connected to four nearest neighbors, with the nearest neighbor bond lengths and angles between pairs of nearest neighbors bonds having specified values. A-Ge has short range order similar to that of c-Ge, in that all atoms have four nearest neighbors in a roughly tetrahedral arrangement. However, the nearest neighbor bond lengths and angles in a-Ge take on values in a narrow distribution centered on their crystalline values. This occurs in such a way that there is no long range order present. Since it takes energy to stretch bonds and change bond angles, a-Ge has a higher energy than c-Ge. A-Ge cannot be continuously deformed into c-Ge, however, since the two structures are topologically inequivalent. C-Ge only has rings with an even number of members, while a-Ge has rings with odd and even numbers of members. This implies that

an energy barrier exists between the two states, and therefore a-Ge is a metastable state of solid germanium.

The structure of two component amorphous solids may also be modelled with a covalent random network. An example of this type would be Ge_xSe_{1-x}. A selenium atom naturally forms covalent bonds with two other selenium atoms, which results in pure Se being made up of isolated polymer chains where each atom has two nearest neighbor bonds. We may then think of producing a compound like Ge_xSe_{1-x} by starting with pure a-Ge and randomly replacing Ge-Ge bonds with Ge-Se-Ge bonds until the desired atomic fractions of x and 1-x are achieved. A schematic picture of this process is shown in Figure 1.

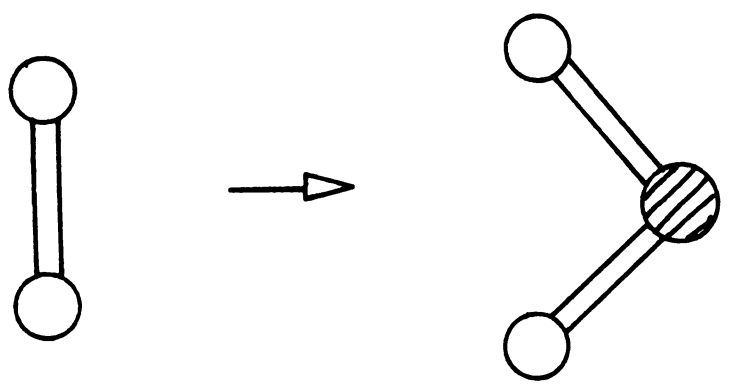

Figure 1. A schematic view of the random substitution of selenium atoms into amorphous germanium.

It is then entirely natural to ask what effect adding Se atoms has on the elastic properties of the material. It is known experimentally that nearest neighbor bond stretching forces (which tend to maintain constant bond lengths) are roughly four to five times stronger than the bond bending forces (which tend to preserve angles between pairs of nearest neighbor bonds) in these kinds of covalent random networks (for a review of the experimental evidence see Zallen 1983). In the substitution shown in Figure 1, we are replacing a strong bond stretching force with a relatively weaker bond bending force. Thus we would expect the elastic moduli of Ge_xSe_{1-x} to soften as x decreases from 1, or equivalently, as $\langle r \rangle$, the mean coordination, decreases from four. The theory of this is worked out in Thorpe (1983) hereafter designated as MFT.

The key result from MFT is a prediction for r_p, the critical value of the mean coordination $\langle r \rangle$ where the elastic moduli of the network go to zero. The elastic moduli can actually soften all the way to zero even when the network is still well connected because with only nearest neighbor bond bending and stretching forces specified there can be units in the network which do not contribute to the elastic strength of the material. An example would be a selenium chain of length ≥ 6 (Thorpe 1983). This transition we call rigidity percolation as opposed to ordinary connectivity percolation, since the network will still be well <u>connected</u> but have <u>zero</u> elastic moduli. This is a result of only

specifying nearest neighbor bond stretching and bending forces. If we included a dihedral angle force (very tiny in real glasses) all connections become rigid and the problem would become a geometrical percolation type problem, where the elastic moduli become zero only when the system is actually geometrically disconnected.

To experimentally achieve the desired range of x so that one can study solids with values of $\langle r \rangle$ both above and below r_p is possible but rather difficult. One must prepare enough samples to be able to cover the relevant range of x properly while maintaining tight chemical control of the value of x. The Ge-Se system is perhaps the best choice for this work. One could put sulfur into germanium but the sulfur tends to form eight-fold rings which would not decrease $\langle r \rangle$ in a random enough way, since we want spatial homogeneity. Experiments are currently being planned to try to test the rigidity percolation ideas, but there is no good experimental evidence as of yet. These are not easy experiments to perform, mostly due to the difficulty of sample preparation.

Lacking any experimental data, we wished to computer-generate covalent random networks with various values of $\langle r \rangle$ and compute their elastic moduli via numerical simulation. In this way we could attempt to verify the mean field prediction for the value of r_p given in MFT.

In doing numerical simulations, one must choose one's model carefully not only for its physical content but more

importantly for its numerical tractability. It is possible to computer-generate covalent random networks of the Ge_xSe_{1-x} type (He 1983) which have reasonable bond length and angle distortions. One randomly inserts two-coordinated sites into a previously generated four-coordinated covalent random network, and then relaxes with bond stretching and bending forces until a local minimum of the potential is found producing a metastable state. However, since elastic energies are small deviations from the local minimum of the potential, in order to do accurate computations of elastic moduli one must know the energy of this minimum with great accuracy. It turns out to be very difficult to impossible to obtain that sort of accuracy on these networks (He 1983).

We are therefore led to try to find a simpler model which exhibits the basic physics we wish to explore. What is needed? An adequate model must have the following properties: 1) unstrained potential energy should be known exactly, 2) mean coordination must be able to be decreased without interfering with 1), 3) rigidity percolation must be able to take place, and 4) the cost of numerical simulations must not exceed the limits of our computer budget!

The class of models whose elastic properties we chose to explore are central force random networks whose randomness is of a special type. We start with a Bravais lattice, the triangular net in two dimensions, the face-centered cubic

and body-centered cubic in three dimensions, where the only interatomic forces are Hooke's law springs between nearest neighbors. We then simultaneously reduce the mean coordination and introduce randomness by randomly removing bonds. The initial elastic energy is always zero, as the lattices have no initial strains in them. The elastic moduli are then found numerically as a function of p= fraction of bonds present, and $\dot{p}$= the bond fraction where the elastic moduli appear to go to zero, is compared with the mean field prediction obtained from constraint counting arguments.

To satisfy 3), there are units in the network which, while fully connected, make no contribution to the restoring force under an external strain. A simple example of one of these units can be seen in Figure 2. More complicated examples will be shown and discussed in Section 1.4. Therefore we claim that results for these central force models will have meaning for the covalent random networks which after all are more physically reasonable models. Condition 4) was also met--with a few cents to spare!

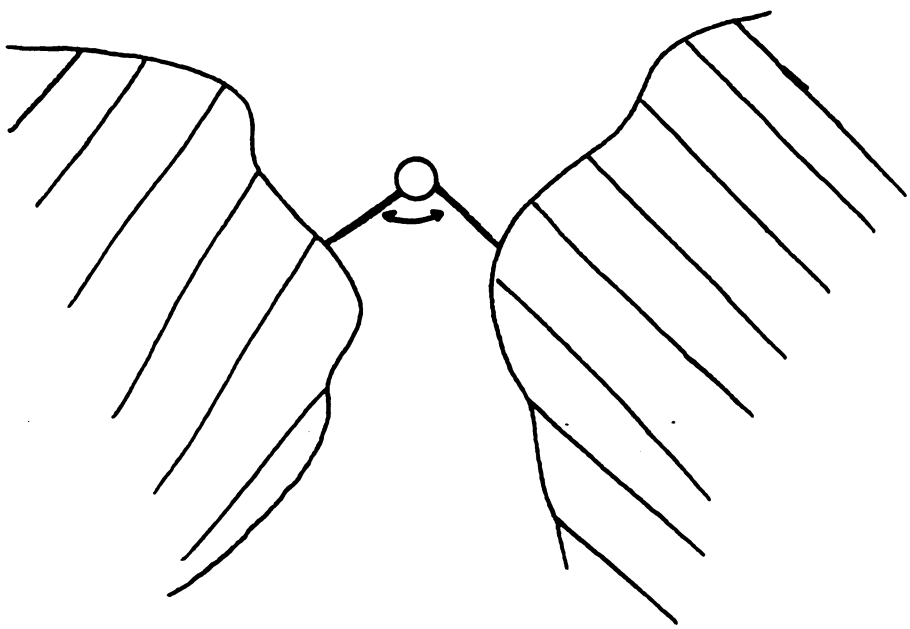

Figure 2. Network unit with no restoring force against external strain

Section 1.2. Mean Field Constraint Counting and Fraction of Zero Frequency Modes

As was stated in Section 1.1 one can construct an estimate for r_p, the value of the mean coordination where the elastic moduli vanish for a covalent random network, using a mean field constraint counting argument. This can also be done for the central force models, which are essentially "covalent" though without any bond bending forces. A change of notation should be noted here. While $\langle r \rangle$, the mean coordination, is the natural variable to use for the covalent random networks, for our central force models where bonds are being randomly removed it is more natural to track the changing coordination through p = the fraction of bonds present. The relationship between p and $\langle r \rangle$ is simple:

$$\langle r \rangle = zp$$

$$r_p = zp^*$$

z = n.n. coordination in the crystal

The constraint counting argument for a central force network in d dimensions goes the following way, which I have adapted from MFT. We define the following quantities for a network with N particles:

N_c = the number of <u>independent</u> constraints in the system which must be satisfied in order to have a zero frequency mode

M_0 = the number of zero frequency vibrational modes of the system

Nd = the total number of degrees of freedom or modes

$f = M_0 / Nd$ = the fraction of vibrational modes with zero frequency

To have a zero frequency mode, one must be able to make some sort of collective motion of the N particles such that all the bonds remain at their equilibrium length l_0, because the lattice potential is

$$V = \tfrac{1}{2} \alpha \sum_{\substack{i \\ \text{(all bonds)}}} (l_i - l_0)^2 \qquad (1)$$

We then have that

$$M_0 = Nd - N_c$$
$$f = 1 - N_c / Nd \qquad (2)$$

One way of seeing the validity of equation (2) is to note that N_c = the rank of the dynamical matrix D(R), so that the nullspace of D(R) has just $Nd - N_c$ elements. Perhaps the easiest way to think of equation (2) is to consider the Nd equations of motion for the network involving the variables $\vec{r}_i$. If we have N_c equations of constraint (each bond length

that must independently remain constant gives an equation like $(\vec{r}_i - \vec{r}_j)^2 = l_0^2$), then we can define $Nd - N_c$ new variables $\vec{q}_j$, which are linearly independent and which automatically satisfy the equations of constraint. We therefore must have $M_0 = Nd - N_c$ zero energy modes involving these variables.

For the central force case, with a lattice potential like (1), N_c is just equal to the number of bonds which <u>independently</u> must have their equilibrium length so that <u>all</u> bonds will be unstretched and thus a zero frequency mode made possible. Our mean field estimate will be that N_c is just equal to the number of bonds actually present, $\frac{1}{2}Nzp$, so that f becomes

$$f = f(p) = 1 - zp / 2d$$

A graph of the mean field prediction for f(p) vs. p is shown in Figure 3. When p = 0, meaning no bonds are present, the system consists of N free particles so that all modes have zero energy. As p increases past p^*, the mean field prediction for f(p) would become negative. A negative value for f is meaningless, however, since f counts numbers of modes. This is evidence of the fact that our mean field estimate of N_c is too high, that each bond does <u>not</u> give an independent constraint. An obvious example in the triangular net is the last bond needed to complete a hexagon. The length of this bond, if all the other bond lengths are

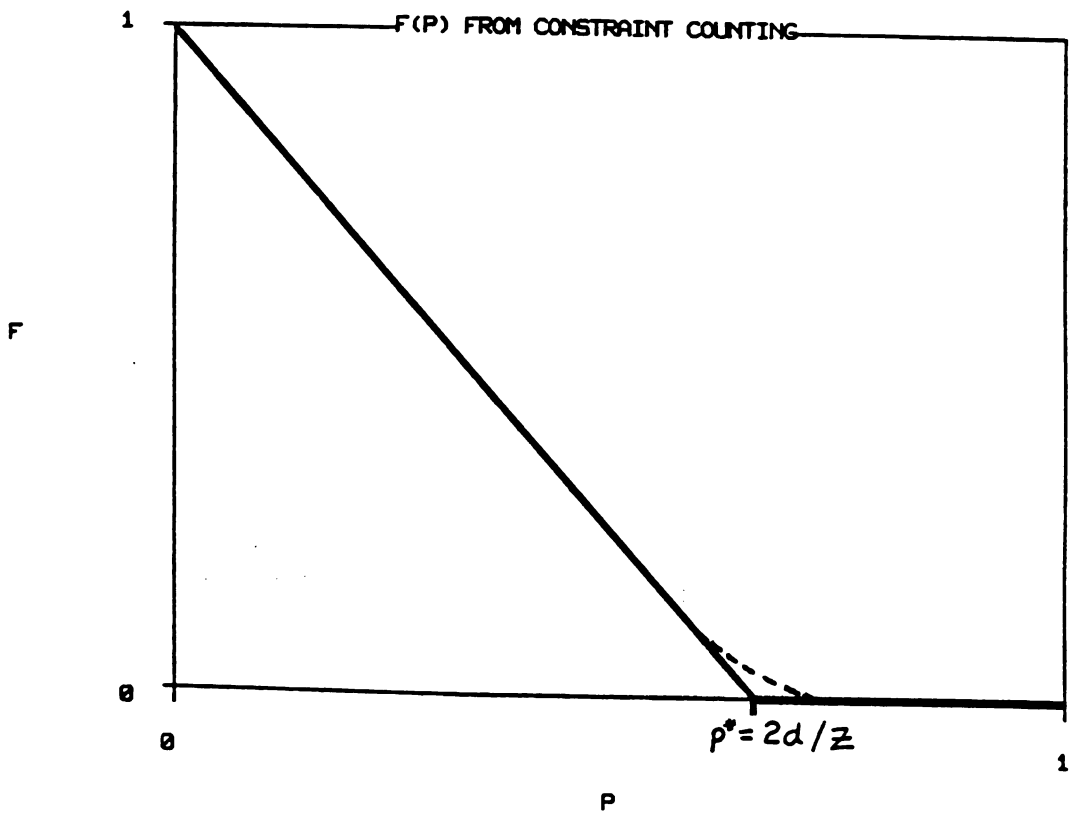

Figure 3. Constraint counting estimate for f(p) = the fraction of zero frequency modes

specified, is not an independent quantity. It is fixed by the other bonds' lengths. So under our mean field theory, f(p) remains zero for $p > p^*$. We call p^* the rigidity threshold, and use its value for our mean field estimate of where the elastic moduli of a central force network will go to zero.

It should be noted that in reality, the elastic moduli will be non-zero when f is non-zero as well. In other words, the rigidity transition will take place when f is actually finite. A network can be macroscopically rigid but still have localized floppy islands. This is the idea of rigidity percolation . In MFT a simple model is solved exactly showing that at the critical threshold f is finite and the third derivative of f is discontinous, implying a third order phase transition. The dotted line in Figure 3 shows an estimate of a more realistic f(p).

Table 1 gives the values of p^* for the three lattices studied. It also gives the known connectivity percolation threshold p_c for each lattice. In all cases p^* is much larger than p_c. In fact, a similar mean field estimate for p_c (Kirkpatrick 1973) gives $p_c = 2 / z = p^* / d$. So the constraint counting theory predicts that the central force networks will have zero elastic moduli while being still very much connected.

Table 1. Comparison of p_c and p^*

Lattice	@ p_c	p^*
triangular	0.3473	0.6666
fcc	0.119	0.5000
bcc	0.179	0.7500

@ Values for p_c taken from Zallen (1983)

Section 1.3. Lattice Potentials and Elasticity Theory for Central Force Crystals

Before we can understand the elastic moduli of a central force random network, we must understand and calculate the elastic moduli of the crystal from which it is generated. The most general way to do this is to set up the dynamical matrix $D(\vec{k})$, calculate the energies of the long wavelength vibrational modes and pick off the values of the elastic moduli. In the remainder of this section $D(\vec{k})$ will be derived for a central force potential, and then in the following sections the triangular net and body-centered cubic (BCC) and face-centered cubic (FCC) lattices will be looked at in detail.

We start with the potential V from equation (1) and rewrite it focussing on the sites rather than the bonds:

$$V = \tfrac{1}{4}\alpha \sum_{\langle \underset{\sim}{l}\underset{\sim}{l}' \rangle} \left(|\vec{r}_{\underset{\sim}{l}} - \vec{r}_{\underset{\sim}{l}'}| - \lambda_0 \right)^2 \qquad (4)$$

where $\langle \underset{\sim}{l}\underset{\sim}{l}' \rangle$ means that $\underset{\sim}{l}$ and $\underset{\sim}{l}'$ must be nearest neighbors, and $\vec{r}_{\underset{\sim}{l}}$ is the total displacement of the atom whose equilibrium position is $\underset{\sim}{l}$. The factor of $\frac{1}{4}$ includes a factor of $\frac{1}{2}$ for a spring potential and a factor of $\frac{1}{2}$ to take care of double counting.

Writing $\vec{r}_{\underset{\sim}{l}} = \underset{\sim}{l} + \vec{u}_{\underset{\sim}{l}}$ and $\vec{r}_{\underset{\sim}{l}'} = \underset{\sim}{l}' + \vec{u}_{\underset{\sim}{l}'}$, equation (4) is

expanded to second order in the u's (harmonic approximation). We then have

$$V = \frac{1}{4}\alpha \sum_{\langle \underline{l}\underline{l}' \rangle} \left[\frac{(\underline{l}-\underline{l}')}{|\underline{l}-\underline{l}'|} \cdot (\vec{u}_{\underline{l}} - \vec{u}_{\underline{l}'}) \right]^2$$

Making the double sum unrestricted and using a well known transformation (Ashcroft and Mermin 1975), the potential takes on the form

$$V = \frac{1}{2} \sum_{\underline{l}\underline{l}'} \sum_{\alpha\beta} D_{\alpha\beta}(\underline{l}-\underline{l}') u_{\underline{l}}^{\alpha} u_{\underline{l}'}^{\beta}$$

$$D_{\alpha\beta}(\underline{l}-\underline{l}') = \left[\delta_{\underline{l}\underline{l}'} \sum_{\underline{l}''} \alpha \hat{S}^{\alpha}_{\underline{l}\underline{l}''} \hat{S}^{\beta}_{\underline{l}\underline{l}''} \delta_{\underline{l}'',\underline{l}+\vec{R}_z} \right] - \alpha \hat{S}^{\alpha}_{\underline{l}\underline{l}'} \hat{S}^{\beta}_{\underline{l}\underline{l}'} \delta_{\underline{l}',\underline{l}+\vec{R}_z} \tag{5}$$

where $\hat{S}^{\alpha}_{\underline{l}\underline{l}'}$ is the alpha component of the unit vector from $\underline{l}$ to $\underline{l}'$, and $\vec{R}_z$ is the vector from site $\underline{l}$ to one of its z nearest neighbors. Fourier transforming, we then obtain

$$D_{\alpha\beta}(\vec{k}) = \frac{\alpha}{m} \sum \hat{R}^{\alpha}_{\bullet} \hat{R}^{\beta}_{\bullet} \left(1 - e^{-i\vec{k}\cdot\hat{R}_{\bullet}}\right) \tag{6}$$

m = mass of atoms on lattice

$\hat{R}_{\bullet}$ = unit vector from a site to one of its nearest neighbors

l_o = nearest neighbor bond length = 1, making k also dimensionless

$D(\vec{k})$ is the dynamical matrix, whose eigenvalues and eigenvectors are respectively the normal mode energies and atomic displacement patterns for the phonon spectrum. Since we are considering only Bravais lattices, $D(\vec{k})$ is a d x d matrix. We can now go on to diagonalize $D(\vec{k})$ for $k \rightarrow 0$ and extract the values of the elastic moduli for various lattices of interest, thus giving the starting values of the elastic moduli for our bond removing computations.

Section 1.4. Triangular Net--Numerical Simulation Results

Details of the Lattice

The triangular net was the first lattice on which we did numerical simulations. It is a two dimensional Bravais lattice with six nearest neighbors per site (z = 6). One can construct a rectangular unit cell for the triangular net, a picture of which is shown in Figure 4. For the simulations, one would like to pick a cell that is as square as possible, so as not to have a preferred direction after cutting bonds. All the elastic moduli simulations were performed on a 20 x 22 supercell, giving 440 sites. Taking the nearest neighbor bond length to be one, this makes the linear dimensions of the supercell 20 x 19, which deviates from a square by only 5 %.

Elastic Moduli for the Crystal

The dynamical matrix $D(\vec{k})$ for the triangular net when $k \rightarrow 0$ is given by

$$D(\vec{k}) = \begin{pmatrix} 3/8\ k^2 + 3/4\ k_x^2 & 3/4\ k_x k_y \\ 3/4\ k_x k_y & 3/8\ k^2 + 3/4\ k_y^2 \end{pmatrix}$$

Solving the eigenvalue equation

$$D(k) \cdot \vec{u} = \omega^2 \vec{u} \qquad (7)$$

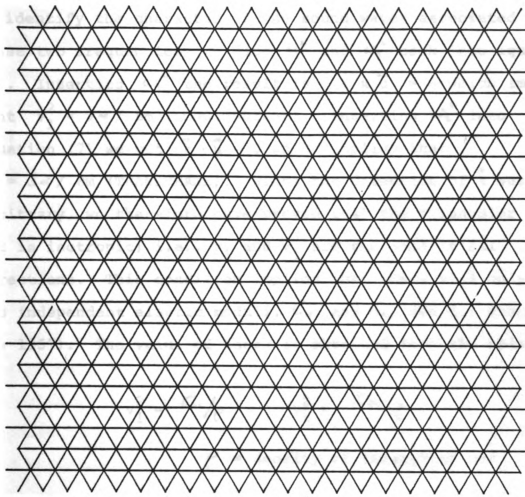

Figure 4. Rectangular unit cell for triangular net (20 x 22)

we find the two solutions are

$$\omega_1^2 = 9\alpha/8m\ k^2$$

$$\omega_2^2 = 3\alpha/8m\ k^2$$

To identify the character of the sound waves associated with these two frequencies, we plug ω_1^2 and ω_2^2 back into equation (7). Inserting ω_1^2 the result is $\vec{k} \times \vec{u} = 0$ which implies that $v_l^2 = 9\alpha / 8m$ (LONGITUDINAL). Inserting ω_2^2 into equation (7) we get $\vec{k} \cdot \vec{u} = 0$ which implies that $v_t^2 = 3\alpha / 8m$ (TRANSVERSE). Since the direction of $\vec{k}$ was arbitrary, we therefore have proved that the triangular net is isotropic; i.e., v_l and v_t are the same in all directions. This condition implies that there will only be two independent elastic moduli, C_{11} and C_{44} (see for example Nye 1957). The value of these is obtained from the relations

$$v_l^2 = C_{11}/\rho \qquad v_t^2 = C_{44}/\rho$$

ρ = density of triangular net

which give the results

$$C_{11} = \frac{3\sqrt{3}\,\alpha}{4} \qquad C_{44} = \frac{\sqrt{3}\,\alpha}{4}$$

Numerical Simulation Techniques

There are two general methods by which one can numerically compute the elastic moduli for a system of mass points

connected by various forces. One method emphasizes computing the stress for a known strain, and thereby extracting the values of the moduli. This method probably requires rigid boundary conditions (Feng and Sen 1984). The other method depends on computing the elastic energy for a known strain, which can be used with periodic boundary conditions. Periodic boundary conditions almost always give better results for a given system size compared to rigid boundary conditions. The energy method with periodic conditions was used for all computations of elastic moduli in this work. There is also more than one way to handle periodic boundary conditions computationally. The method used in this work was that of having an extra boundary layer of "imaginary" sites surrounding the 440 "real" sites, where the imaginary sites were periodic images of real sites, thus maintaining the proper environment for each real site. There is only a small cost in extra computer memory involved in this technique, as opposed to a somewhat larger savings in computational ease and efficiency.

The general method of computing the elastic moduli via the strain energy for a given bond fraction p is as follows: one first initializes the coordinates of all the sites, then bonds are removed randomly until a fraction p are left. Then, depending on whether C_{11} or C_{44} is being computed, the coordinates of the sites are transformed corresponding to a certain external strain.

To compute C_{11}, one makes the transformation

$$x' = (1 - \epsilon_x)x$$
$$y' = (1 - \epsilon_y)y$$

where ϵ_x , ϵ_y are not both non-zero at the same time. For the triangular net, C_{11} was computed as an average over the x and y directions by taking the following combinations of ϵ_x and ϵ_y :

$$\begin{aligned} &(x) \quad \epsilon_x = 10^{-5} \qquad \epsilon_y = 0 \\ &(y) \quad \epsilon_x = 0 \qquad\quad \epsilon_y = 10^{-5} \end{aligned} \tag{8}$$

Averaging over the x and y directions helps to get rid of finite size noise, because for an infinite triangular network which starts out isotropic, randomly removing bonds should not break that isotropy. Averaging over x and y helps to restore this symmetry which can be broken for a cell of finite size.

To compute C_{44} , the necessary coordinate transformation is:

$$x' = x + \epsilon_x y$$
$$y' = y + \epsilon_y \cdot x \tag{9}$$

where $\epsilon_x = 10^{-5}$ and $\epsilon_y = 0$. In two dimensions one need not average over direction, as the requirement that the system have a net torque of zero guarantees the same result as when $\epsilon_x = 0$, $\epsilon_y = 10^{-5}$ (Kittel 1967).

Whatever the applied strain is, one then proceeds to allow each site to move to its equilibrium position under the condition that its nearest neighbors' positions are fixed. Of course, as a site's neighbors are themselves relaxed, the original site will no longer be at the equilibrium position, but as this process is repeated many times the system as a whole will converge to its equilibrium configuration. It is important to note here that periodic boundary conditions are maintained throughout this process which reflect the new shape of the unit cell under the given external strain. If the new shape of the unit cell were not maintained via the periodic boundary conditions the sites would just relax back out to their unstrained positions. The relaxation process finds the equilibrium configuration of the cell for the strained cell shape. In other words we find the microcopic atomic configuration which gives rise to the macroscopic elastic modulus.

By summing over all bonds we then obtain the final relaxed elastic energy per unit volume U, from which the values of C_{11} and C_{44} are extracted according to the following relations:

$$U = \tfrac{1}{2} C_{11} \epsilon^2$$

or

$$U = \tfrac{1}{2} C_{44} \epsilon^2$$

depending on which kind of external strain was used.

By varying p one proceeds to map out C_{11} and C_{44} as functions of p. When this process is done one then repeats it by choosing the bonds to be removed with a different set of random numbers. We used three sets of random numbers, and averaged the elastic moduli over these three configurations. This damps out finite size noise, giving a better approximation to the thermodynamic limit.

There is one aspect of the numerical simulation technique which must be mentioned in connection with rigidity percolation. As was mentioned before, when the sites in the random network are connected by only Hooke's law springs, certain configurations of sites and bonds arise upon bond removal which, while still quite thoroughly connected to the main network, have no contribution to the final relaxed elastic energy. The simplest example is the dangling bond which can always stretch to its equilibrium length no matter where the rest of the sites relax to. All dangling bonds can be successively removed without affecting the final relaxed strain energy.

A non-trivial unit of the type mentioned above is the site with two bonds. By simple geometry one can see that no matter where its two neighbors move to (for small strains), such a site can always adjust its position so that its two bonds have their equilibrium length. So all such sites, along with their bonds, may be successively removed until none remain without affecting the final relaxed elastic energy.

This has a major effect, since such sites, as opposed to dangling bond sites, play a real role in the connectivity of the network. This process of iteratively removing all one and two coordinated sites we call trimming. Figure 5 shows a network with 65% of its bonds present after random cutting. Figure 6 shows the same network after trimming. One can clearly see that many bonds have been removed, even bonds belonging to sites which originally were 3,4,5 or 6 coordinated. This is an effect of the nonlocal aspect of trimming, that one can only tell whether a certain bond will be trimmed by looking at other bonds more than one or two bond lengths away. One might wonder whether pairs of colinear bonds which exist in the triangular net can always be trimmed as well, because they can buckle uner compression but are rigid under tension. This is an important point, and will be discussed fully under Diode Effect.

There are higher order units which are functionally just generalizations of the one and two coordinated sites. An example of each is shown in Figure 7 a) and b). These also will not contribute to the final relaxed elastic energy. The unit shown in Figure 7 c) is somewhat different. Any cluster of sites which is only connected to the rest of the network by three bonds can also relax fully, since such a cluster always has three degrees of freedom, two translational and one rotational, so the three constraints represented by maintaining the attached bonds'equilibrium lengths can always be achieved. All of the above configurations are

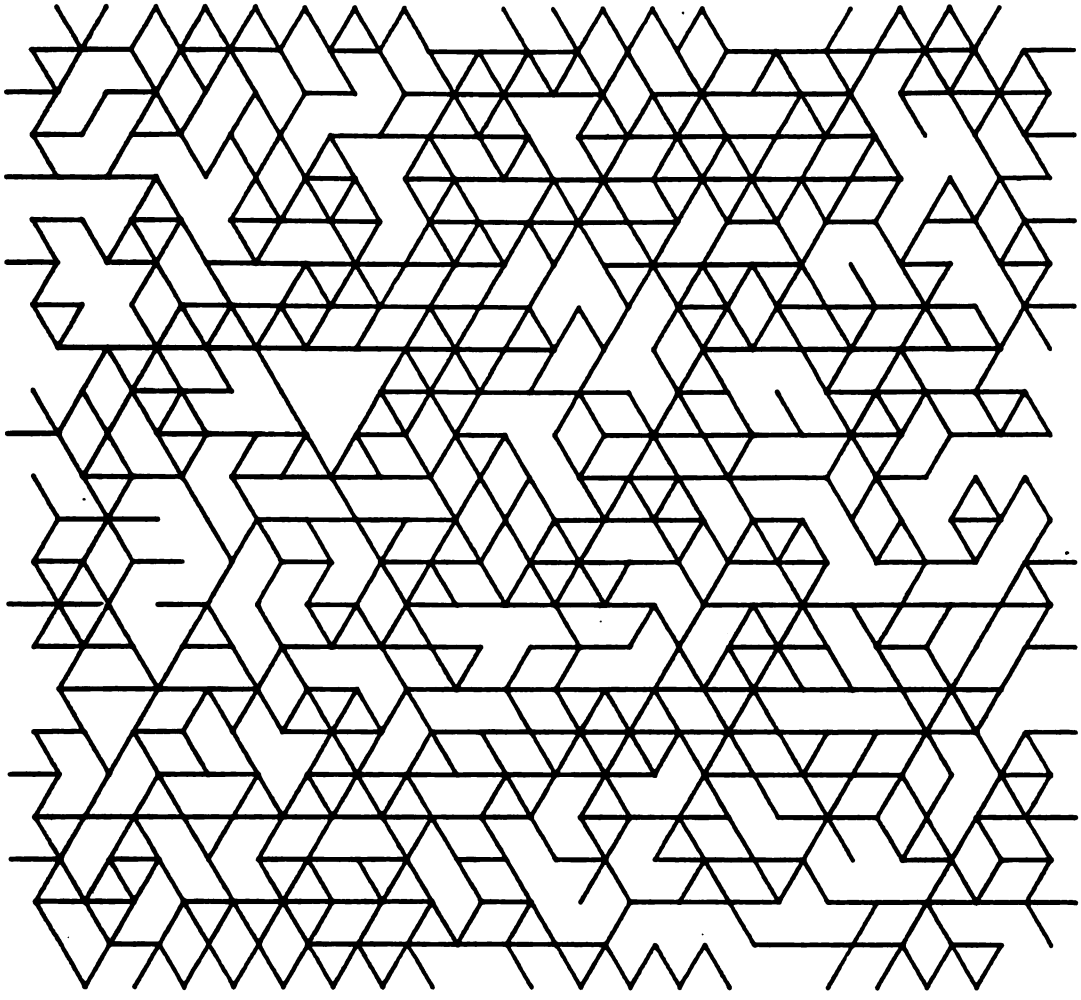

Figure 5. 20 x 22 triangular cell with p=0.65

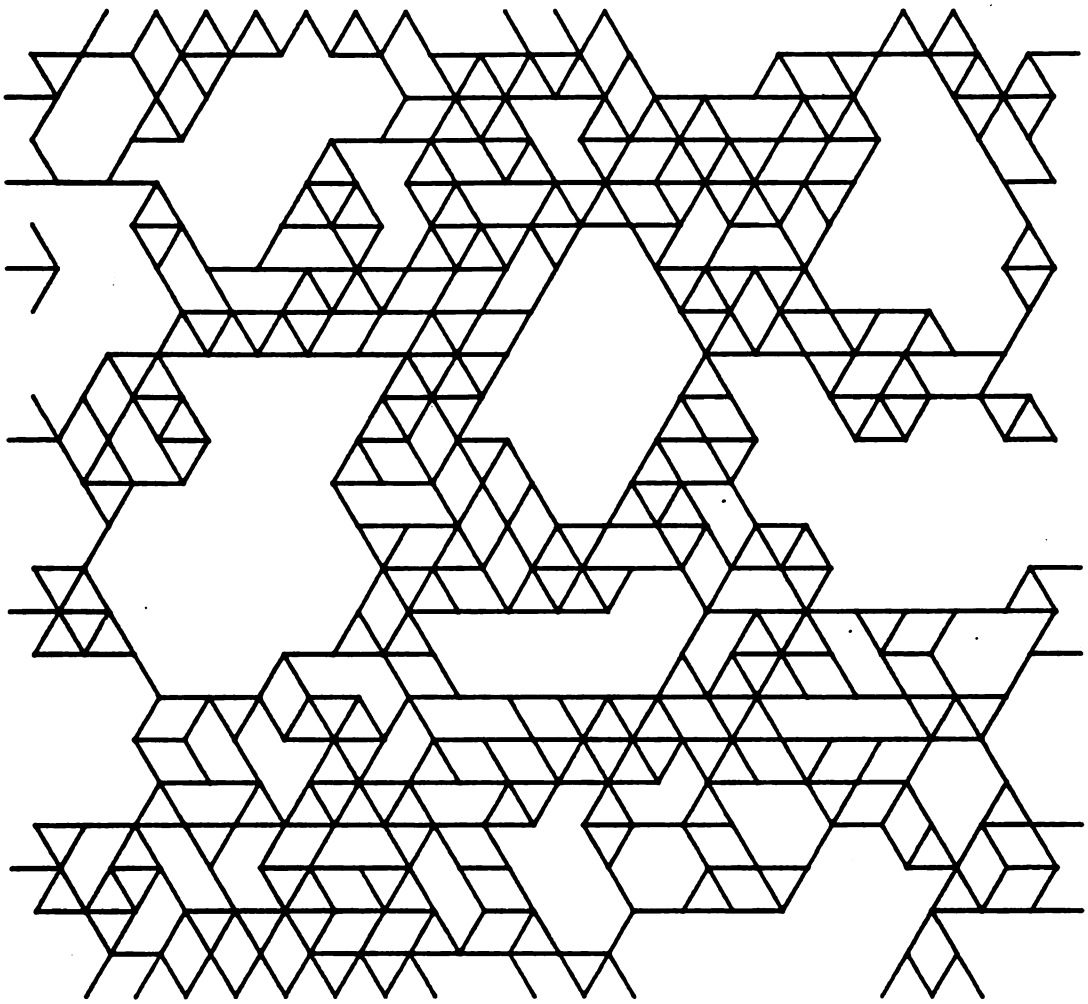

Figure 6. Network from Figure 5 after trimming

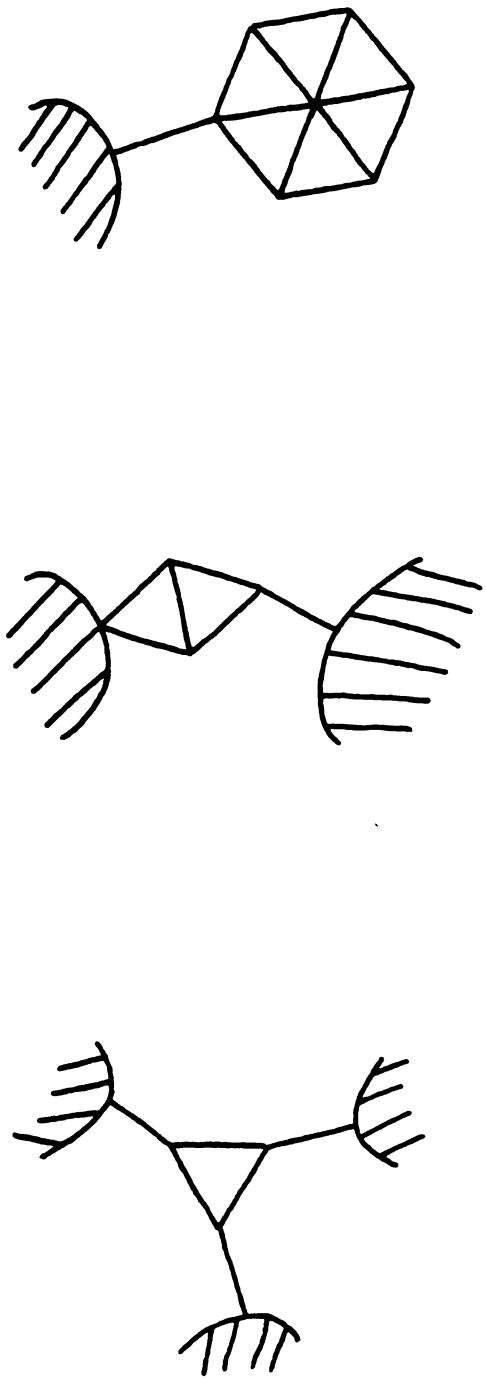

Figure 7. Examples of three types of supertrimmable units

removed by hand before relaxing the network by a process we call supertrimming. The removal of such units sometimes creates new one and two coordinated sites, which leads to further trimming, which can lead to further supertrimming, etc. These two processes are iterated sequentially until no new units can be identified by these criteria. There are certainly other units which could be removed as well, but we have not been able to identify them. A complete set of rules for all supertrimmable units which we have found is listed in Appendix A. Figure 8 shows the same network as in Figure 5 but now supertrimmed as well as trimmed.

The effects of trimming and supertrimming are to greatly accelerate the relaxation process and save computer time by not wasting relaxation steps on sites which will not contribute to the elastic energy anyway. One can also find a lower bound for p^* by finding the point at which the networks breaks up under the combined effects of trimming and supertrimming. Figure 9 shows p' as a function of p, where p' = the fraction of bonds left after trimming or trimming plus supertrimming. This gives a lower bound for p^* of about 0.61. A more careful computation has been done, using ten configurations of 60 x 72 triangular supercell. One trims and supertrims until the network breaks up in all directions. The value of p for which this occurs is the lower bound for p^*. After averaging, one finds that $p^* \geq 0.62$.

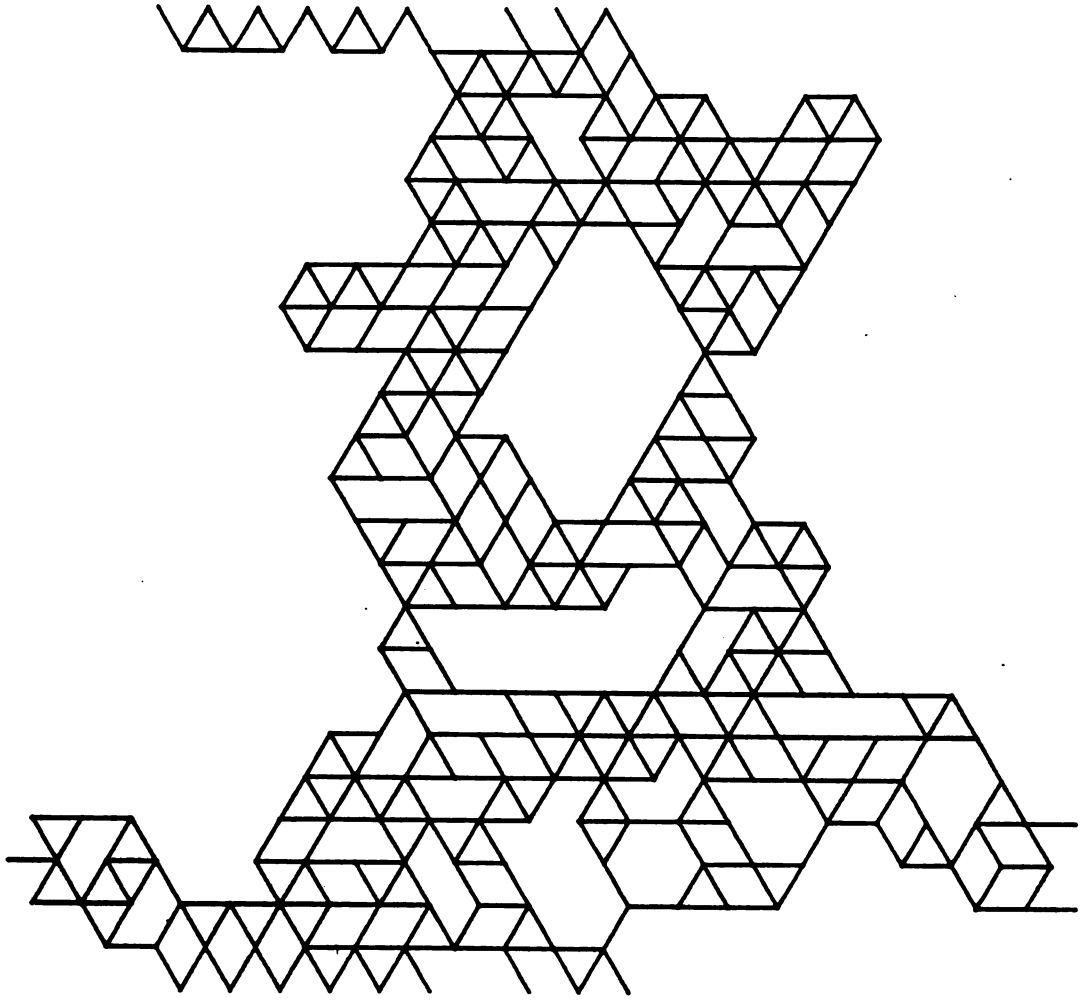

Figure 8. Network from Figure 5 after trimming and supertrimming

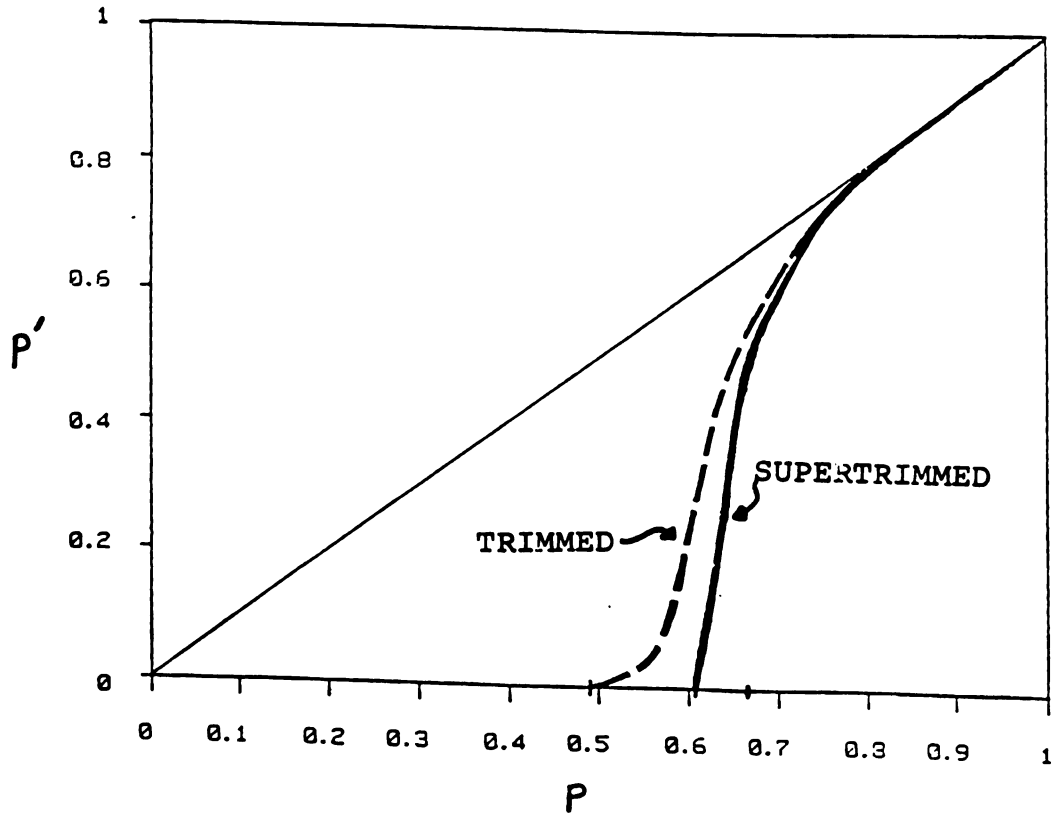

Figure 9. P' vs. p for 20 x 22 triangular network

Diode Effect

As was mentioned previously, when one cuts bonds on the triangular lattice, there can exist sites with two bonds which are colinear. These kinds of sites introduce a non-linearity into the system, since under compressive strain this connection will buckle, providing no restoring force, while under tension this connection does have a restoring force and so is rigid. This point is illustrated in Figure 10. We call this problem the "diode effect." The difficulty is summarized in the expression "You can't push things with a rope!" A system with these kind of connections will then have different elastic moduli depending on the sign of the strain, which is a violation of classical elasticity theory. What must be done to remedy this situation is perhaps best illustrated by considering a simple example.

Consider a two bond "system" as shown in Figure 11 with a potential energy

$$V = \sum_{i=1}^{2} \frac{1}{2} \alpha (l_i - l_0)^2 + \frac{1}{2} \beta (\theta - \theta_0)^2$$

We can now put a horizontal strain ϵ on this system, where $\epsilon > 0$ means compression and $\epsilon < 0$ means tension. The elastic "modulus" C which couples to this strain can be calculated with a little algebra to give

$$C = \frac{2 \alpha \beta \sin \frac{1}{2}\theta_0}{l_0 \left(\alpha \cos^2 \frac{1}{2}\theta_0 + \frac{2\beta}{l_0^2} \sin^2 \frac{1}{2}\theta_0 \right)}$$

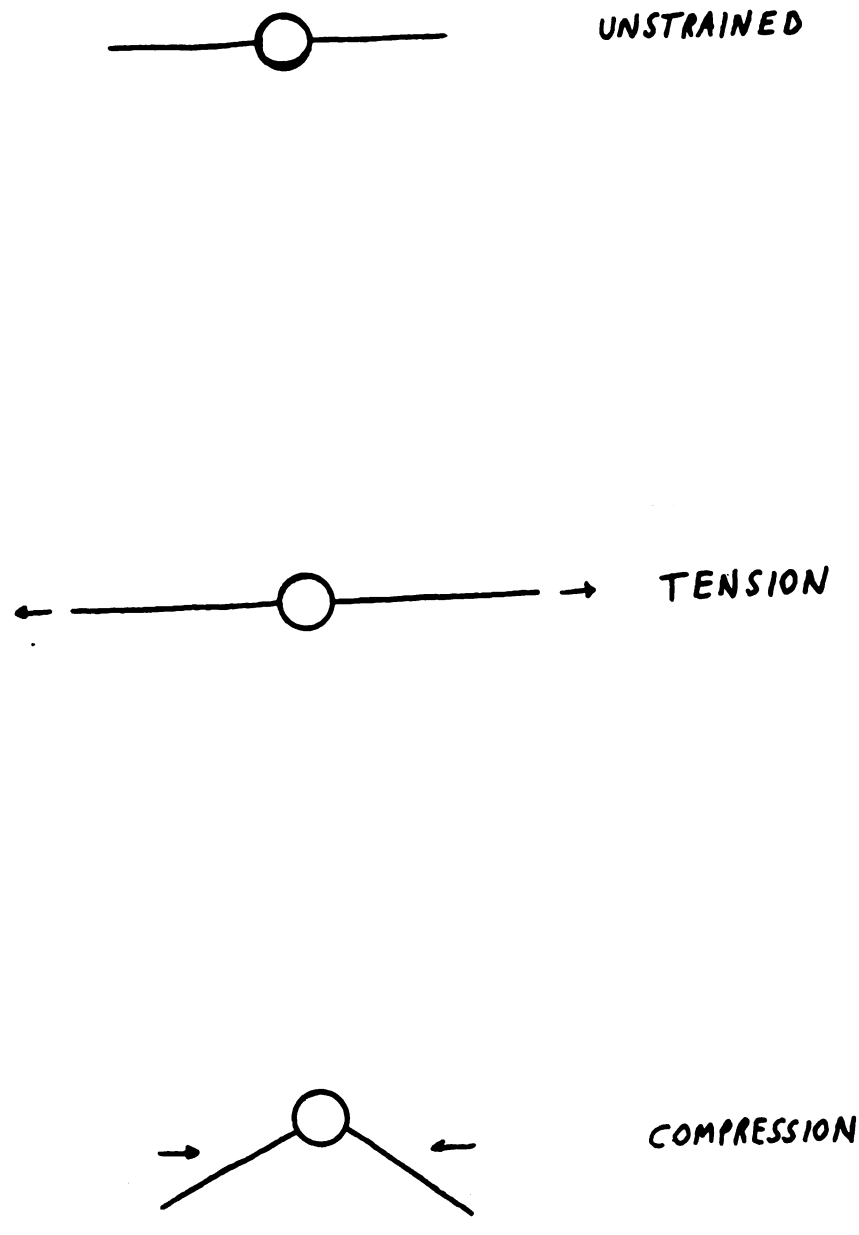

Figure 10. Illustration of the diode effect

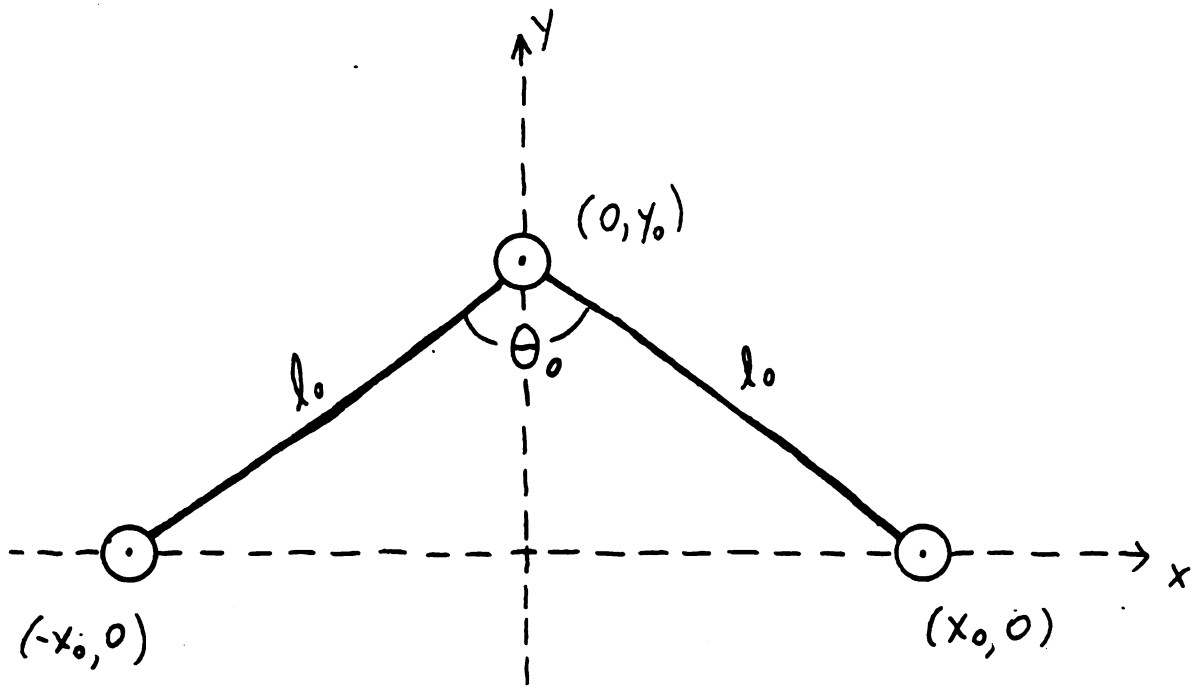

$$l_o^2 = x_o^2 + y_o^2$$

$$\cos\left(\frac{\theta_o}{2}\right) = \frac{y_o}{l_o}$$

Figure 11. Two bond elastic "network"

Now, to make this example illustrate the situation in the triangular net, we need to take the two limits $\beta \to 0$ and $\theta_0 \to 180^0$. There are two orders in which to take these limits of course.

$$\lim_{\theta_0 \to \pi} \lim_{\beta \to 0} C(\theta_0, \beta) = 0 \tag{10}$$

$$\lim_{\beta \to 0} \lim_{\theta_0 \to \pi} C(\theta_0, \beta) = \alpha l_0 \tag{11}$$

Equation (11) illustrates the diode effect. C will be finite under tension and zero under compression. Equation (10) is then the proper order in which to take the two limits. It is clear how we are to do the calculation on the triangular net. Taking $\beta = 0$ gives us our central force potential. Then we perturb the triangular lattice so that the angle between all pairs of straight bonds is less than 180^0. This perturbation must be of the order $\epsilon^{1/2}$, so as to allow all straight pairs of bonds to fully relax under both tension and compression. As the strain $\to 0$, so will the perturbation, and we will get back the proper result for the triangular net.

Computationally, we use $\epsilon = 10^{-5} << 1$, and do the simulation by simply trimming all two coordinated sites and leaving the rest of the lattice unperturbed. For small strains this is equivalent to the ideal limiting process.

Numerical Simulation Results

The actual results for C_{11} and C_{44} as a function of p for the triangular net are presented in Figure 12. These results are averaged over three configurations, where each network was trimmed by a computer program then supertrimmed by hand interactively. The straight line in the graphs is the result of the effective medium theories described in Sections 1.7 and 1.8. The agreement between theory and "experiment" is clearly very good, much better than we usually get for simple effective medium theories. The data is almost exactly linear nearly all the way down to p^*. The constraints counting prediction for $p^* = 2 / 3$ is very accurate. The small tail past p^* has contributions from finite size effects and incomplete relaxation in this region. Near p^*, each connected site in the network had to be relaxed many thousands of times to even approach convergence. A confirmation of our result has recently come from Tremblay (1984). He and his co-workers used finite-size scaling to obtain a value of 0.649 for p^*, with a critical exponent of 1.4 ± 0.2, which is consistent with our results.

Figure 13 presents the numerical result for f(p). f(p) was computed for three configurations of a 12 x 14 triangular network by setting up the full 336 x 336 dynamical matrix and numerically diagonalizing it, then counting how many modes had zero frequency. These networks were small because of central memory limitations in the MSU CYBER 750, and were untrimmed and unperturbed. The difference that a lattice

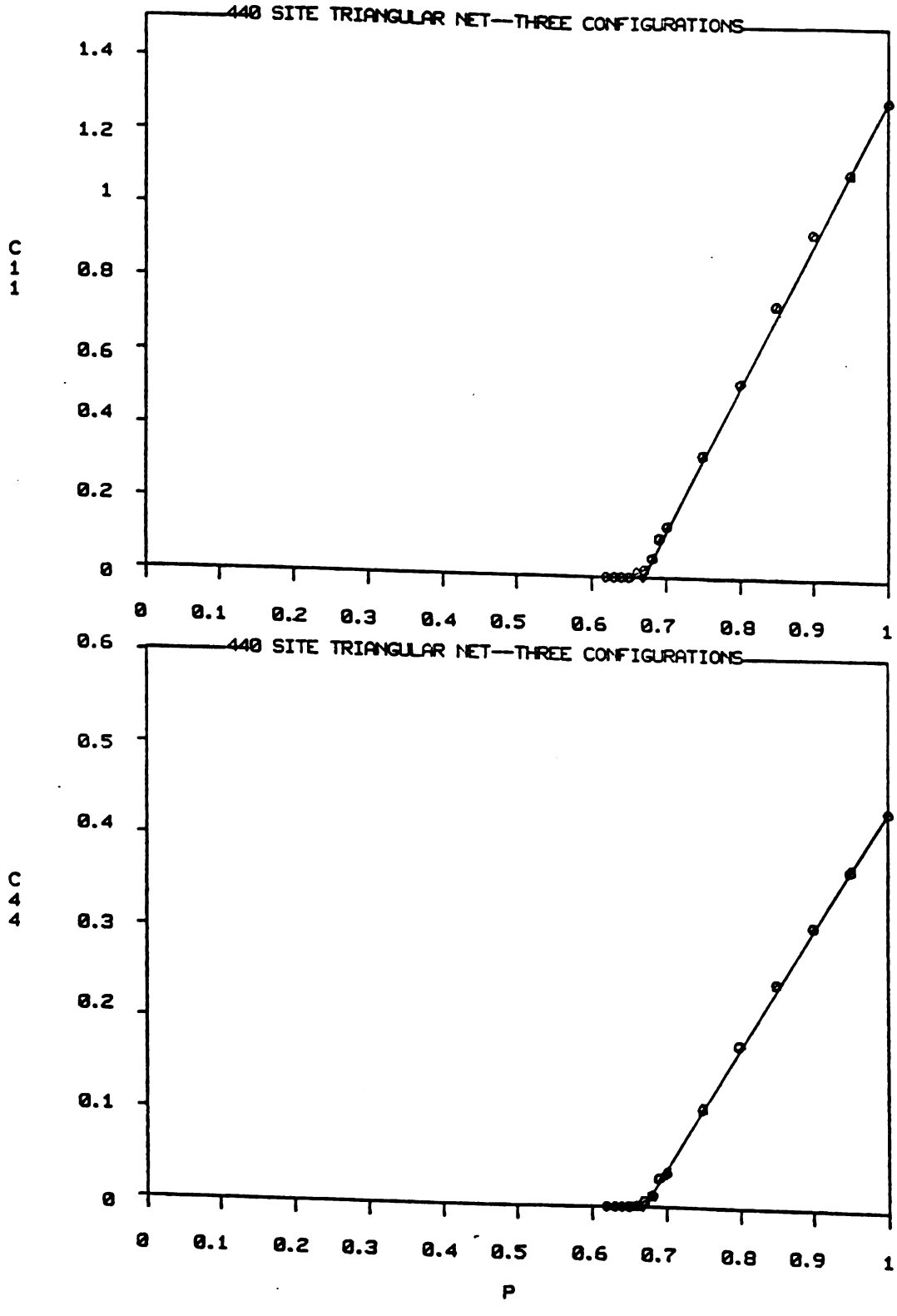

Figure 12. C_{11} and C_{44} vs. p for the triangular network

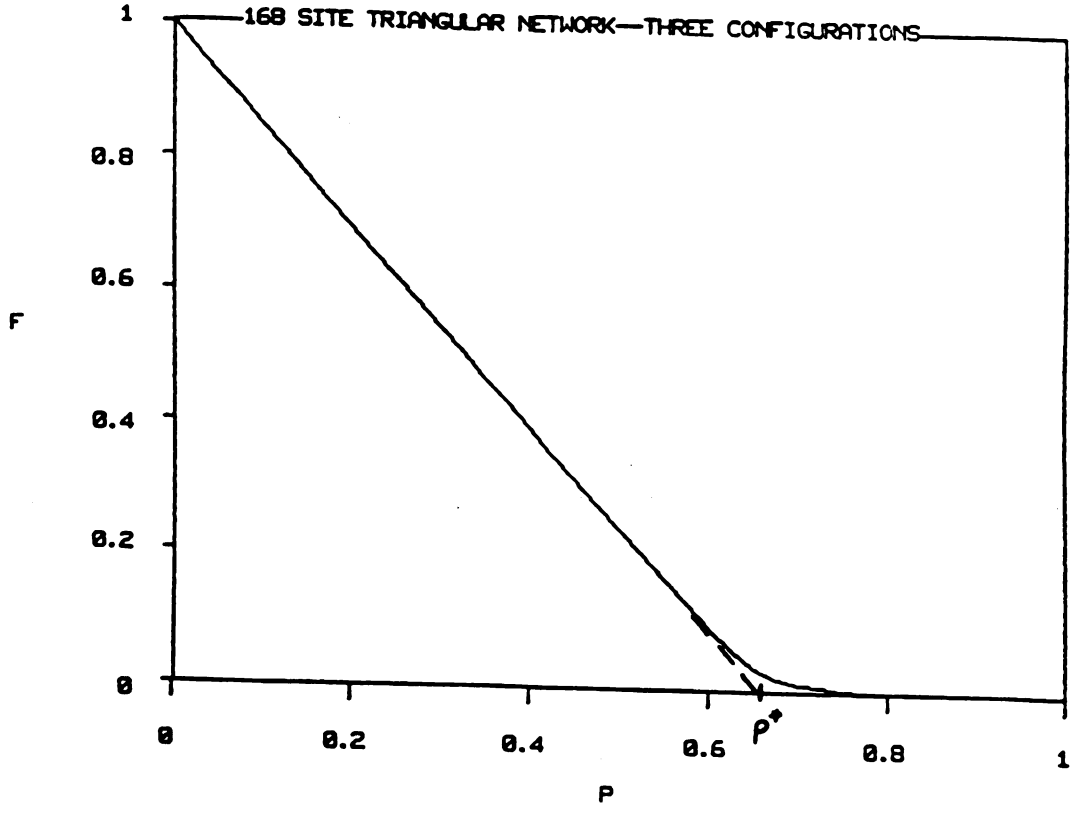

Figure 13. f(p) vs. p for the triangular network

perturbation like that described earlier makes in f(p) will be shown explicitly in the FCC results. The difference is very small. The numerical result for f(p) matches the mean field prediction very well indeed, as can be seen by comparing Figures 3 and 14. The slight curvature around $p^* \simeq 0.65$ is due partly to finite size effects and partly to real critical effects, as we do not expect mean field theory to be exact (see Thorpe 1983).

Section 1.5. FCC Numerical Simulation Results

Details of the lattice

One of the two lattices in three dimensions upon which we have tested the constraint counting theory is the face centered cubic (FCC) Bravais lattice. Every site in this lattice has twelve nearest neighbors (z = 12). One can think of the FCC lattice as being made up of four interpenetrating simple cubic sublattices, where each site's twelve nearest neighbors are on a different sublattice from itself. The nearest neighbor bond lengths are all a $/\sqrt{2}$, where a is the edge length of the standard cubic unit cell. For computational purposes it was convenient to take a $=\sqrt{2}$, so that the n.n. bond lengths all became equal to unity.

Elastic Moduli for Crystal

Using the dynamical matrix formalism for central forces set up in Section 1.3, and letting $k \to 0$, we can write out the elements of $D(\vec{k})$ for the FCC lattice:

$$D_{xx} = \frac{\alpha a^2}{4m}\left(k^2 + k_x^2\right) \qquad D_{xy} = \frac{\alpha a^2}{2m} k_x k_y$$

$$D_{yy} = \frac{\alpha a^2}{4m}\left(k^2 + k_y^2\right) \qquad D_{xz} = \frac{\alpha a^2}{2m} k_x k_z$$

$$D_{zz} = \frac{\alpha a^2}{4m}\left(k^2 + k_z^2\right) \qquad D_{yz} = \frac{\alpha a^2}{2m} k_y k_z$$

I will now take the mass m = 1 as this was what was done in the numerical simulations. The FCC density then becomes $\rho = 4 / a^3$, since there are four sites per standard cubic unit cell. $D(\vec{k})$ is particularly easy to diagonalize in the (100), (110), and (111) directions. We can find v_l^2 and v_t^2, the longitudinal and transverse sound velocities in these three directions and then find C_{11}, C_{12}, and C_{44} using a result from Kittel (1967) relating the moduli and sound velocities. For cubic symmetry there are only three independent elastic moduli which it is standard practice to take to be C_{11}, C_{12}, and C_{44}. For the FCC lattice we find that

$$C_{11} = 2\alpha/a \qquad C_{12} = \alpha/a \qquad C_{44} = \alpha/a$$

Letting $a = \sqrt{2}$ and $\alpha = 1$ to match up with the units used in the numerical simulations, the final form of the elastic moduli for the FCC crystal is

$$C_{11} = \sqrt{2} \qquad C_{12} = C_{44} = \sqrt{2}/2$$

The equality of C_{44} and C_{12} comes from a Cauchy relation. For a Cauchy relation to hold, all sites must have inversion symmetry and the forces between sites must be purely central (Love 1944).

Numerical Simulation Results

All the elastic moduli computations for the FCC networks

were done on a cubic cell which was made up of 125 standard cubic unit cells (5 x 5 x 5), giving 500 sites altogether, with 3000 bonds present initially. Periodic boundary conditions were maintained throughout the computation in a manner similar to that used on the triangular net. The values of the bond fraction p ranged from 1.0 to 0.46. C_{11} and C_{44} were averaged over the x,y, and z directions for each configuration, and these results plus the bulk modulus K were averaged over three configurations. C_{12} was obtained by using the computed values of C_{11} and K in the relation

$$K = \frac{1}{3}(C_{11} + 2C_{12}) \quad .$$

The diode effect is present in FCC as well as in the triangular net. Here, however, one cannot escape dealing with the problem directly as up to four bonds attached to one site may all lie in the same plane, thus giving different elastic response for in-plane tension or compression. This difficulty is resolved by perturbing the FCC lattice through moving each sublattice so that all bonds become non-planar by an amount proportional to $\epsilon^{1/2}$ (ϵ = applied strain = 10^{-5}). In effect, each site is "puckered" slightly out of each of the three cubic faces of which it was formerly a member. This is a small perturbation, and only appreciably affects the elastic moduli very near the critical region.

Trimming and supertrimming are both possible for FCC.

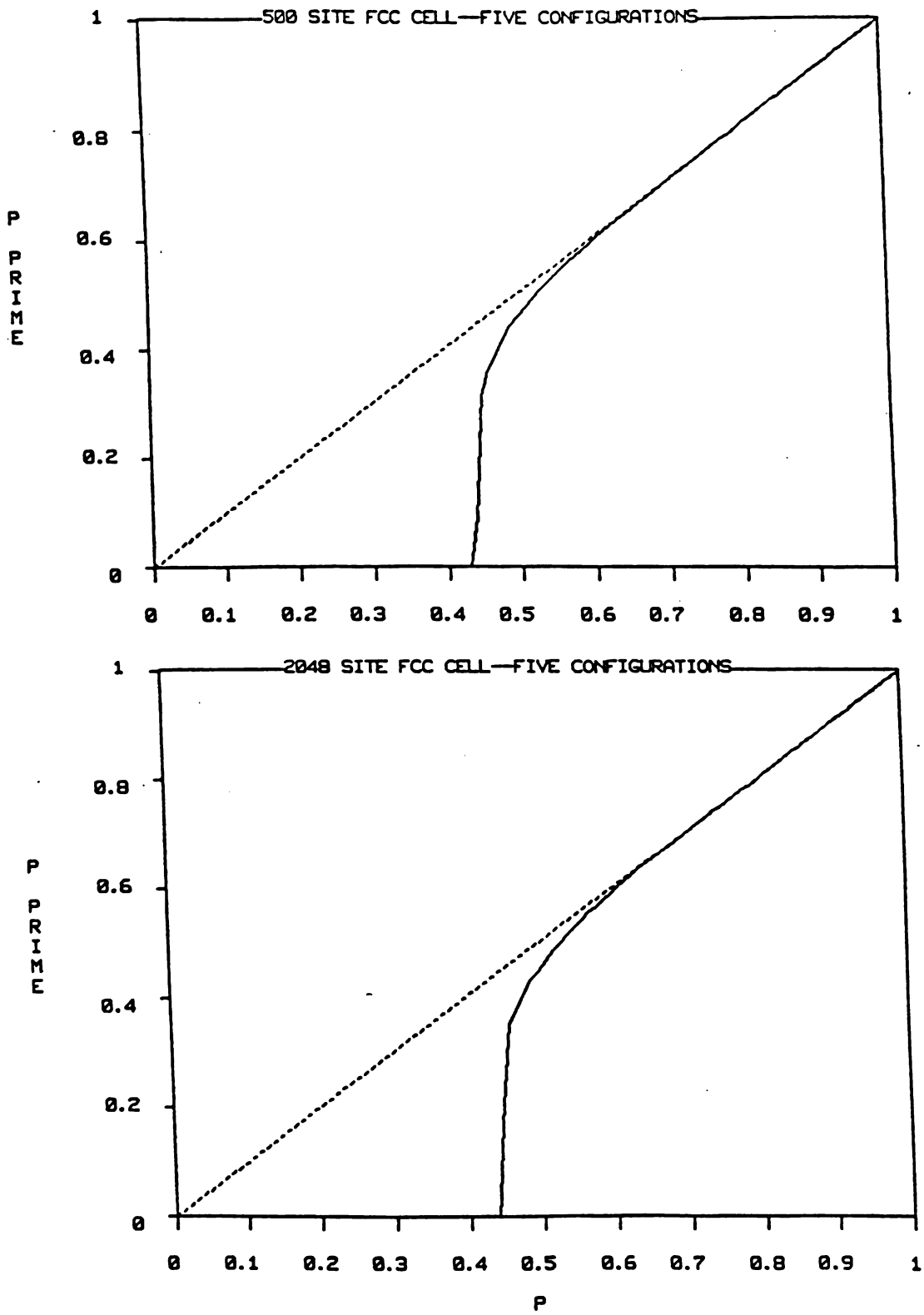

Figure 14. P′ vs. p for 500 and 2048 site FCC networks

In three dimensions any site with three bonds or less will not contribute to the final relaxed elastic energy so can be removed. There are certainly higher order units which do not contribute to the strain energy, as in two dimensions, but these we have not identified because we cannot draw three dimensional pictures. It fortunately turns out that super-trimming appears to be of lesser importance in three dimensions, as a 500 site network is broken up by trimming alone on the average at about $p = 0.43$, which is already quite close to $p^* = 0.50$. It would seem that ordinary trimming is more effective in three dimensions than in two, if we compare Figure 14 with Figure 9. Figure 14 shows the small dependence of trimming on the size of the network. For 2048 sites, the trimming lower bound for p^* is about 0.44.

Figures 15 and 16 present the results of the numerical computations of C_{11}, C_{44}, C_{12}, and K. For all cases, the p dependence of the elastic moduli is very close to linear all the way down to $p^* = 0.50$, with a small tail which is partly a finite size rounding of the transition and partly a real critical effect. It is very difficult to completely relax the network for values of p close to p^*, so that incomplete relaxation could also have made a contribution to the tail. In fact, for $p \lesssim 0.64$, an extrapolation scheme was used to extend the relaxation procedure. The details of this scheme can be found in Appendix B. The straight lines drawn in Figures 15 and 16 are the result for C_{ij} (p) obtained from the effective medium theories

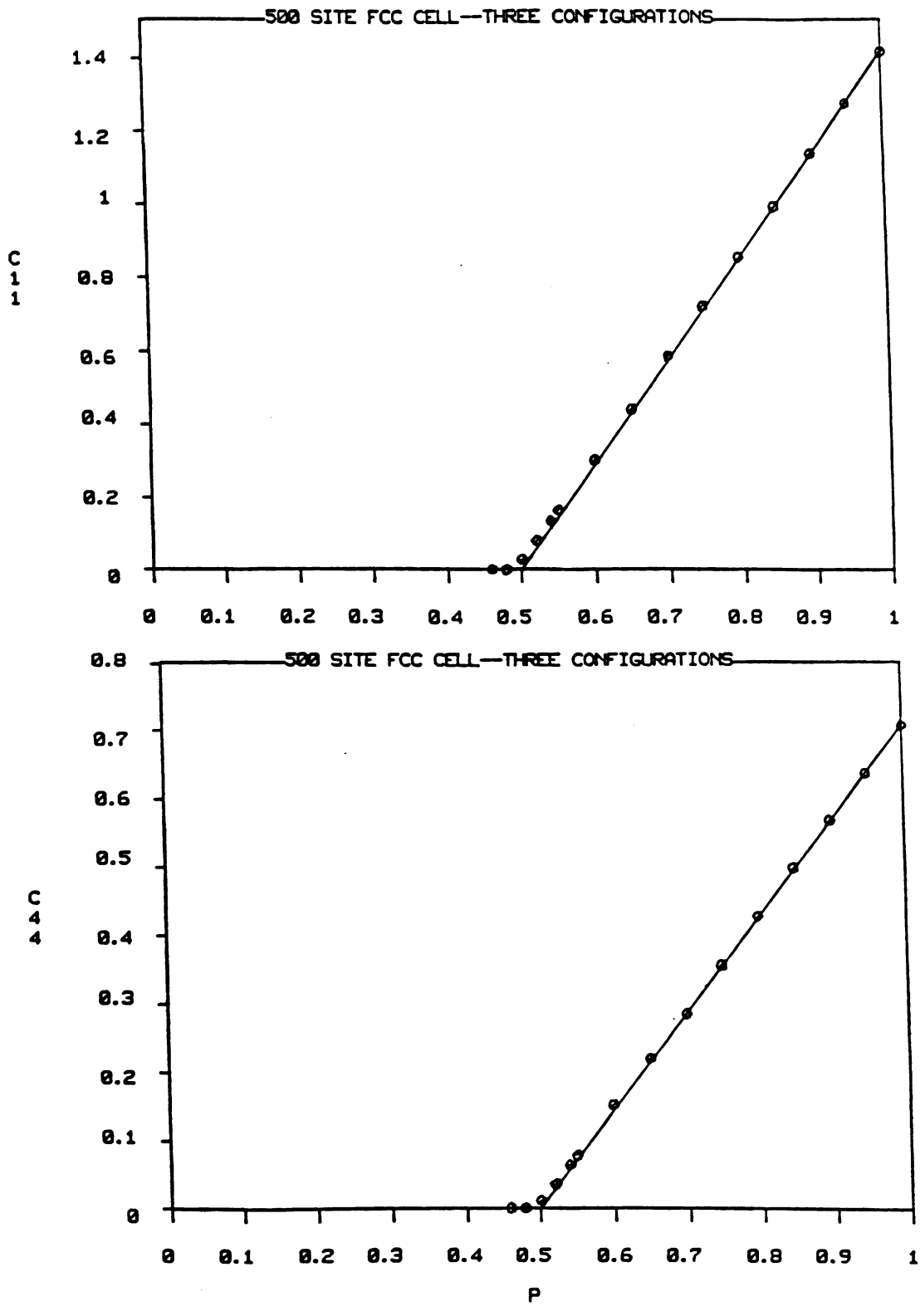

Figure 15. C_{11} and C_{44} vs. p for FCC network

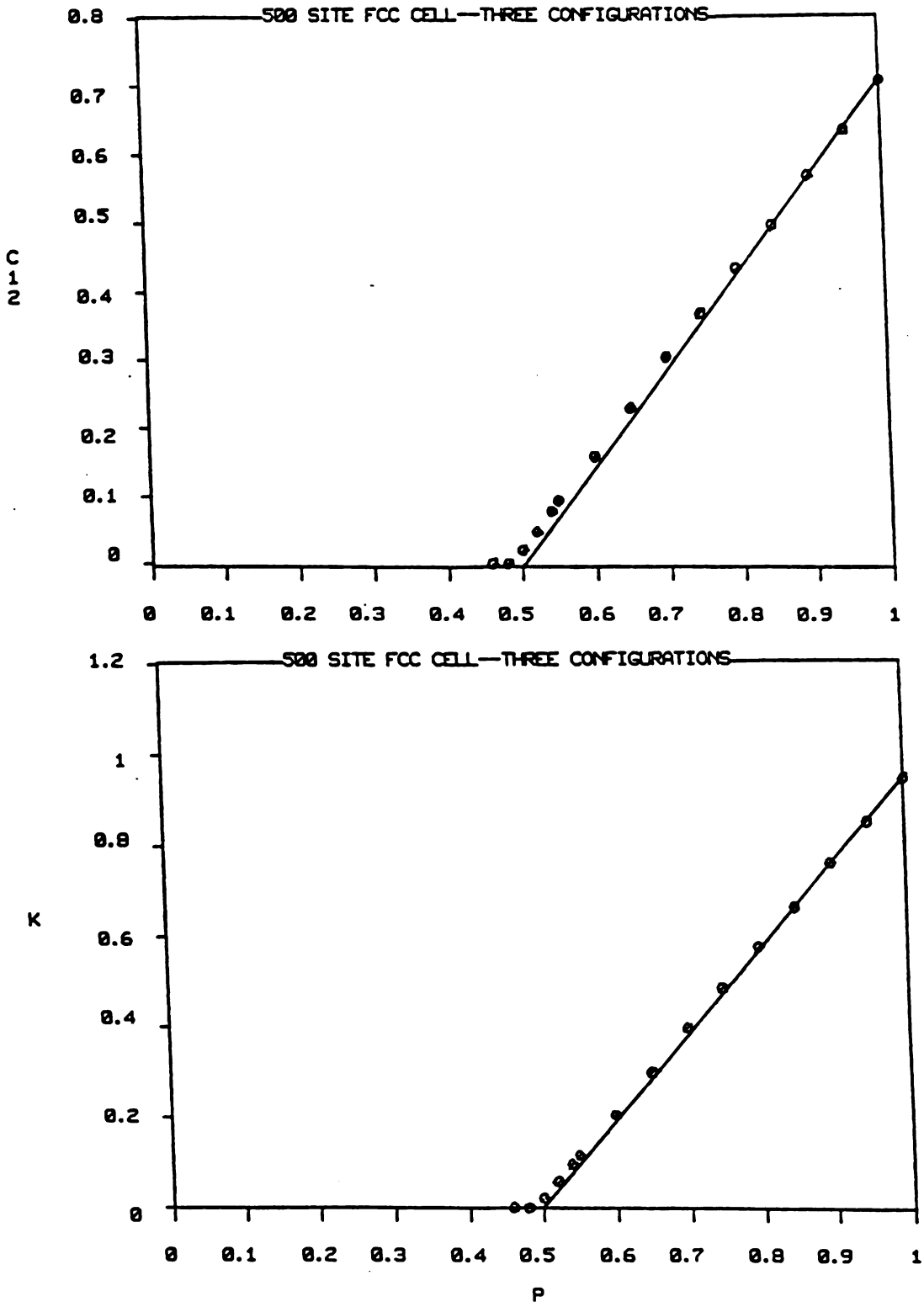

Figure 16. C_{12} and K vs. p for FCC network

described in Sections 1.7 and 1.8. The agreement of numerical simulation with theory is seen to be very good indeed, and the agreement of the mean field estimate for p^* with the computational results is also quite good. It is interesting to note that the near perfect linearity of C_{44} and C_{12} all the way into the critical region implies that the Cauchy relation $C_{12} = C_{44}$ is also obeyed with high accuracy over a wide range of p. It is not known why this should be so, as inversion symmetry at each site is lost as bonds are cut.

Figure 17 shows the numerical result for the fraction of zero frequency modes f for both perturbed and unperturbed networks. These curves were obtained by setting up the full 3N x 3N real space dynamical matrix for the FCC network at various values of p, then diagonalizing it and counting the actual number of zero frequency modes. The three Goldstone modes are subtracted out at the beginning. Because of central memory limitations on the MSU CYBER 750 computer, this computation was done for a 108 site cubic cell (3x3x3), and averaged over three configurations. The constraint counting prediction for f(p) agrees quite well with the numerical simulations. There are only small differences at the 2% level around p^* due in part to finite size effects and actual critical effects, since we do not expect mean field theory to be perfectly accurate.

Figure 18 at the top shows a blow-up of the region in which f(p) for the perturbed and unperturbed lattices differs at all. The bottom graph shows $f^{un}(p) - f^{per}(p)$.

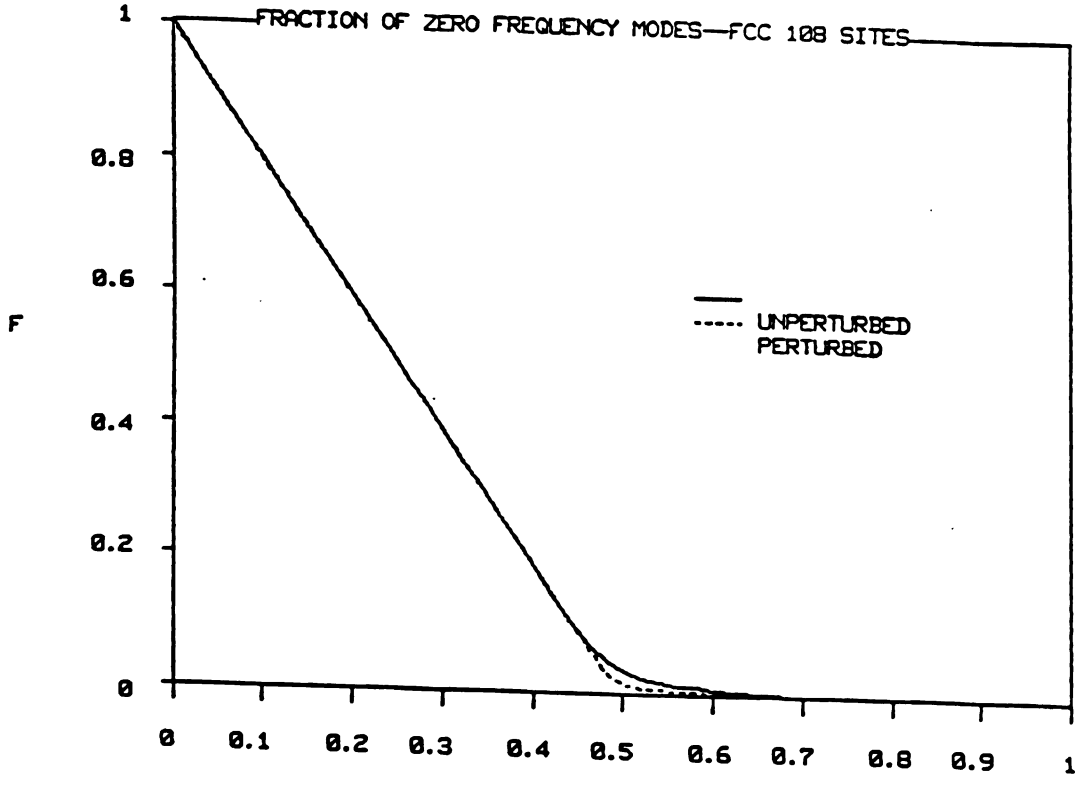

Figure 17. f(p) vs. p for perturbed and unperturbed 108 site FCC networks

The maximum difference comes at about p^*. The unperturbed f is always larger than the perturbed f since for central forces, out of the plane motion of a site with coplanar bonds has zero frequency. This symmetry is broken for the perturbed lattice giving this kind of motion a small finite frequency.

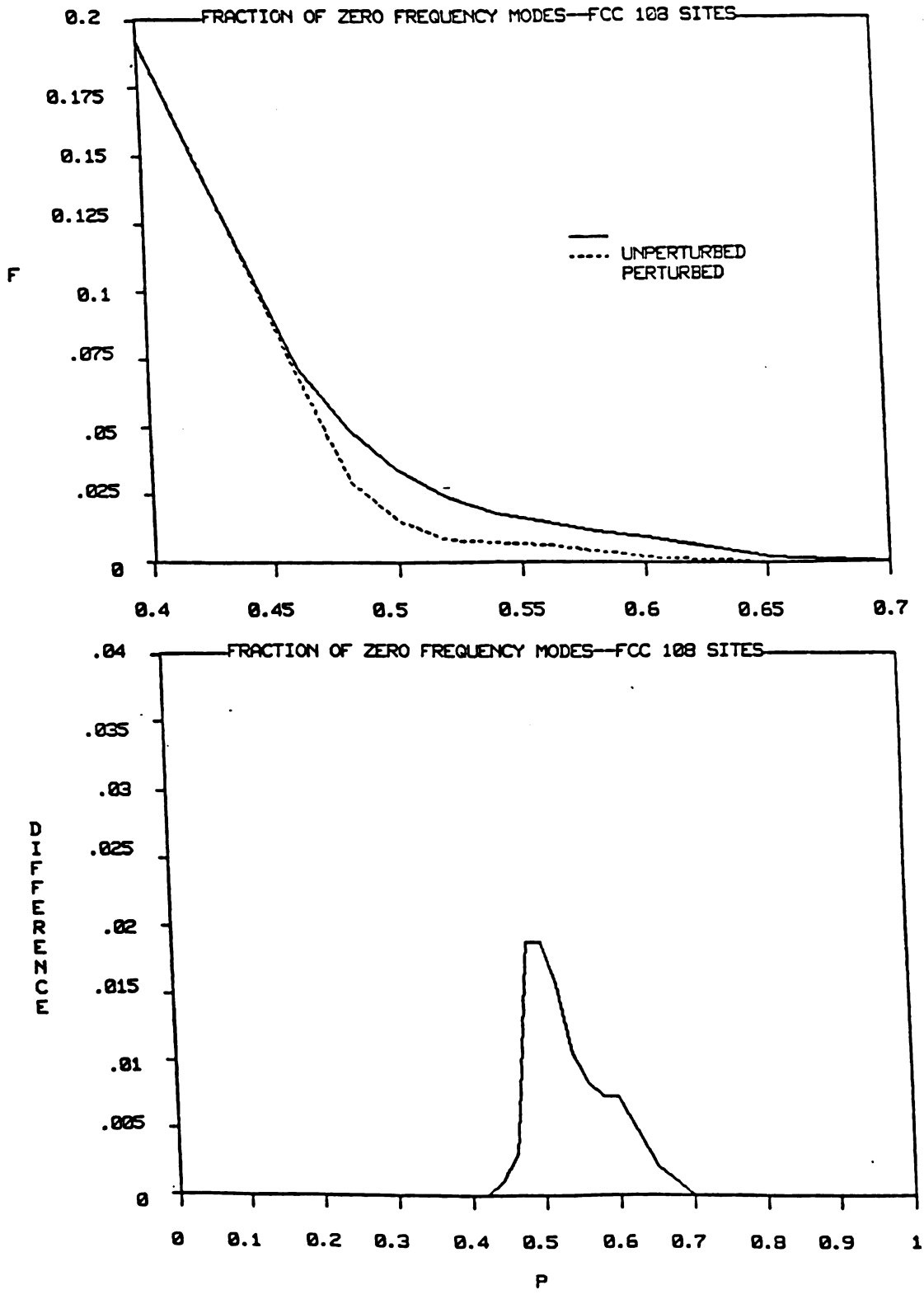

Figure 18. f and Δ f vs. p for 108 site FCC networks

Section 1.6. BCC Numerical Simulation Results

Details of the Lattice

Numerical simulations to compute $C_{ij}(p)$ were also done on the body centered cubic (BCC) lattice. The BCC lattice can be thought of as consisting of two interpenetrating simple cubic sublattices. A site on sublattice A has all its eight nearest neighbors (z = 8) on sublattice B and vice versa. The nearest neighbor bond lengths are all $\sqrt{3}\,a\,/\,2$, where a = edge length of the standard cubic unit cell. For computational purposes it was convenient to take $a = 2/\sqrt{3}$ so that the nearest neighbor bond lengths were normalized to one.

Elastic Moduli for the Crystal

Following the same procedure as was done for FCC, we write out in the $k \to 0$ limit $D(\vec{k})$:

$$D_{xx} = D_{yy} = D_{zz} = \frac{1}{3} k^2 a^2$$

$$D_{xy} = D_{yx} = \frac{2}{3} K_x K_y a^2$$

$$D_{xz} = D_{zx} = \frac{2}{3} K_x K_z a^2$$

$$D_{yz} = D_{zy} = \frac{2}{3} K_y K_z a^2$$

We diagonalize $D(\vec{k})$ in the (100), (110), and (111) directions and calculate the elastic moduli similarly as for FCC. This gives the somewhat surprising result:

$$C_{11} = C_{12} = C_{44} = \frac{2}{3}\frac{\alpha}{a}$$

When we let a = 2 /$\sqrt{3}$ to rescale the nearest neighbor bond lengths we obtain:

$$C_{11} = C_{12} = C_{44} = \frac{\sqrt{3}}{3}\alpha$$

The equality of C_{12} and C_{44} is due to the existence of a Cauchy relation (Love 1944). C_{44} and C_{12} being equal is a consequence of the BCC lattice symmetry. A curious result of this second degeneracy is that v_{t2}, the transverse sound velocity in the (110) direction where the atomic displacements are in the plane, is identically zero. In fact, one can easily show by considering $D(\vec{k})$ for a general $\vec{k}$ that one of the three branches of $\omega^2(k)$ is identically zero in the (110) direction. Thus even with all bonds present the BCC lattice still has non-trivial zero frequency modes. The number of these is insignificant in the thermodynamic limit, but for the small systems used in the simulations their fraction was large enough to make the determination of f(p) meaningless. It was therefore pointless to compute f(p), but the behavior of the elastic moduli was still of interest.

Numerical Simulation Results

The cell used for the BCC simulations contained 216 standard cubic cells (6 x 6 x 6) for a total of 432 sites.

There were 1728 bonds present when p = 1.0. Periodic boundary conditions were maintained, and the values of p investigated ranged from 1.0 to 0.67. Regular trimming was done in all cases, with effectiveness comparable to that in the FCC networks. Regular trimming caused the breakup of the elastic backbone on the average at about p = 0.64. The effect cell size had on this number can be seen in Figure 19 where p' vs. p is graphed for both a 432 site and a 2000 site cell. P' = the fraction of bonds left after trimming. All other numerical techniques were the same as those used for the FCC networks.

The diode effect is present in the BCC networks. There are planes of four bonds attached to one site which will have a different elastic response depending on whether the in-plane local strain is tension or compression. Such bond configurations can persist after trimming. We therefore perturb the lattice by shifting the two sublattices with respect to each other by an amount proportional to $\epsilon^{1/2}$, where ϵ = the applied strain = 10^{-5}. This breaks up all the planes of bonds, assuring the same result for the elastic moduli for $\pm \epsilon$. As in the case of FCC, this lattice perturbation has its only significant effect near the critical region.

Figures 20 and 21 present the results for C_{11} , C_{44} , C_{12} , and K. The results are comparable in quality to those for the triangular net. The straight line on the graphs come from the effective medium theories described in Sections

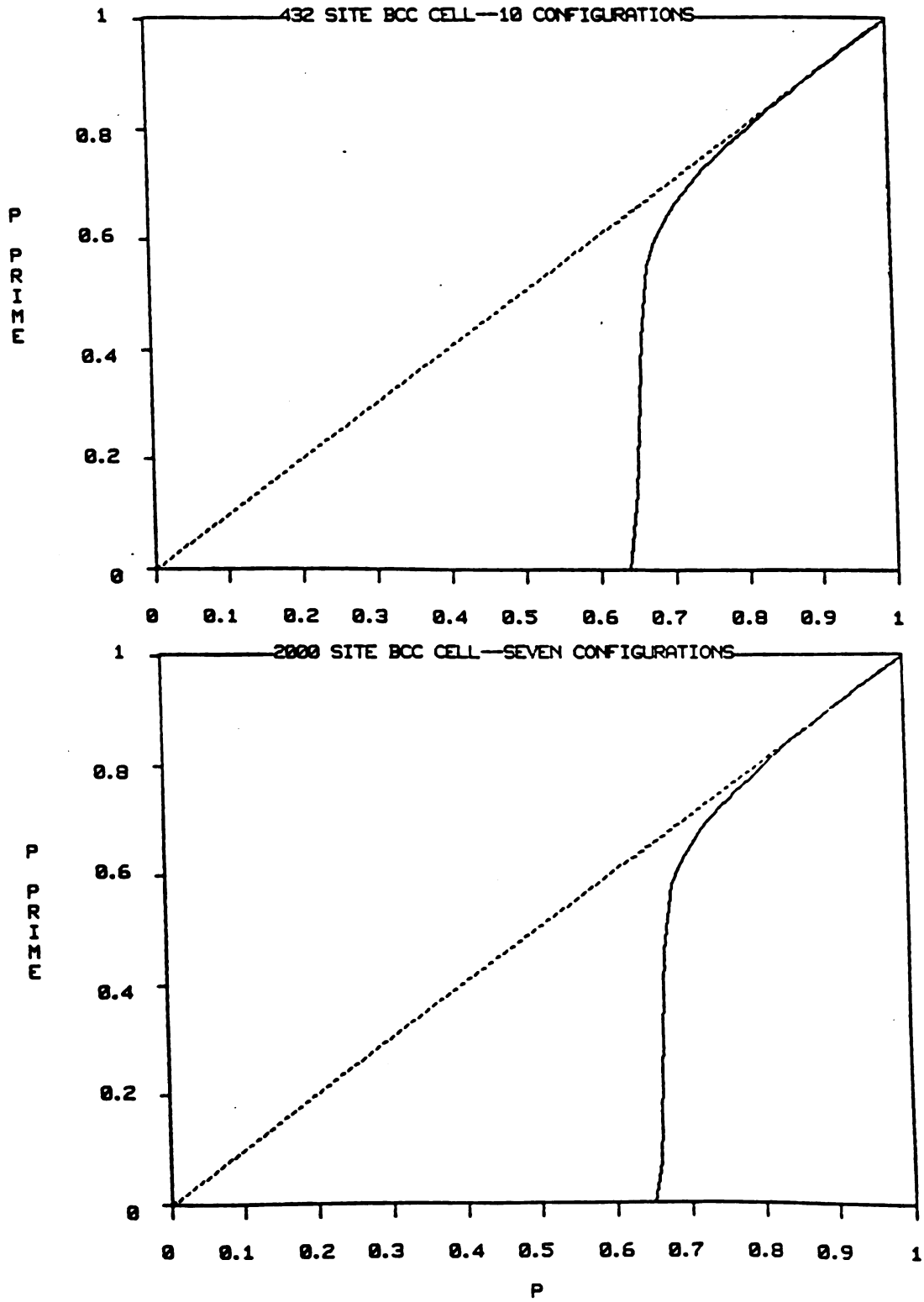

Figure 19. P' vs. p for 432 and 2000 site BCC networks

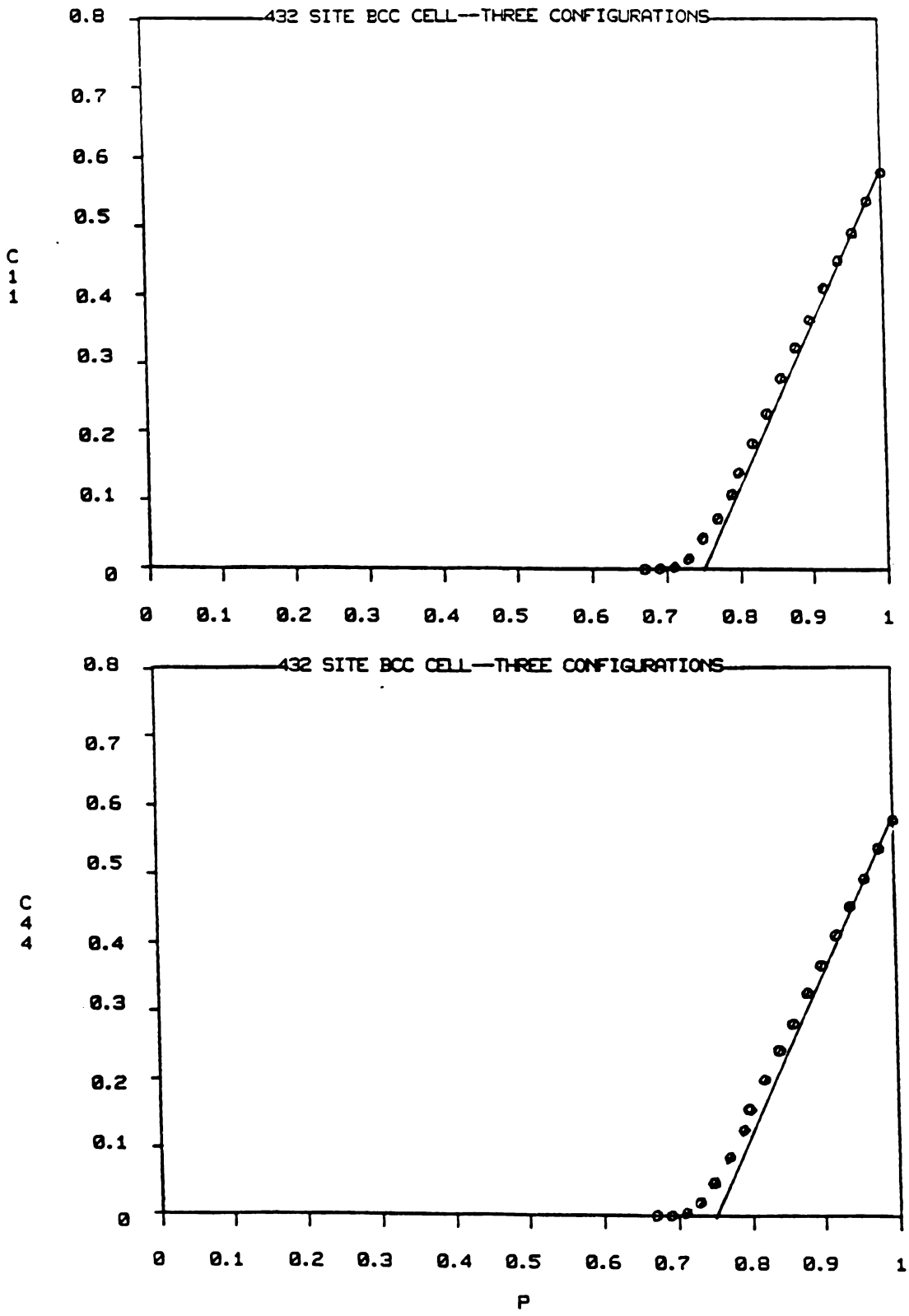

Figure 20. C_{11} and C_{44} vs. p for BCC network

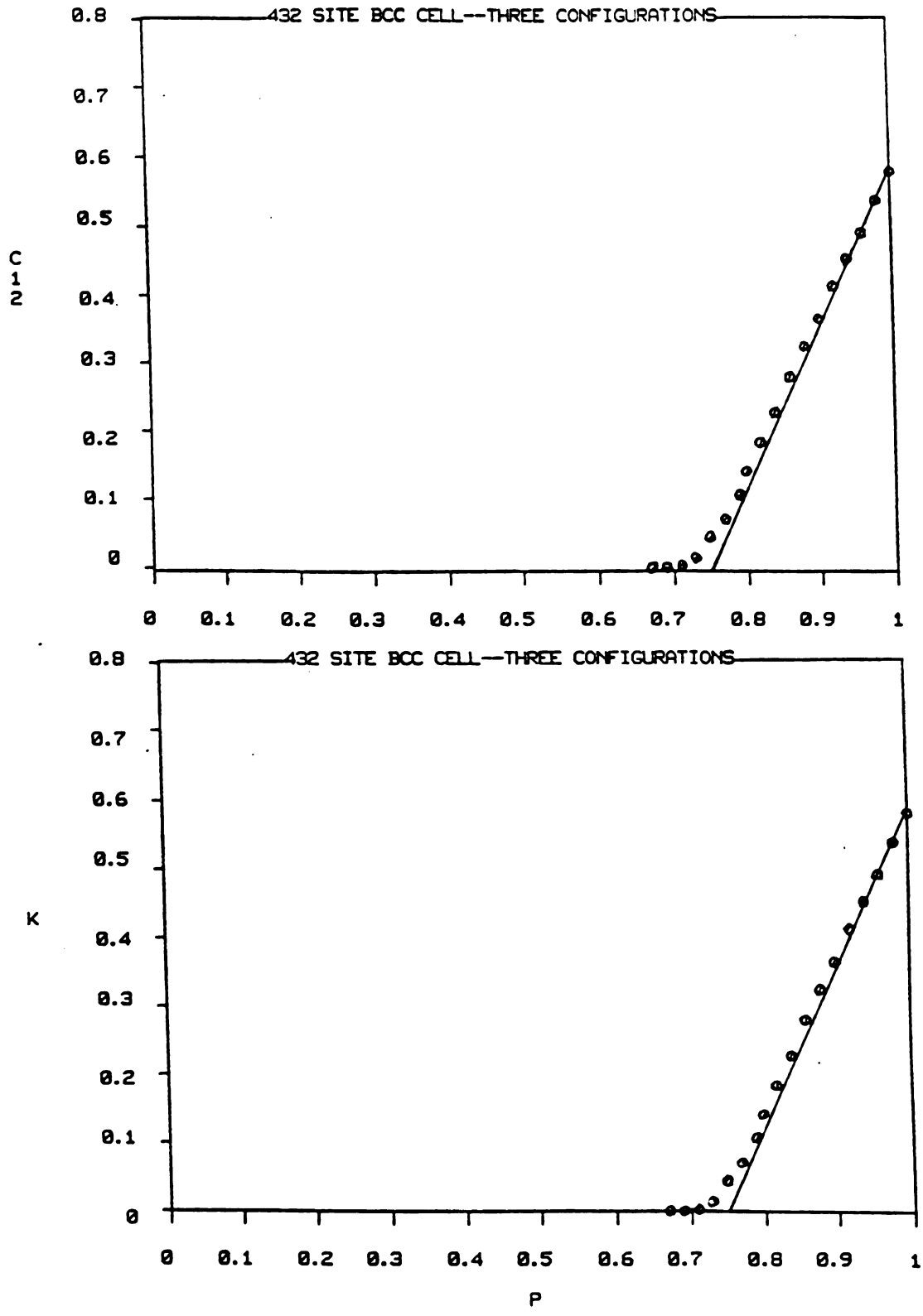

Figure 21. C_{12} and K vs. p for BCC network

1.7 and 1.8. The agreement is quite good between theory and experiment, though not quite as good as for FCC. The constraint counting prediction for p^* is 0.75. This prediction agrees quite well with the data, although the size of the critical tail for BCC is larger than that for FCC. As noted before, the tail is no doubt due to finite size rounding of the transition and relaxation difficulties in the critical region. The Cauchy relation $C_{44} = C_{12}$ and the $C_{44} = C_{12}$ relation are maintained with a high degree of accuracy all the way into the critical region. The reason for the persistence of this behavior over a large range of p when random bond cutting should have long ago destroyed the summetries on which these degeneracies depend is unclear at the present time.

Section 1.7. Effective Medium Theory--Static Method

There are two ways that we know of to develop an effective medium theory that gives a functional form for the elastic moduli as a function of p, and that gives a prediction for p_c. The method described in this section we call the static method. It is based on an effective medium theory (EMT) used by Kirkpatrick (1973) to describe the dependence of the conductivity of a resistor network on the fraction of resistors randomly present. This static method was developed by S. Feng, and is described in Feng (1984), which has been included in this thesis as Appendix C.

Let us start with a triangular net, with all interatomic force constants equal to α. Now apply a uniform stress to the system, which can be hydrostatic, uniaxial, etc. For sake of definiteness let us consider a hydrostatic stress, so that all bonds have the same relative displacement u_h. Now let us focus on two sites, labelled 1 and 2, where the spring constant between 1 and 2 has been changed to γ with $\gamma < \alpha$. (This last assumption is not needed. γ can have any value. Note that in the numerical simulations, $\gamma = 0$.) After this substitution, the spring between 1 and 2 will compress by an additional amount δu, since it is not strong enough to resist the rest of the lattice and maintain a relative displacement of only u_h. This scenario is depicted in Figure 22. Now if we were to apply an external force F to move sites 1 and 2 back to their original positions, F

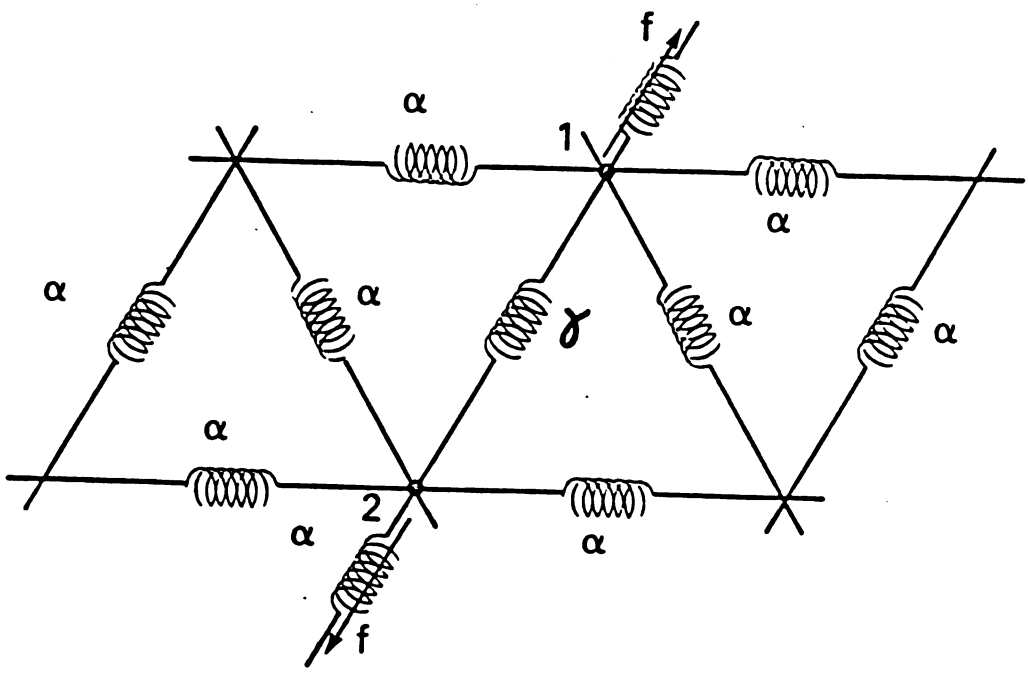

Figure 22. "Wrong bond" substitution in triangular net

would have to be such that

$$F + \gamma u_1 = \alpha u_1$$

$$\text{or} \quad F = (\alpha - \gamma) u_1$$

The external force F "stiffens" the weak spring γ . Now suppose we were to apply the same F to sites 1 and 2 <u>without</u> the uniform stress being applied to the system first. This force would induce a relative displacement δw between 1 and 2. By the principle of superposition,

$$\delta w = \delta u$$

The relation between F and δu can be obtained in the following manner. When all the spring constants are α and we apply F to sites 1 and 2, we can define an effective spring constant between 1 and 2 by

$$\alpha_{eff} \equiv F / \delta u$$

We can write α_{eff} as $\alpha_{eff} = \alpha / a_{cen}$, where $0 < a_{cen} < 1$, since α_{eff} will be greater than α because all the other indirect connections between 1 and 2 will give a positive contribution to α_{eff}. If we then remove the α spring between 1 and 2 and replace it with a γ spring, α_{eff} becomes

$$\alpha_{eff} = \alpha / a_{cen} - \alpha + \gamma$$

Equating the two expressions for F,

$$F = u_h (\alpha - \gamma)$$
$$F = \alpha_{eff} \, \delta u \qquad (12)$$

we have that

$$\delta u = \frac{u_h (\alpha - \gamma)}{(\alpha / a_{cen} - \alpha + \gamma)}$$

δu can be thought of as the "fluctuation" in the relative displacement of sites 1 and 2 that resulted from changing the spring constant from α to γ. The key idea of the effective medium theory enters the argument at this point. Let us renormalize α to α_m, and try to choose α_m in such a way so that a network where <u>all</u> bonds are α_m has the same elastic properties as the original network with γ bonds substituted in for some of the α bonds. The obvious way to choose α_m would be so that δu is zero for every bond. This is clearly not possible. However, we <u>can</u> try to choose α_m so that the average value $\langle \delta u \rangle$ of δu is zero. The average is defined by the following formula:

$$\langle h(\gamma) \rangle \equiv \int P(\gamma)\, h(\gamma)\, d\gamma$$

where $P(\gamma)$ = probability distribution for values of γ .

This gives the usual kind of effective medium or mean field result, with fluctuations treated in only an average sort of way. Setting $\langle \delta u \rangle = 0$ gives the following equation:

$$\left\langle \frac{\alpha_m - \gamma}{\alpha_m / a_{cen} - \alpha_m + \gamma} \right\rangle = 0 \qquad (13)$$

where we note that α has been replaced by α_m . The probability distribution of interest for percolative processes is

$$P(\gamma) = p\, \delta(\gamma - \alpha) + (1-p)\, \delta(\gamma)$$

Evaluating (13) and simplifying gives the result

$$\alpha_m = \alpha \left(\frac{p - a_{cen}}{1 - a_{cen}} \right)$$

Since we know that all the elastic moduli scale with α , this shows that they all will be linear in p, and go to zero at $p = a_{cen}$. The value of a_{cen} can be calculated exactly (see Appendix C) and turns out to agree with the

constraints counting result:

$$a_{cen} = 2d / z = p^*$$

So the final result for the elastic moduli is

$$C_{ij}(p) = C_{ij}(1)\left(\frac{p - p^*}{1 - p^*}\right)$$

Section 1.8. Effective Medium Theory--CPA Method

The coherent potential approximation (CPA) effective medium theory gives the same result for $C_{ij}(p)$ and p^* as does the static method. The CPA gives more than this, however. As will be seen below, the CPA method gives a self-consistent equation for the effective medium density of states at all frequencies. This effective medium theory was worked out by M.F. Thorpe. The presentation which follows is taken from Feng (1984). This paper may be consulted in Appendix C of this thesis (see Elliot, Krumhansl, and Leath for a general reference on the CPA).

One starts with the Hamiltonian

$$H = H_o + V$$

where

$$H = \sum_i \frac{p_i^2}{2m} + \frac{1}{2}\alpha \sum_{\langle ij \rangle} \left[(\vec{u}_i - \vec{u}_j) \cdot \hat{r}_{ij} \right]^2$$

$$\text{and} \quad V = \frac{1}{2}(\gamma - \alpha) \left[(\vec{u}_1 - \vec{u}_2) \cdot \hat{r}_{12} \right]^2$$

H_o is the Hamiltonian of the system with all bonds present, and V contains the effect of changing the force constant on the bond between sites 1 and 2 from α to γ . We define the Green's function for H_o by:

$$\vec{\vec{P}}_{ij} = \sum_n \left[\frac{\langle o | \vec{u}_i | n \rangle \langle n | \vec{u}_j | o \rangle}{\omega - \omega_n + \omega_o} - \frac{\langle o | \vec{u}_j | n \rangle \langle n | \vec{u}_i | o \rangle}{\omega + \omega_n - \omega_o} \right]$$

where $\{|n\rangle\}$ is a complete set of energy eigenstates. $\overleftrightarrow{G}_{ij}$ is defined similarly for the full Hamiltonian. It should be noted here that i, j run over sites, and $\overleftrightarrow{G}_{ij}$ and $\overleftrightarrow{P}_{ij}$ are d x d matrices for each pair i, j. V can be rewritten in matrix form as

$$\overleftrightarrow{V}_{ij} = (\gamma - \alpha)\, \hat{r}_{12} \hat{r}_{12}\, m_{ij}$$

where

$$m_{ij} = (\delta_{1i}\delta_{1j} + \delta_{2i}\delta_{2j} - \delta_{1i}\delta_{2j} - \delta_{2i}\delta_{1j})$$

It can be shown that $\overleftrightarrow{G}$, $\overleftrightarrow{P}$, and $\overleftrightarrow{V}$ satisfy the Dyson equation which is of the form

$$\overleftrightarrow{G} = \overleftrightarrow{P} + \overleftrightarrow{PVG} \qquad (14)$$

We are only considering a single defect, so that summing over all repeated scatterings from this same bond we can rewrite (14) as

$$\overleftrightarrow{G} = \overleftrightarrow{P} + \overleftrightarrow{PTP}$$

where $\overleftrightarrow{T}$ is called the "t-matrix" (for obvious reasons) and is given by

$$\overleftrightarrow{T}_{ij} = \frac{\gamma - \alpha}{1 - 2(\gamma - \alpha)\, \hat{r}_{12} (\overleftrightarrow{P}_{11} - \overleftrightarrow{P}_{12})\, \hat{r}_{12}}\, \hat{r}_{12} \hat{r}_{12}\, m_{ij}$$

It should be noted that $\overleftrightarrow{T}_{ij}$ has the same matrix <u>form</u> as $\overleftrightarrow{V}_{ij}$, but with a different overall multiplicative factor. The heart of the coherent potential approximation now is setting the <u>average</u> t-matrix equal to zero, allowing α to be renormalized to α_m, the effective medium value:

$$\left\langle \frac{\gamma - \alpha_m}{1 - 2(\gamma - \alpha_m)\hat{r}_{12}(\overleftrightarrow{P}_{11} - \overleftrightarrow{P}_{12})\hat{r}_{12}} \right\rangle = 0 \qquad (15)$$

The physical idea here is that we have somehow eliminated the leading order corrections to our effective medium, defined by (15). The average is again defined as in Section 1.7:

$$\langle h(\gamma) \rangle = \int p(\gamma)\, h(\gamma)\, d\gamma$$

where $p(\gamma)$ is the probability distribution for the values of γ. Using the percolative distribution we obtain the result

$$\frac{p(\alpha - \alpha_m)}{1 - 2(\alpha - \alpha_m)\hat{r}_{12}(\overleftrightarrow{P}_{11} - \overleftrightarrow{P}_{12})\hat{r}_{12}} + \frac{(1-p)(-\alpha_m)}{1 + 2\alpha_m \hat{r}_{12}(\overleftrightarrow{P}_{11} - \overleftrightarrow{P}_{12})\hat{r}_{12}} = 0 \qquad (16)$$

We can use the equation of motion for P_{11}, given by

$$m\omega^2 P_{11} = 1 + \frac{2\alpha_m}{d}\hat{r}_{12}(\overleftrightarrow{P}_{11} - \overleftrightarrow{P}_{12})\hat{r}_{12} \qquad (17)$$

to simplify (16). It should be noted that $\alpha \rightarrow \alpha_m$ in the definition of $\overset{\leftrightarrow}{P}_{ij}$ as well as in the average t-matrix equation. Combining (16) and (17) we obtain finally

$$\alpha\left[\rho + \frac{2d}{z}\left(n\omega^2 P_{11} - 1\right)\right] - \alpha_m\left[1 + \frac{2d}{z}\left(n\omega^2 P_h - 1\right)\right] = 0 \qquad (18)$$

If we let $\omega^2 \rightarrow 0$, one can readily see that (18) becomes

$$\alpha_m = \alpha\left(\frac{\rho - \rho^*}{1 - \rho^*}\right) \quad , \quad \rho^* = \frac{2d}{z}$$

the same result as obtained in Section 1.7. Equation (18) serves as the starting point for the analysis of Chapter 2.

Section 1.9. Conclusions

The original purpose of the work that has been described in Chapter 1 was to attempt to verify the predictions of a simple constraints counting argument for p^*, the point at which the elastic moduli of a central force random network vanish. The data presented in Sections 1.4, 1.5, and 1.6 show clearly that this simple argument works remarkably well. An extra bonus in this work has been the excellent agreement between the numerical results for the elastic moduli and effective medium theory.

I should note at this point that numerical simulations for the bulk and shear modulus of the triangular net and FCC networks were first done by Feng and Sen (1984). Using a potential that was strictly harmonic, they obtained the result $p^* = 0.58$. Their value for p^* is less than ours because in their model pairs of straight bonds could contribute to the elastic energy and so the network could hold together elastically for lower values of p. They essentially did a different problem than we did because their potential was the harmonic approximation to ours. Our work was carried out independently from Feng and Sen.

The application of the constraints counting argument to more realistic models of glasses now seems hopeful. The central force models, while very simple and unrealistic, have the essential physics of the glasses: decreasing average connectivity produces units in a random network that do not contribute to the elastic energy under an applied

external strain. Therefore rigidity percolation, of which these are an example, is a different class of problem from ordinary percolation. Just how different remains to be seen as work progresses. A more realistic model of a glass has been analyzed using numerical simulations, and the results agree quite well with the constraints counting ideas (He 1984). The central force models provide a base for this and further work in this rapidly developing area.

Chapter 2. Effective Medium Theory Vibrational Density of States for Central Forces

Section 2.1. Introduction

The success of effective medium theory in describing the behavior of the elastic moduli in central force random networks led us to see if other applications would be as successful. The values of the elastic moduli essentially give us the small ω^2 behavior of the vibrational density of states (see last section of Appendix C). The CPA-based effective medium theory described in Section 1.8 can give the density of states for all ω^2 under this approximation. The so-called static method of Section 1.7 can also be modified to give this information (Feng 1984 and Appendix C) but it is simpler to use the already existing CPA result. This method will be described in Section 2.3.

The numerical "experimental data" for the vibrational density of states $g(\omega^2)$ with which the CPA theory is to be compared has been obtained using the negative eigenvalue method (Bell 1972, 1976, 1982; Dean 1972), modified for use with large randomly sparse matrices. This method gives $g(\omega^2)$ vs. ω^2 in histogram form. The accuracy of the histogram is limited only by the size of the system and the amount of computer time one wishes to invest. This method will be

described in Section 2.2.

All the work in this chapter was done on the triangular net rather than on the BCC or FCC networks. The reasons for this choice were the following: 1) we can get effectively larger unit cells in two dimensions thus reducing finite size effects, 2) the size of the dynamical matrix is only 2N x 2N instead of 3N x 3N, where N= the number of sites, 3) the number of non-zero elements in the dynamical matrix which actually have to be stored is proportional to the nearest neighbor coordination, and 4) the integrals over the first Brillouin zone which must be done in solving the CPA equation are much cheaper to compute in two as opposed to three dimensions.

Section 2.2. Negative Eigenvalue Method

The following brief description of the standard negative eigenvalue method is drawn from Bell (1982).

We start from the usual eigenvalue equation for ω^2, the phonon frequencies:

$$\underline{D} \cdot \vec{u} = \omega^2 \vec{u}$$

where $\underline{D}$ is the real space dynamical matrix (sometimes called the force constant matrix):

$$D_{ij}^{\alpha\beta} = \begin{cases} -\hat{\delta}_{ij}^{\alpha} \hat{\delta}_{ij}^{\beta} & \text{if } i \neq j, \langle ij \rangle \\ \sum_{\hat{\delta}_{ij}} \hat{\delta}_{ij}^{\alpha} \hat{\delta}_{ij}^{\beta} & \text{if } i = j \\ 0 & \text{otherwise} \end{cases} \qquad (1)$$

$\hat{\delta}_{ij}$ = unit vector from i to j

All masses are equal to unity. We can rewrite (1) as

$$\underline{A} \cdot \vec{u} = 0 \qquad (2)$$

$$\underline{A} \equiv \underline{D} - \omega^2 \underline{I}$$

The eigenvalues of $\underline{A}$ will be equal to those of $\underline{D}$ but shifted downward by an amount $-\omega^2$. Since the eigenvalues of $\underline{D}$ are all non-negative, this implies that the only eigenvalues of $\underline{A}$ which are negative will be those corresponding to eigenvalues of $\underline{D}$ less than ω^2. So the number of vibrational modes with frequency less than ω^2 will just be equal to the number of negative eigenvalues $M(\underline{A})$ of $\underline{A}$. To compute this number without actually having to diagonalize $\underline{A}$ is made possible by the negative eigenvalue theorem.

This theorem in its simplest form relates $M(\underline{A})$ to $M(\underline{A}_1)$ and $M(\underline{A}_2)$, where $\underline{A}_1$ and $\underline{A}_2$ are two smaller matrices related to a partition of $\underline{A}$. We partition $\underline{A}$ (symmetric because $\underline{D}$ is symmetric) in the following way:

$$\underline{A} = \begin{bmatrix} \underline{A}_1 & \underline{C}_1 \\ \underline{C}_1^T & \underline{B}_1 \end{bmatrix} \tag{3}$$

where $\underline{A}$ is n x n, $\underline{A}_1$ is m x m, $\underline{B}_1$ is (n-m) x (n-m), and $\underline{C}_1$ is n x (n-m). The result of the negative eigenvalue theorem is that

$$M(\underline{A}) = M(\underline{A}_1) + M(\underline{A}_2) \tag{4}$$

where

$$\underline{A}_2 = \underline{B}_1 - \underline{C}_1^T \underline{A}_1^{-1} \underline{C}_1$$

We can continue this process with $\underline{A}_2$, eventually giving the result

$$M(\underline{A}) = \sum_{i=1}^{l} M(\underline{A}_i)$$

where we have iterated the partitioning process l times. It is most convenient to choose the next $\underline{A}_i$ to be 1 x 1, so that

$$M(A_i) = 1 \quad \text{if } A_i < 0$$
$$M(A_i) = 0 \quad \text{if } A_i \geq 0$$

Processing the matrix $\underline{A}$ in this way, after n steps (if $\underline{A}$ is n x n) we will have computed $M(\underline{A})$.

In realizing this process on the MSU CYBER 750 computer, one quickly runs into the problem of limited central memory. In symmetric storage mode, which requires N(N+1)/2 words of storage for an N x N matrix, N must be at most about 400 or so. For the triangular net this means one can only compute the density of states for a system of 200 sites or less. By way of contrast, the results for the elastic moduli were obtained on a 440 site network, more than twice as large. A fairly large number of sites is crucial for these density of states computations in order to see the details of the spectrum.

It happily turns out that the matrix $\underline{D}$ is very sparse because we have nearest neighbor forces only and therefore so is $\underline{A}$. Less happily, this sparseness is not predictable in any useful way. One must then store the non-zero elements in

a one dimensional array, with an associated array giving their position in $\underline{A}$ according to some numbering scheme. The numbering arrangement used in this work is illustrated in Figure 23 for a system with 3 sites (N=3) which gives a 6 x 6 dynamical matrix. There are two entries in $\underline{A}$ per neighbor plus two self terms for each degree of freedom, which gives 14 entries per row and there are 2N rows. We only need to store roughly half of the entries because $\underline{A}$ is a symmetric matrix. Therefore the initial storage requirement is approximately 14N for an N site triangular net. This figure of course decreases as we cut bonds. This storage requirement only increases by about 50% at most during a typical computation so that values of N up to 440 can easily be handled. The storage requirement does not go up nearly as much as one might expect, because although each $\underline{A}_i$ has some new non-zero elements in it, the size of the $\underline{A}_i$'s is decreasing as well. These computations are quite long, however, and require a lot of central processor time. But they <u>are</u> possible on the MSU CYBER 750 system. In this method, one essentially trades the "hard" limitation of central memory availability for the "soft" limitation of computing time (and cost).

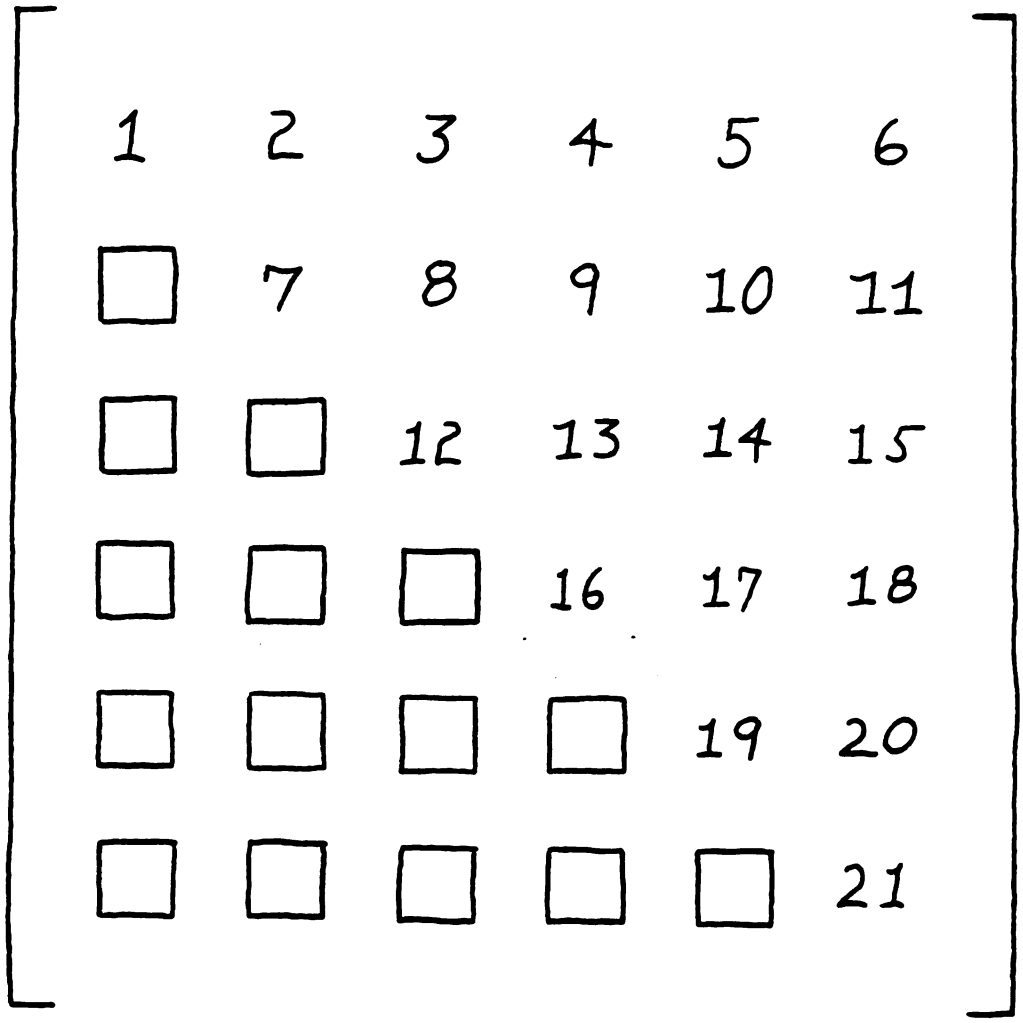

Figure 23. Sparse storage indexing scheme for the negative eigenvalue method

Section 2.3. CPA Equation

The starting point for the calculation of the CPA density of states, $g_c(\omega^2)$, is equation (18) of Section 1.8, which is reproduced here as equation (5):

$$p + p^*(\omega^2 P_{11} - 1) - \alpha_m \left[1 + p^*(\omega^2 P_{11} - 1)\right] = 0$$

where
- p = fraction of bonds present
- α_m = effective force constant, which is complex in general
- ω^2 = phonon frequency squared
- P_h = complex Green's function for the effective medium (all bonds present with force constant α_m)

Equation (5) really consists of two equations, one for the real and one for the imaginary part, since P_{11} is complex and α_m will acquire an imaginary part in general. P_{11} is complex according to the prescription

$$P_{11}(\omega^2) = \frac{1}{Nd} \sum_{K,s} \frac{1}{\omega^2 - \omega_s^2(K)}$$

$$P_{11}^R = \lim_{\eta \to 0} Re\, P_{11}(\omega^2 + i\eta)$$

$$P_{11}^I = \lim_{\eta \to 0} Im\, P_{11}(\omega^2 + i\eta) \qquad (6)$$

$$g_c(\omega^2) = \frac{-1}{\pi} P_{11}^I(\omega^2)$$

For the triangular net d=2 and z=6, so that equation (5) becomes

$$p + \frac{2}{3}(\omega^2 \rho_{11} - 1) - \alpha_m \left[1 + \frac{2}{3}(\omega^2 \rho_{11} - 1) \right] = 0 \qquad (7)$$

What does equation (7) mean? Equation (7) is a pair of coupled equations in the variables α_m^R and α_m^I . They are self-consistent in the sense that we cannot explicitly solve for α_m^R and α_m^I in terms of the parameters of the problem. This is because ρ_{11}^R and ρ_{11}^I depend on the real and imaginary parts of α_m in a very complicated way, involving sums over the first Brillouin zone in k-space. Therefore we must solve them by <u>iteration</u> at every p and ω^2 . In the usual way with the CPA method, α_m becomes energy dependent.

The procedure for solving equation (7) is the following. Starting with a trial solution for α_m^R and α_m^I , we calculate ρ_{11}^R and ρ_{11}^I . This is done by changing the k-space sum of equation (6) into an integral then performing the integration by Gaussian quadratures. The small imaginary part η of the energy is taken to be zero, since for $p \neq 1.0$, α_m^I will be non-zero so that no extra convergence factor is needed. The imaginary part of α_m will broaden the delta functions in the integral in equation (6) into Lorentzians which can be evaluated numerically. One then feeds the values of ρ_{11}^R and ρ_{11}^I into equations (7a) and (7b), and solves this pair of linear equations simultaneously for the new values of α_m^R and α_m^I . Equations (7) are linear since ρ_{11}^R and ρ_{11}^I are taken to be parameters of the equations. One then begins again with these new values, iterating the entire process

until α_n and P_{11} are seen to converge reasonably well. This typically took 5-12 iterations depending on the energy and on the initial guess. The final calculation of $P_{11}^I(\omega^2)$ is saved, with the CPA density of states given by

$$g_c(\omega^2) = \frac{-1}{\pi} P_{11}^I(\omega^2) .$$

Section 2.4. Pure System

A few comments about the properties of the triangular net with all bonds present are appropriate as background for the $p<1.0$ results presented in the next section.

For the harmonic lattice potential given in Section 1.3, we can solve for $\omega^2(\vec{k})$ for the triangular net, with the result:

$$\omega^2(\vec{k}) = \frac{\alpha}{m}\left[F \pm \sqrt{G}\right] \tag{8}$$

$$F = 3 - \cos k_x a - 2\cos\tfrac{1}{2}k_x a \cos\tfrac{\sqrt{3}}{2}k_y a$$

$$G = \left(\cos\tfrac{1}{2}k_x a \cos\tfrac{\sqrt{3}}{2}k_y a - \cos k_x a\right)^2 + 3\sin^2\tfrac{1}{2}k_x a \sin^2\tfrac{\sqrt{3}}{2}k_y a$$

One should recall that $m=1$ and $a=1$ for the pure net, while α_m replaces α when $\omega^2(\vec{k})$ appears in the effective medium Green's functions used in the CPA method. The maximum frequency squared is equal to $6\alpha/m$.

Given this dispersion relation (8), one can easily generate the density of states $g(\omega^2)$ by randomly picking points in k-space and counting how many fall into a given range of ω^2. If enough points are selected (typically about 100,000) the result converges to the correct value. Figure 24 shows the density of states for the triangular net which was generated by this procedure. The four discontinuities in slope labelled on the graph refer to Figure 25, which shows the dispersion relation (8) graphed along the first Brillouin zone path Γ-A-B-Γ defined in Figure 26. Features (1), (3), and (4) clearly arise from local extrema in $\omega^2(\vec{k})$. At $\omega^2 = 4.5$ the lower branch (obtained by always taking the (-) sign

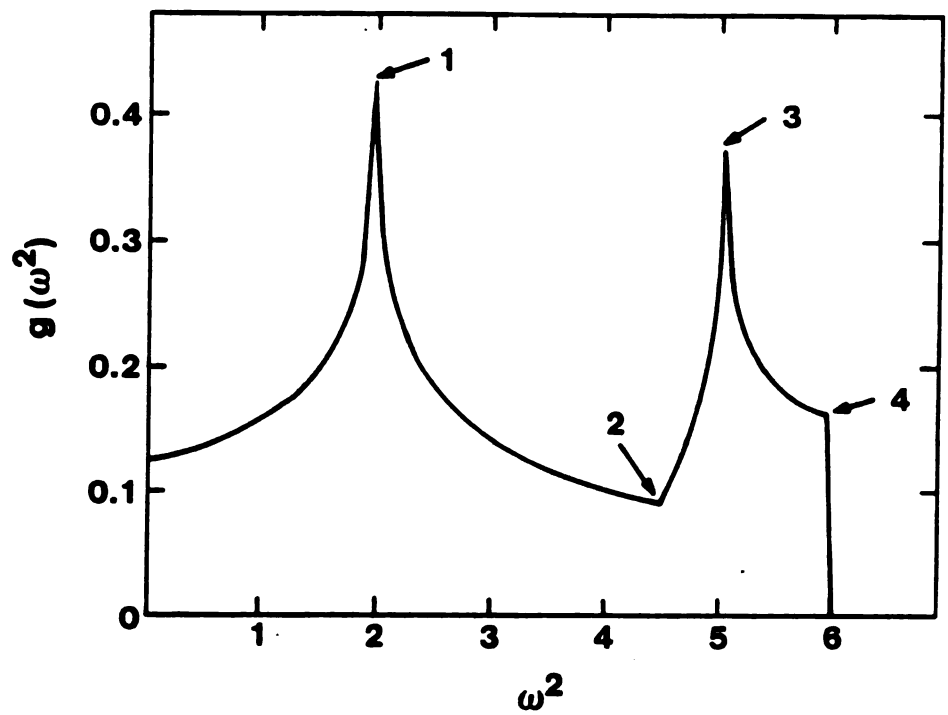

Figure 24. Density of states for the triangular net

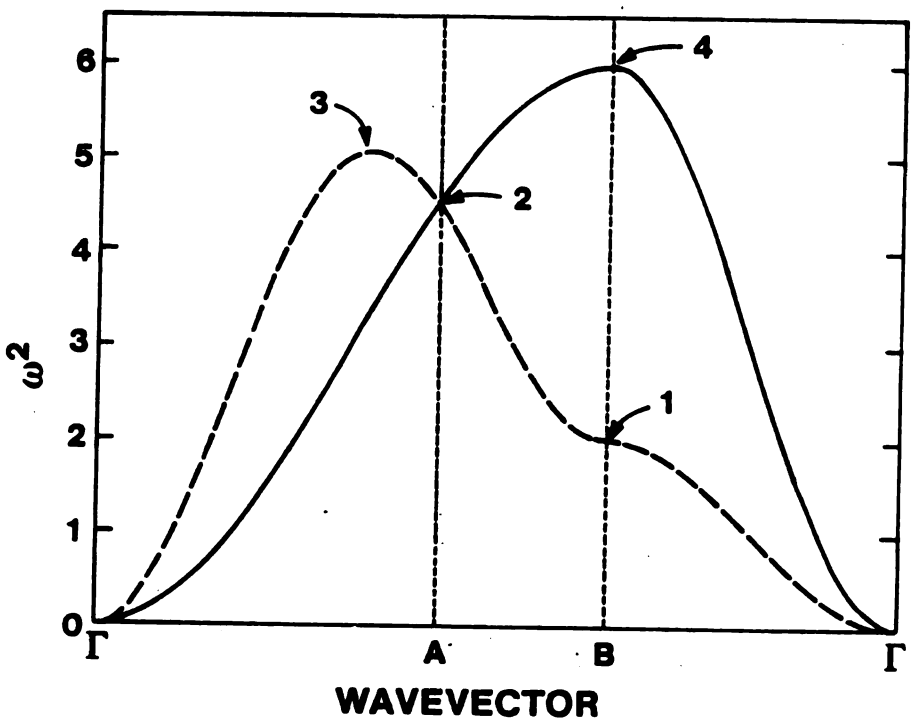

Figure 25. Dispersion relation for the triangular net

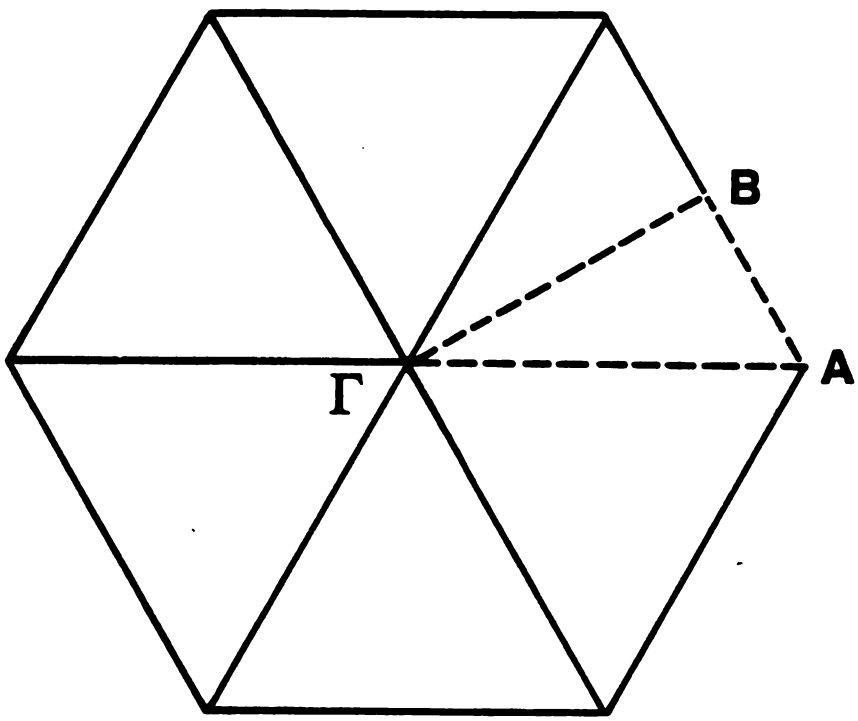

Figure 26. First Brillouin zone for the triangular net

in (8)) has its maximum, not explicitly shown in Figure 25, which gives rise to feature (2).

The fact that $g(\omega^2) \rightarrow$ constant as $\omega^2 \rightarrow 0$ is perhaps a little disconcerting at first if one is used to looking at a three dimensional density of states, but one can easily prove that in d dimensions

$$g(\omega^n) \sim \omega^{d-n} \quad \text{as} \quad \omega^n \rightarrow 0$$

so that $g(\omega^2) \sim$ constant as $\omega^2 \rightarrow 0$ for the triangular net.

Figure 24 then is our starting point. As we remove bonds we will be able to see how $g(\omega^2)$ evolves from its pure system form.

Section 2.5. Results

Choice of values of p

Four values of p, the fraction of nearest neighbor bonds present on the triangular network, have been selected at which to compare the CPA density of states $g_c(\omega^2)$ to the negative eigenvalue method "exact experimental" results. These four values of p are: 1) p=0.85, 2) p=0.70, 3) p=0.50, 4) p=0.20. The first value was chosen to be well above the critical region and close enough to the crystal so that the CPA should do well there if it does well anywhere, and yet far enough from the pure system so that some real differences from the crystal might be seen. Point 2) was chosen to be just above p^* to give a stringent test of the accuracy of the CPA in the critical region. Also, trimming and supertrimming have a fairly large effect at p=0.70, so we desired to see how the density of states divided itself between the rigid "backbone" and supertrimmable pieces which together make up the network. The third value of p investigated is interesting because when 50% of the bonds are present, the triangular network is still connected geometrically but is disconnected elastically. It should be noted that p=0.50 is less than even Feng and Sen's (1984) result for p^*=0.58, so that there is no question about the elastic moduli being zero or not. And finally, point 4) is below p_c for regular connectivity percolation. The network consists of isolated clusters only at p=0.20.

1) p=0.85

Figure 27 shows the two results for the density of states of the triangular network. The dashed line is the CPA result while the histogram with area normalized to 1 is the negative eigenvalue method (NEM) "experimental " result. It should be noted here that all the NEM results are an average over three configurations of a triangular network with 440 sites, in fact the same three used in Section 1.4 for the elastic moduli computations. The agreement between NEM and CPA in Figure 27 at the level of accuracy of the histogram is quite good. One can see the memory of the crystal in the peaks which remain at $\omega^2 = 2$ and 5, while the effect of bond cutting shows in the increase in the small frequency density of states, due to the fact that

$$g(\omega^2) \sim \left(C_{11}^{-1} + C_{44}^{-1}\right) \sim (p-p^*)^{-1} \quad \text{as} \quad \omega^2 \to 0$$

All these features including the decrease of the right band edge are reproduced well by the CPA. The integrated weight under the CPA curve is equal to 1, as it should be.

2) p=0.70

The density of states results for p=0.70 are shown in Figure 28. The agreement between CPA and NEM (untrimmed) is similar to that in the previous figure. The CPA has a very narrow peak that goes up off the graph to about 1.9 and then comes back down to the correct $\omega^2 = 0$ EMT result. The bin size used in the NEM was not small enough to check if this behavior was real or an artifact of the CPA. To get higher

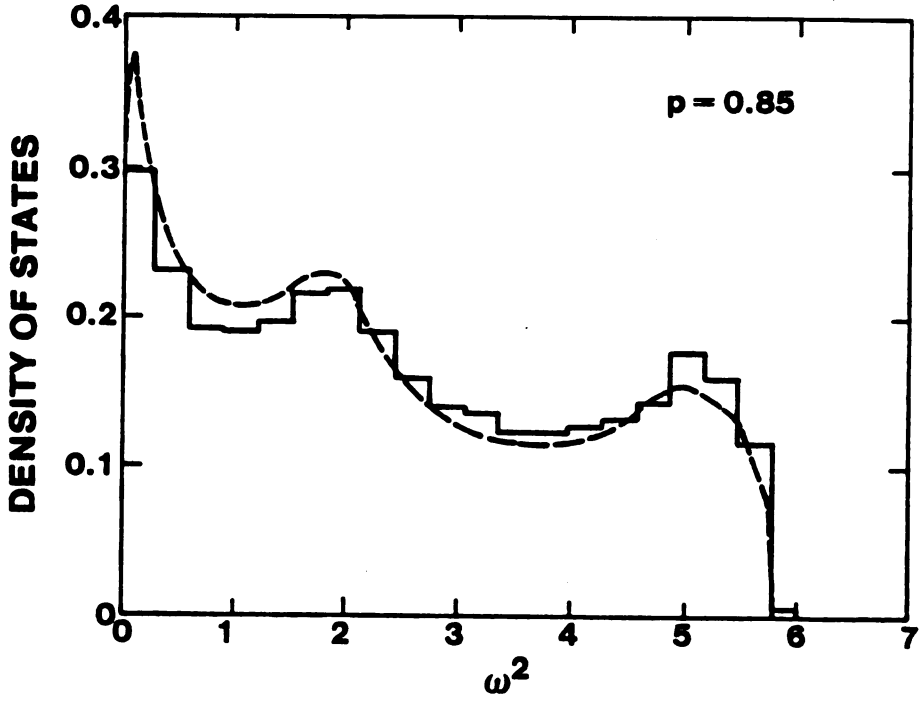

Figure 27. CPA vs. NEM for p = 0.85

accuracy with the NEM, one should go to smaller bin sizes along with larger networks so as to keep the noise level tolerable in each bin. The average number of modes per bin is really what determines the noise in the histogram. In Figure 28 one can clearly see the beginning of the divergence of g(0) as the elastic moduli go to zero. The right band edge continues to come in from the pure system value of 6.0 with the CPA tracking this behavior quite well.

Figure 29 gives the NEM results for the p=0.70 networks as well as these same networks trimmed and supertrimmed. The supertrimmed histogram is normalized to the fraction of sites present in the remaining backbone (about 0.85) with all the zero frequency modes from the missing sites subtracted out. The untrimmed histogram's integrated weight is normalized to 1. The solid lines are the contribution from the "rigid" backbone while the dashed lines show the contribution from the supertrimmed parts. The effect of supertrimming seems to be to deplete $g(\omega^2)$ by about the same amount across all frequencies except for a larger amount at low frequency. This is perhaps not so surprising when we recall that supertrimming can remove sites with all possible connectivities (one to six) so that the complicated pieces of the network removed could support the whole range of allowable frequencies. As a final comment, one should recall the statement made in Section 1.4 that the supertrimming rules we formulated were not complete, but were probably almost so. This was seen clearly to be true in comparing the NEM data for the p=0.70 networks. After supertrimming,

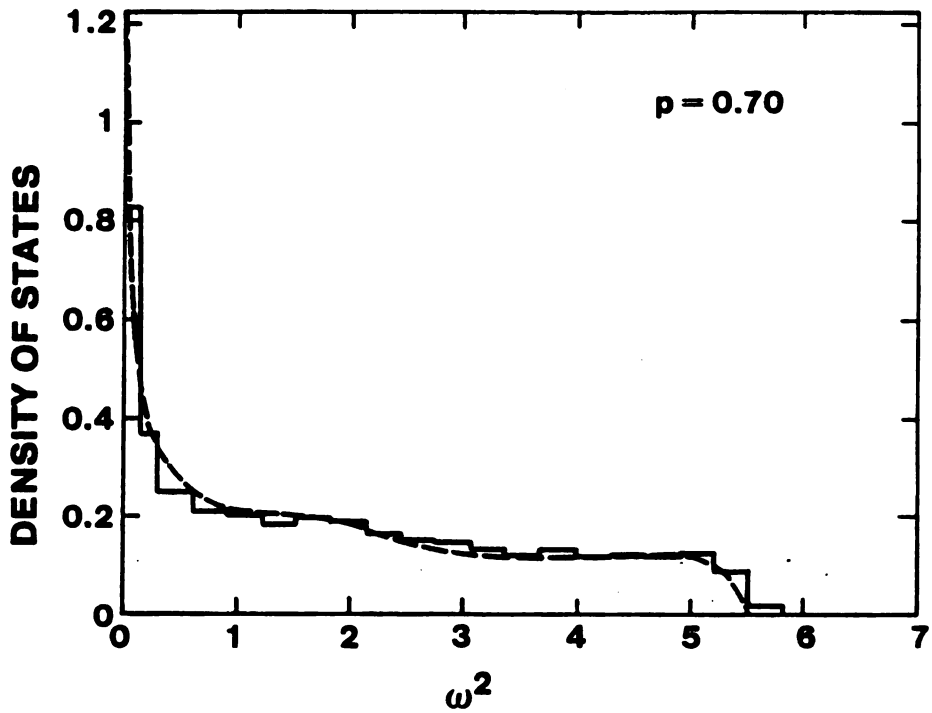

Figure 28. CPA vs. NEM for p = 0.70

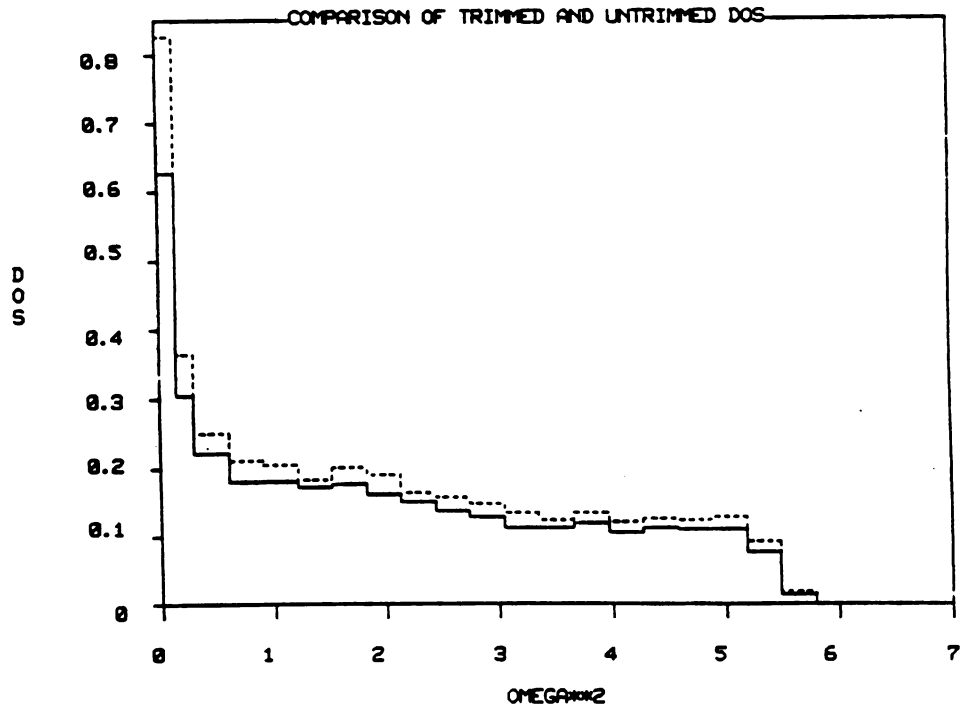

Figure 29. Effect of supertrimming on density of states for p = 0.70

the networks still had a few (one or two) non-trivial zero frequency modes left. Therefore supertrimming, as formulated, does not identify all the possible floppy regions in the network.

3) p=0.50

At p=0.50, the network is connected geometrically but disconnected elastically. Figure 30 presents the CPA and NEM results for this value of p. Again, the overall shape of the NEM density of states is reproduced by the CPA to the level of accuracy of the histogram. The one systematic deviation is at the right band edge where the CPA cuts off before the actual band edge. The CPA shows a gap opening up at small frequencies, with the new band edge at about ω^2 =0.05. The histogram does not have fine enough resolution to see this. It is very difficult to solve the CPA equation for small ω^2, since in this region, to get the band gap, the solution has to jump from the Riemann sheet that was valid above the transition to a new solution sheet in the gap. It is easier to see the small gap in the p=0.20 results. At p=0.50, the value of f, the fraction of zero frequency modes, should be

$$f(p) = 1 - p/p^* = 0.25$$

Therefore the weight in the band should be 0.75. The weight under the CPA density of states comes out to this value, and the NEM results agree. The contribution of the zero frequency

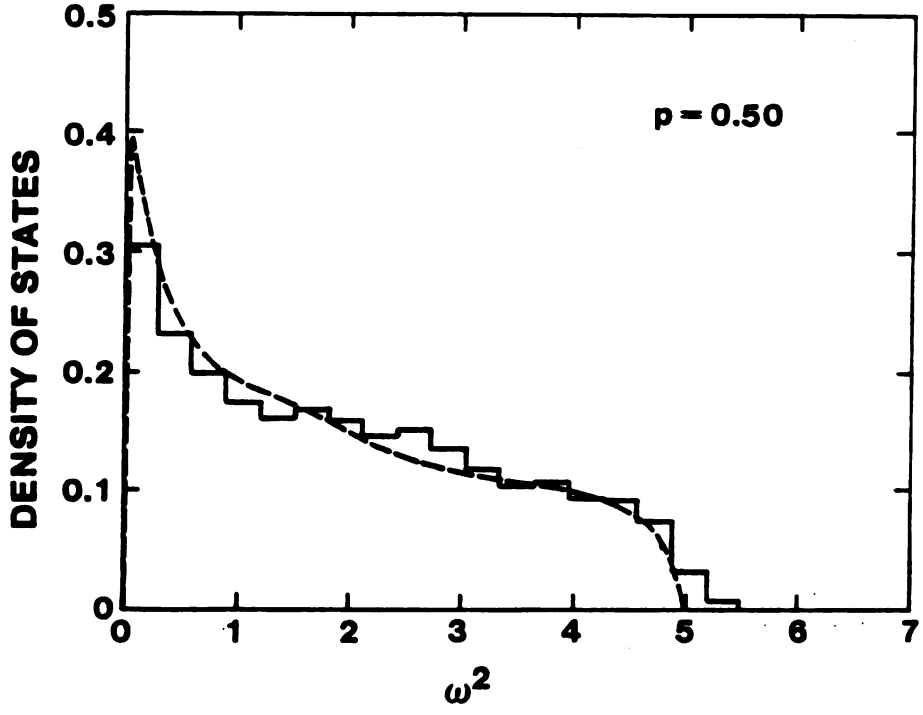

Figure 30. CPA vs. NEM for p = 0.50

modes to the density of states will be a delta function at the origin with weight 0.25. This is not shown in Figure 30. However the CPA does predict this delta function accurately, as will be shown in the p = 0.20 results.

4) p = 0.20

At p = 0.20, the network consists of isolated clusters of sites and bonds, with the most probable clusters containing one or two bonds. This is reflected in the NEM results shown in Figure 31. The large bins at ω^2 = 2.0, 1.5, and 2.5 come from one and two bond clusters respectively. These are isolated cluster modes, and obviously a simple effective medium theory cannot be expected to get these right. However the CPA does not do too badly in reproducing the other features of the density of states. There is a band gap at about ω^2 = 0.3 which the CPA puts at ω^2 = 0.5. The low density of states in the first bin probably shows a Lifshitz (1964) tail, which the real infinite system must have. This is an exponential tail which comes from the band edge into zero. The right band edge has moved in to about ω^2 = 4.3 which the CPA puts at 4.0. The overall shape of the density of states is reproduced fairly well by the CPA. At p = 0.20 the weight at zero frequency is 0.7, so that the weight in the band is 0.3. The weight under the CPA and NEM curves is equal to this value within computational error.

The CPA below p^* predicts a delta function at the origin with weight 1 - p / p^* (see Section 1.2). This comes about in the following way. Assume $\alpha_m \omega^2 \to 0$ for $p < p^*$. Then eq. (5) is

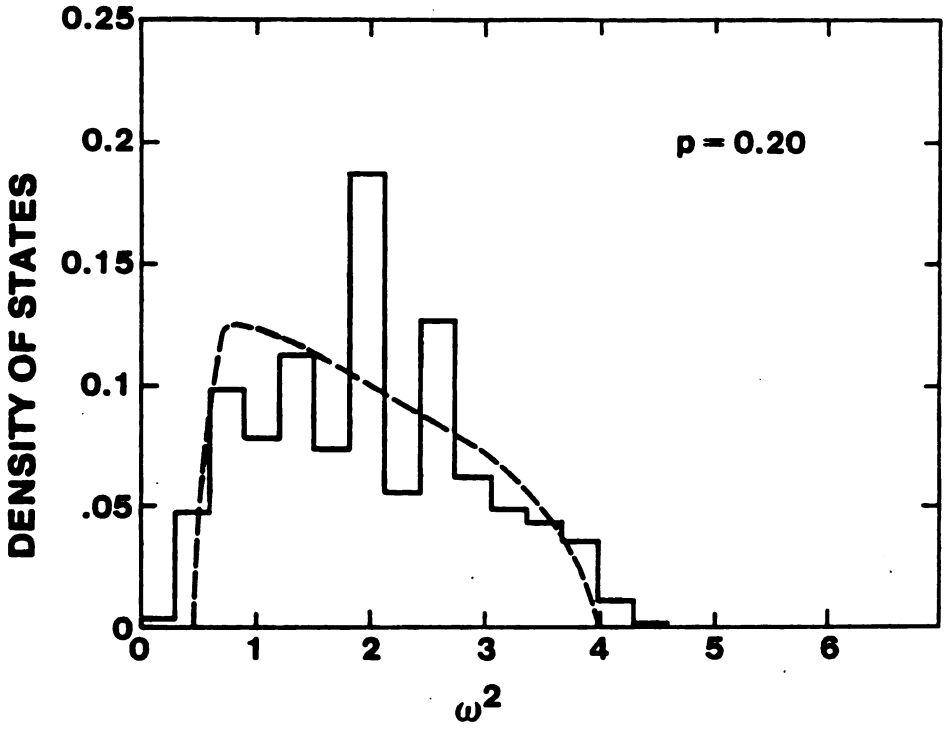

Figure 31. CPA vs. NEM for p = 0.20

$$p + p^*(\omega^2 P_{11} - 1) = 0$$

or

$$P_{11} = (1 - p/p^*)\frac{1}{\omega^2}$$

When we take the imaginary part of P_{11} to get $g_c(\omega^2)$, we get

$$g_c(\omega^2) = \frac{-1}{\pi} \operatorname{Im} P_{11} = (1 - p/p^*)\,\delta(\omega^2)$$

which agrees with constraint counting. In Figure 32 the real and imaginary parts of α_m are graphed as functions of ω^2 for p=0.85 and 0.20. For p=0.20 it is clearly seen that <u>both</u> α_m^R and α_m^I go to zero with ω^2, so that the CPA does predict the right delta function at the origin for $p<p^*$. The graph of α_m for p=0.85 shows the real part going to

$$0.55 = \left.\frac{p-p^*}{1-p^*}\right|_{p=0.85}$$

which is the correct result as was seen in Chapter 1. One should also note on both the p=0.85 and p=0.20 graphs that α_m^I is zero outside the band. This is because the only way $g_c(\omega^2)$ can be non-zero is if P_{11}^I is non-zero, and that will occur only when α_m has a finite imaginary part.

Other features of interest in Figure 32 are the cusp-like behavior of α_m^R (p=0.20) for small frequencies. This is an indication of the change of solution sheets going from in the band to below the band, as was mentioned previously. The solution

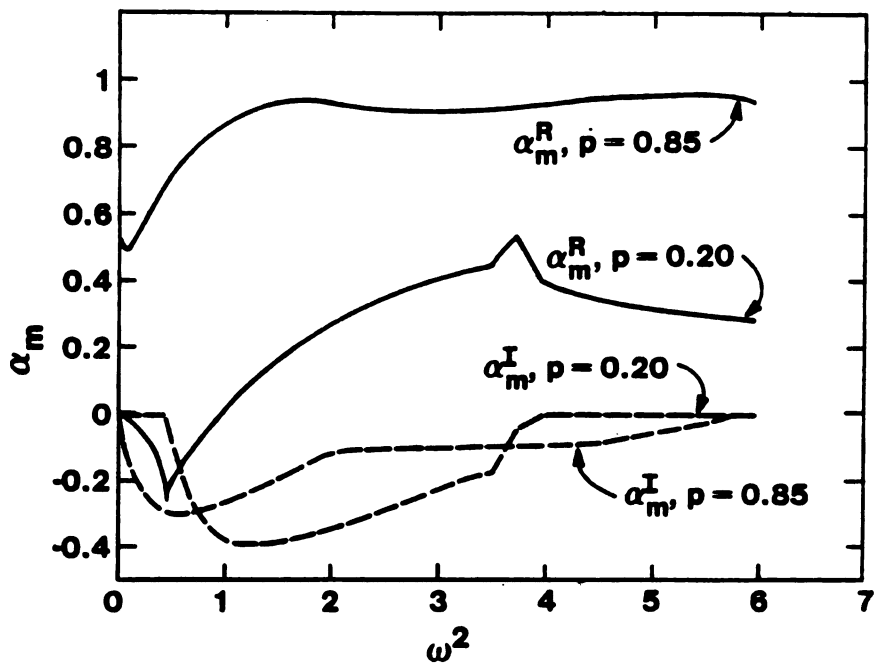

Figure 32. Real and imaginary parts of effective force constant vs. energy

$$\alpha_m^R(\omega^2=0) = \frac{p-p^*}{1-p^*}$$

remains a solution below p^* as well as above, but below p^* it is not the correct solution as it gives elastic behavior at small frequencies. For $p<p^*$, at small frequencies one must carefully search numerically for the other solution which is the correct one in this region. The less prominent cusp-like feature in α_m^R and α_m^I (p=0.20) at $\omega^2=4.0$ is probably at least partially a numerical artifact as it was difficult to solve the CPA equation at the right band edge for $p<p^*$.

Section 2.6. Conclusions

It has been demonstrated that not only does a simple effective medium theory give a good description of the zero frequency elastic properties of nearest neighbor central force random networks, but it also gives a quite good description of the finite frequency behavior as well. This is true over a range of values of p where the network varies from being geometrically and elastically connected to being geometrically connected and elastically disconnected and finally becoming completely disconnected. Band edges and the zero frequency delta functions are also reproduced by the CPA as well as the overall shape of the density of states.

In the next chapter the results of Chapter 1 are extended to longer range central forces with again a spectacular success of effective medium theory. The finite frequency behavior of these systems has not yet been investigated, but it is interesting to speculate that the CPA equation, suitably generalized, might be quite successful in that case as well.

Chapter 3. Rigidity Percolation on Elastic Networks with 1st and 2nd Neighbor Central Forces

Section 3.1. Introduction

In Chapter 1 rigidity percolation was studied on various random networks which had nearest neighbor central forces only. Effective medium theory and constraint counting arguments described the elastic moduli and rigidity threshold very well indeed for these systems. It was of interest to us to see if the same kind of results would be obtained for systems with longer range central forces. Perhaps the success of our theory was due only to the nearest neighbor character of the atomic interactions in our model. Also, since more realistic models of covalent glasses have angle forces, higher neighbor central forces are interesting too because in the right context, a second neighbor central force is not so much different from a nearest neighbor angle force.

The second thrust of this work was to explore some ideas that have appeared recently concerning the universal critical behavior of the ratio of C_{11}/C_{44} as $p \longrightarrow p_c^*$. Bergman (1984) and Schwartz (1984) have shown that in certain models, C_{11}/C_{44} approaches a limiting value as the critical threshold is approached that does not depend on the initial value of the ratio.

Section 3.2 presents the details of the model we studied,

Section 3.3 describes the constraint counting arguments plus numerical results for the fraction of zero frequency modes as a function of p for this model, Section 3.4 derives the effective medium theory we used, Section 3.5 presents the results of numerical simulations for the elastic moduli and ratio and compares these to the effective medium theory, and Section 3.6 draws conclusions from this work.

Section 3.2. Details of the Model

The model we studied was a square net with first and second neighbor Hooke's law springs. The first neighbor force constant was α and the second neighbor force constant was γ. Figure 33 shows a piece of this lattice with all bonds present. The solid lines are first neighbor bonds and the dashed lines are second neighbor bonds. The full potential for this model is

$$V = \frac{1}{2}\alpha \sum_i (l_i - l_1)^2 + \frac{1}{2}\gamma \sum_j (l_j - l_2)^2 \qquad (1)$$

where the sums over i and j respectively are over all first and second neighbor bonds present. First neighbor bonds are present with probability p_1 and second neighbor bonds with probability p_2. It should be noted that p_1 and p_2 are <u>independent</u> probabilities. The phase space for this system is then the p_1-p_2 plane, with $0 \leq p_1, p_2 \leq 1.0$. Figure 34 is a diagram of this phase space. The lines labelled 1,2, and 3 are the three phase space tracks actually used in the various simulations. The three tracks are defined as follows:

$$\begin{aligned} &\text{Track 1:} \quad p_2 = p_1 \\ &\text{Track 2:} \quad p_2 = 2.37p_1 - 1.37 \\ &\text{Track 3:} \quad p_2 = 2.37p_1 \end{aligned} \qquad (2)$$

The reasons for the choice of these three particular tracks are given in Section 3.5.

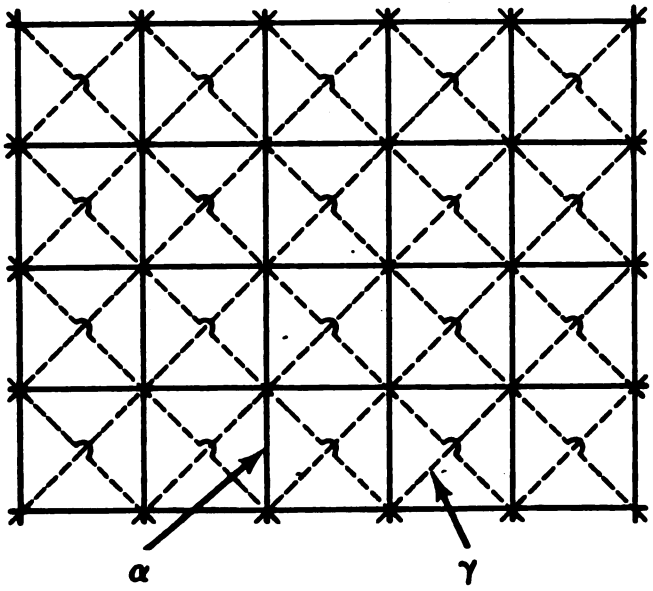

Figure 33. Diagram of square net with first and second neighbor springs

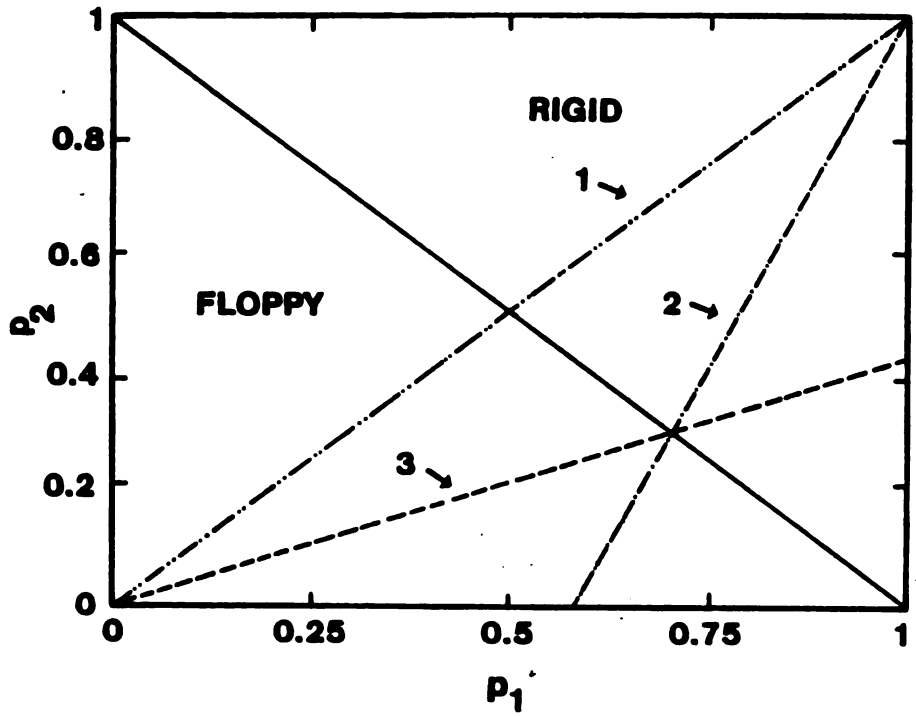

Figure 34. Phase space for square net model

Using the methods described in Chapter 1 we can easily show that the elastic moduli for the pure system are:

$$C_{11} = \alpha + \gamma$$
$$C_{44} = C_{12} = \gamma \qquad (3)$$

Since we still have only central forces, and each point is a center of inversion, C_{44} and C_{12} are related by a Cauchy relation (Love 1944) equating them.

Section 3.3. Constraint Counting and Fraction of Zero Frequency Modes

As in Chapter 1 the fraction of zero frequency modes f is given by

$$f = M_0/dN = \frac{dN - N_c}{dN}$$

$$= 1 - \frac{(N_1 + N_2)}{dN}$$

$$f = 1 - (p_1 + p_2) \qquad (4)$$

where z_1, z_2 are the first and second neighbor coordinations in the pure system and are both equal to four in this case, and N_1 and N_2 are the number of first and second neighbor bonds actually present. The critical line in the p_1-p_2 phase plane is given by f=0 or

$$p_1^* + p_2^* = 1$$

This result is shown as the solid line in Figure 34. Note that equation (4) predicts that f depends only on the sum of p_1 and p_2 and not on their individual values. In fact, if we use $p=\frac{1}{2}(p_1+p_2)$, the actual fraction of all bonds present, we can rewrite (3) as

$$f(p) = 1 - 2p$$

We have done numerical simulations to test the validity of (3). Using the negative eigenvalue method as described in Section 2.2 we have selected values of p_1 and p_2 along tracks 1 and 3 and computed f by counting the number of modes with frequencies

less than some very small number x ($x \lesssim 0.00001$). These results were averaged over three configurations and graphed vs. p. The result for f along tracks 1 and 3 is shown in Figure 35. The straight line is the prediction from equation (5). Note that the agreement between tracks 1 and 3 is almost perfect except for some very small deviations in the critical region around $p^{*}=0.50$, and both separately agree quite well with equation (5). As at least some of the curvature in the critical region is due to finite size effects, we can conclude that the fraction of zero frequency modes is dependent only on the sum p_1+p_2, with only very small fluctuations in the critical region from individual variations in p_1 and p_2.

One final note: the critical line being defined as in (4) implies that p_1^{*} for each of the three tracks will be as given in Table 2.

Table 2. Critical values of p_1^{*} for tracks 1-3

Track	p_1^{*}
1	0.50
2	0.703
3	0.703

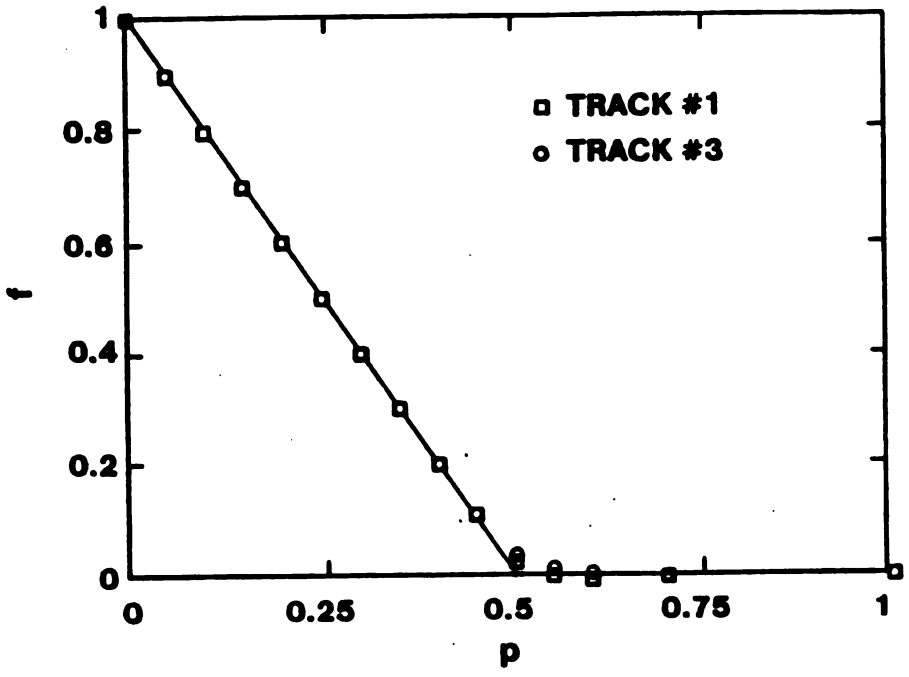

Figure 35. Fraction of zero frequency modes for tracks 1 and 3

Section 3.4. Effective Medium Theory

We use the static method described in Section 1.7 to develop an effective medium theory for our model. Since we have two independent effective force constants, α_m and γ_m, we end up with two equations like equation (13) in 1.7:

$$\alpha_m = \alpha \frac{(\rho_1 - a_1)}{1 - a_1} \tag{6a}$$

$$\gamma_m = \gamma \frac{(\rho_2 - a_2)}{1 - a_2} \tag{6b}$$

where a_1 and a_2 are defined similarly as in Appendix C:

$$a_1 = \frac{2\alpha_m}{N z_1} \sum_{k,\hat{\delta}} Tr\left[\left(1 - e^{i a \vec{k}\cdot\hat{\delta}}\right)\left(\hat{\delta}\hat{\delta}\right) \cdot D^{-1}(\vec{k})\right] \tag{7a}$$

$$a_2 = \frac{2\gamma_m}{N z_2} \sum_{k,\hat{\delta}'} Tr\left[\left(1 - e^{i b \vec{k}\cdot\hat{\delta}'}\right)\left(\hat{\delta}'\hat{\delta}'\right) \cdot D^{-1}(\vec{k})\right] \tag{7b}$$

$\hat{\delta}$ = 1st neighbor unit vectors
$\hat{\delta}'$ = 2nd neighbor unit vectors
a = 1st neighbor distance = 1
b = 2nd neighbor distance = $\sqrt{2}$

$\bar{D}^{-1}(k)$ is the inverse of the dynamical matrix of our model but with α and γ replaced by α_m and γ_m. The dynamical matrix D(k) is easily shown to be

$$D_{xx}(\vec{k}) = 2\alpha_m (1 - \cos k_x a) + 2\gamma_m (1 - \cos k_x a \cos k_y a)$$

$$D_{xy}(\vec{k}) = D_{yx}(\vec{k}) = 2\gamma_m \sin k_x a \sin k_y a$$

$$D_{yy}(\vec{k}) = 2\alpha_m(1-\cos k_y a) + 2\gamma_m(1-\cos k_x a \cos k_y a)$$

The elastic moduli go to zero at $p_1^* = a_1$ and $p_2^* = a_2$, and since the following sum rule is easily proved from (7)

$$a_1 + a_2 = 1 \tag{8}$$

that implies that

$$p_1^* + p_2^* = 1$$

which agrees with the constraint counting result of Section 3.3. The existence of the sum rule (8) means that only a_1 need be independently computed. The definition of a_1 in (7) involves a 1st Brillouin zone summation which can be changed to an integral and evaluated numerically. This double integral cannot be evaluated analytically but instead was computed with a 22 x 22 point Gaussian quadrature. The explicit form of the integral for a_1 is not important but it should be noted that $a_1 = a_1(\gamma_m/\alpha_m)$ only.

To solve equation (6) along a given track, we divide (6b) by (6a) and solve for p_1, eliminating p_2 by the relation (2) of interest and a_2 via the sum rule (8). This gives an equation of the form

$$p_1 = h(\gamma_m/\alpha_m)$$

This is a non-self consistent equation for p_1. We can substitute in values of γ_m/α_m, starting with the initial value of γ/α and continuing until the known critical value of γ_m/α_m is reached. Each of these points give a value of p_1 which can then be substituted back into equations (6) along the calculated value of a_1 to calculate α_m and γ_m thus the elastic moduli via (3). The value of γ_m/α_m at the critical point is known, since on the critical line $p_1^* = a_1$. Thus for a given track p_1^* is known and so

$$\left.\frac{\gamma_m}{\alpha_m}\right|_{\text{critical point}} = a_1^{-1}(p_1^*)$$

Figure 36 shows how the value of C_{11}/C_{44} varies along the critical line. The elastic modulus ratio is simply related to γ_m/α_m by

$$C_{11}/C_{44} = 1 + \left(\frac{\gamma_m}{\alpha_m}\right)^{-1}$$

All of the above theory can be easily generalized to account for an arbitrary number of Hooke's law forces of arbitrary range. If there are z_i bonds from a given site to its ith neighbors, each randomly present with probability p_i, and if we have forces out to the nth neighbor, then equations (6) will be generalized to

$$\alpha_m^i = \alpha^i \frac{(p_i - a_i)}{1 - a_i} \qquad i = 1, n$$

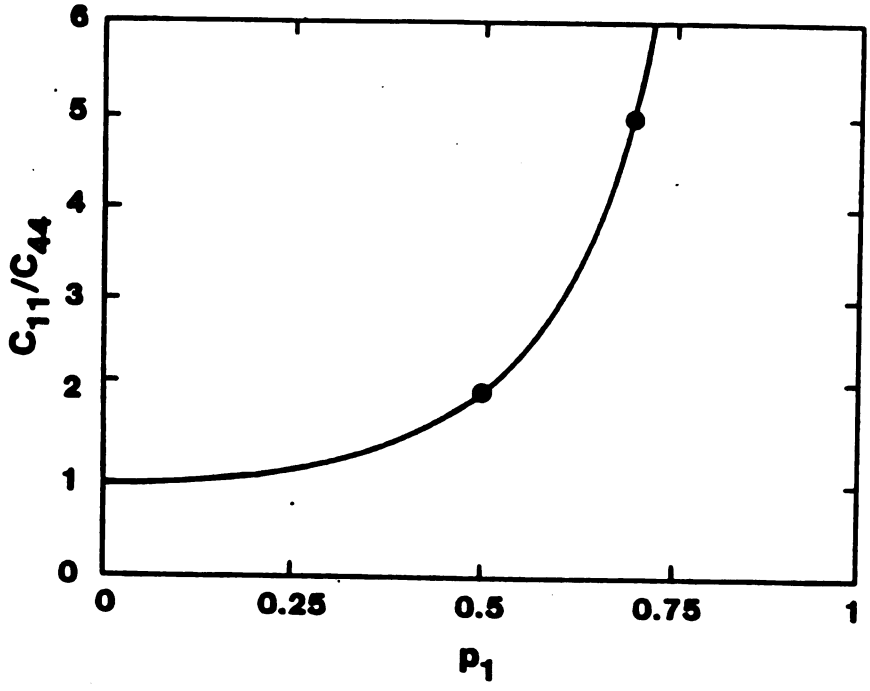

Figure 36. Elastic modulus ratio along critical line (EMT)

$$a_i = \frac{2\alpha_m^i}{N z_i} \sum_{K,\hat{\delta}_i} Tr\left[\left(1 - e^{i b_i \vec{K}\cdot\hat{\delta}_i}\right)\left(\hat{\delta}_i \hat{\delta}_i\right)\cdot \bar{D}^{-1}(K)\right]$$

Sum rule (8) can be generalized to

$$\sum_{i=1}^{n} z_i a_i = 2d$$

so that the critical surface becomes defined by

$$\sum_{i=1}^{n} z_i p_i^* = 2d$$

This also the result which would be obtained from constraint counting in this general case.

Section 3.5. Numerical Simulation Results

We present results for the elastic moduli computed along tracks 1 and 2 in the p_1 - p_2 phase plane. The results are displayed as a function of $p = \frac{1}{2}(p_1 + p_2)$, the total fraction of bonds present. The rigidity threshold is then $p^* = 0.50$ for both tracks. All the simulations were done on 40 x 40 square nets with periodic boundary conditions. Five independent configurations were averaged over for each track. Regular trimming of one and two bond sites was performed, but supertrimming, though possible, was not attempted. The regular trimming took care of the "diode effect" as it did for the triangular net in Section 1.4. All other details of the simulations were as described in Chapter 1.

Three different values of r/d were used for each track. These are given in Table 3 along with the related initial value and critical value of C_{11}/C_{44}.

Figures 37 and 38 present the results for C_{44} and C_{12}. Within the scatter of the simulations they are equal over the whole range of p. As in Chapter 1 this is a surprising result, since inversion symmetry at each site is lost as bonds are cut, so that the Cauchy relation equating C_{44} and C_{12} should become invalid. It is possible that Cauchy's thoerem may be true under more general conditions than have been previously assumed.

Figure 39 shows the simulation results for C_{11} and C_{44} for each track and each value of r/d. The lines shown are from the effective medium theory (EMT) of Section 3.4.

Table 3. γ/α ratios used for numerical simulations

Track	γ/α	$C_{11}/C_{44}^{initial}$	$C_{11}/C_{44}^{critical}$
1	0.25	5.0	2.0
	1.0	2.0	2.0
	2.0	1.5	2.0
2	0.1	11.0	5.0
	0.25	5.0	5.0
	2.5	1.4	5.0

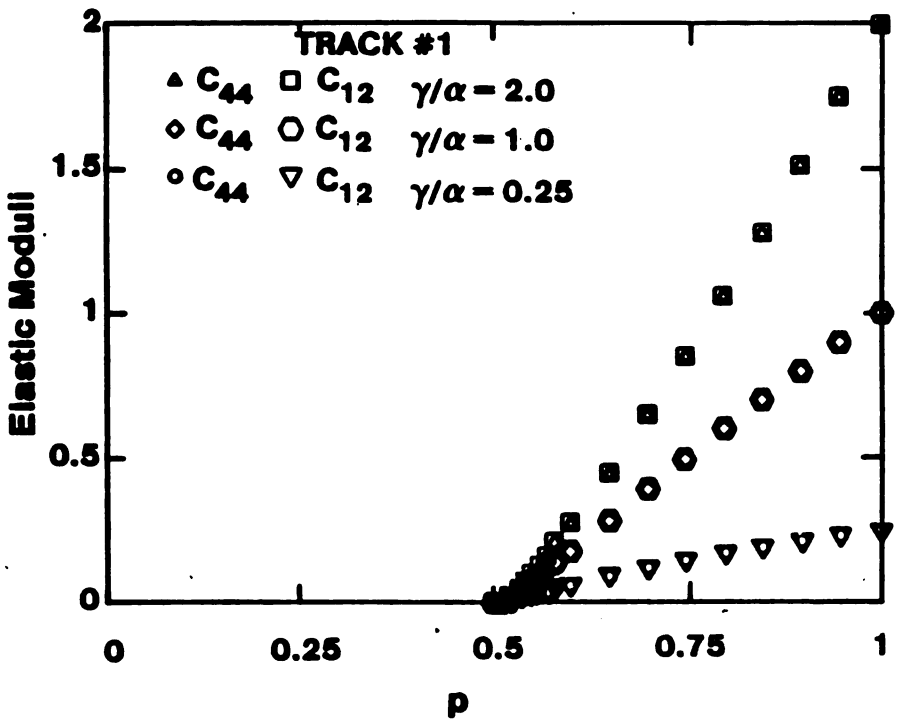

Figure 37. C_{44} and C_{12} vs. p for track 1

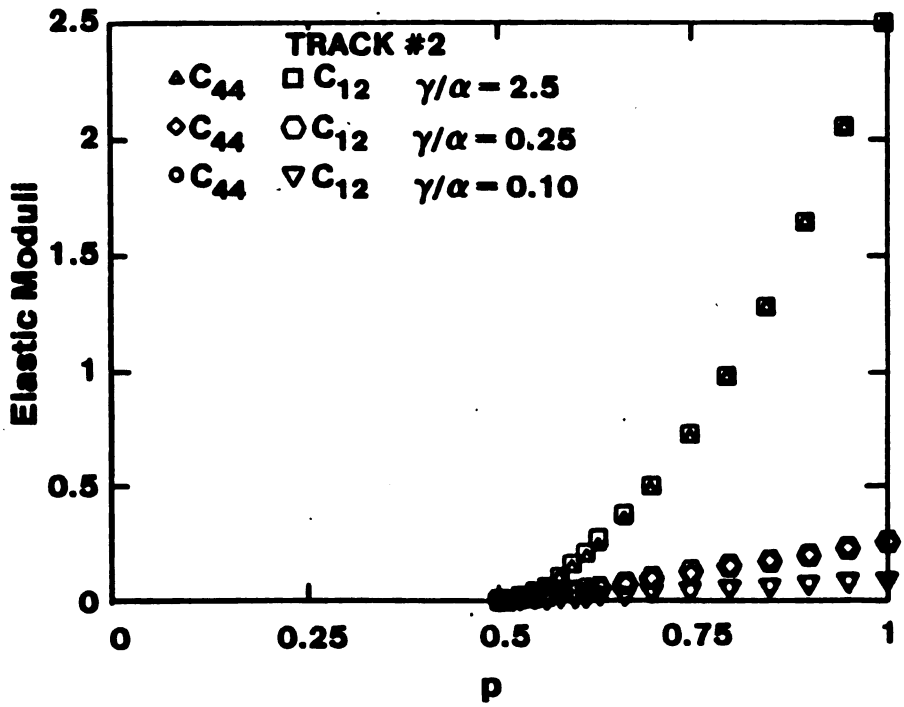

Figure 38. C_{44} and C_{12} vs. p for track 2

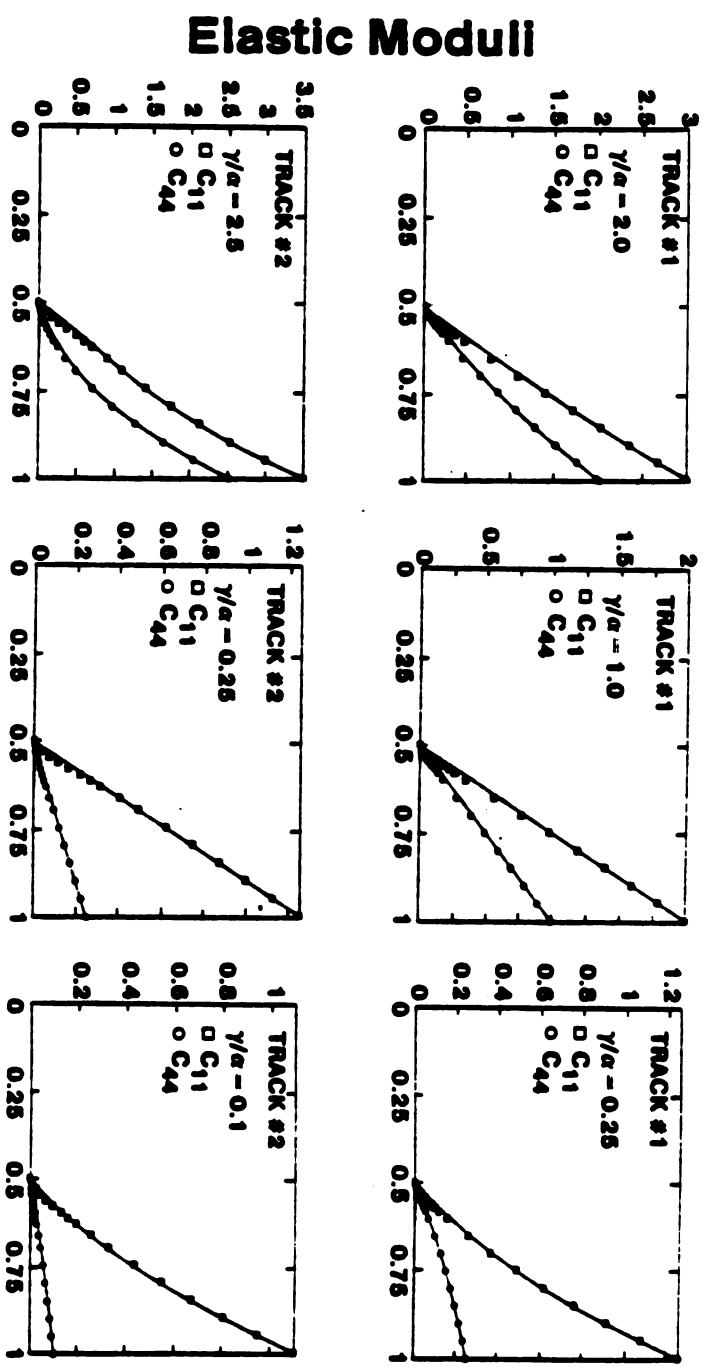

Figure 39. Elastic moduli for tracks 1 and 2

In all six graphs the agreement between EMT and simulation is excellent, and perhaps even more impressively so than in Chapter 1, as the shape of the curves is no longer simply linear. As the rigidity threshold $p^* = 0.5$ is closely approached, however, there are what appear to be very small systematic deviations of the simulations from EMT, with the experimental points being below the EMT curves. These deviations mean that EMT is probably not exact for this model, but since they are very small, EMT describes this sytem quite well indeed.

The EMT predicts that the ratio C_{11}/C_{44} should go to a fixed value at the critical point of any given track which is independent of its initial value. The simulation results for this ratio along tracks 1 and 2 are presented in Figures 40-41 and 42-43 respectively.

For track 1 the EMT predicts the critical value of C_{11}/C_{44} to be 2.0 ($\gamma_m/d_m = 1$). Figure 40 shows the numerical simulation result. Within the numerical scatter, the simulations appear to agree with the EMT result. Figure 41 shows the same result for the ratio but computed on three configurations of a 20 x 20 square net. The finite size effects encountered in using too small systems are clearly seen. For track 1, the difference between Figures 40 and 41 are not that great but the larger system with more configurations clearly is an improvement. One should note that even with the excellent agreement of the moduli with EMT, small finite size errors in the moduli are amplified in the

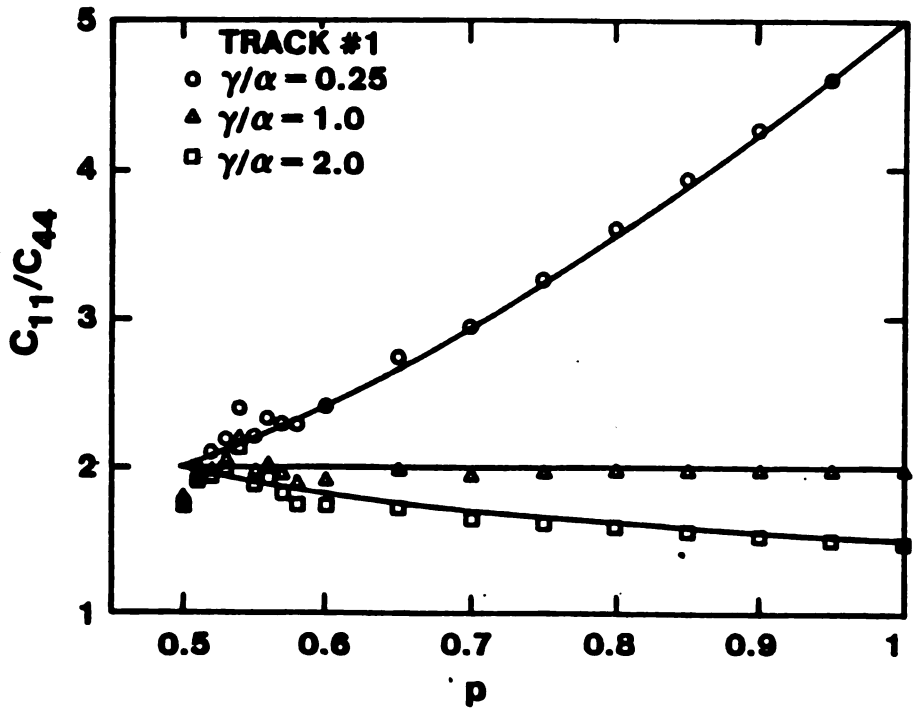

Figure 40. C_{11}/C_{44} flow diagram for track 1

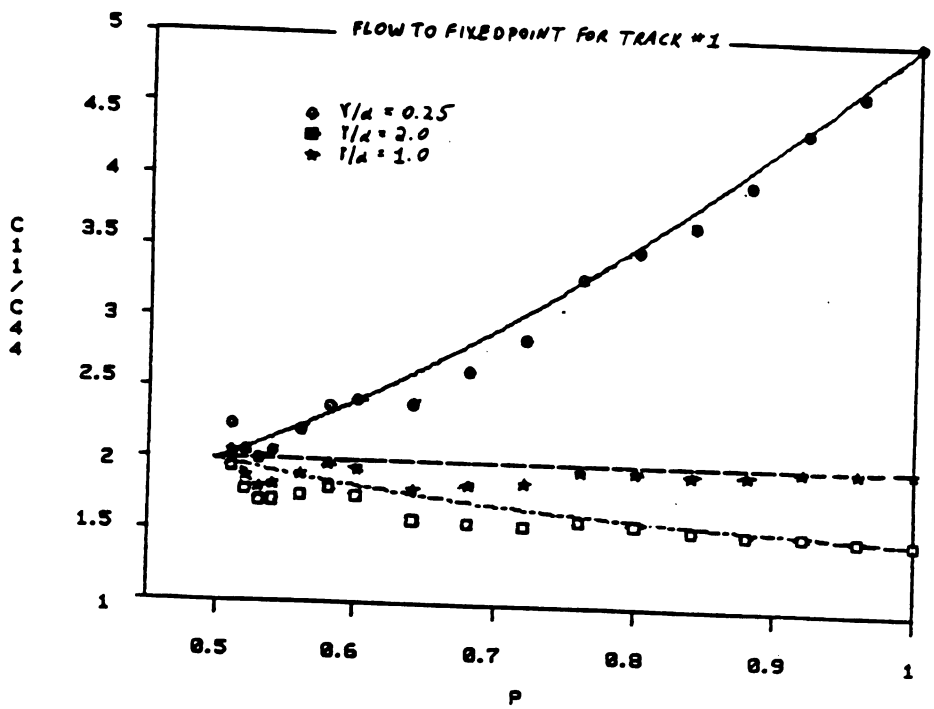

Figure 41. C_{11}/C_{44} flow diagram for track 1 (small system)

ratios because we are dividing two very small numbers.

Finite size noise has a much greater effect for the track 2 results. Figure 42 shows that within numerical scatter, the ratio C_{11}/C_{44} seems to become asymptotically equal to 5.0, in agreement with the EMT result for this track. Figure 43 shows the smae ratios computed using the smaller systems described above. Based on Figure 43 alone, we would have said that there is large numerical disagreement with the EMT result. Because we are computing critical ratios, our results are quite sensitive to finite size noise in the critical region, when the appropriate correlation length becomes of the order of the size of the system.

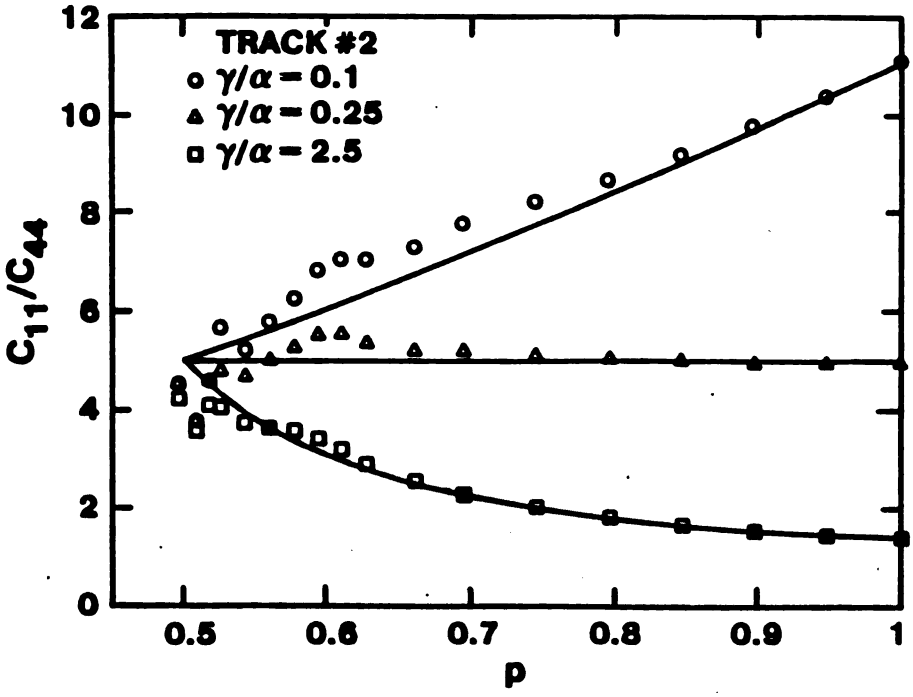

Figure 42. C_{11}/C_{44} flow diagram for track 2

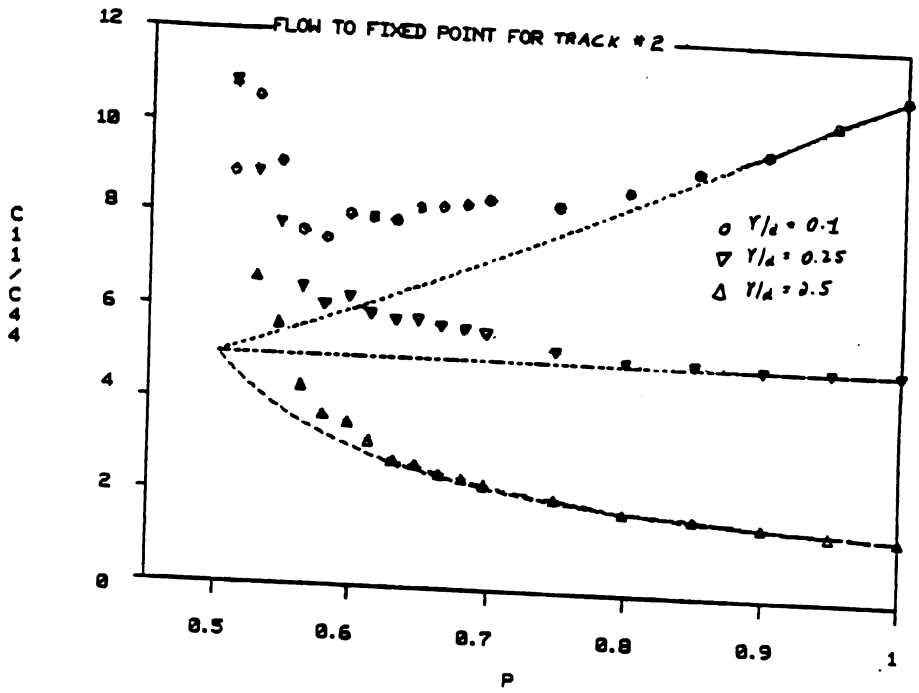

Figure 43. C_{11}/C_{44} flow diagram for track 2 (small system)

Section 3.6. Conclusions

We can conclude that EMT does as well or better for first and second neighbor central forces as it did for nearest neighbor bonds only. This agreement between EMT and simulation is far better than in most other problems where EMT has been applied. The reason for this may be that since the EMT always gets the initial slope right for any problem. and in this case EMT also predicts the critical threshold quite accurately, that with both ends of the curve fixed there is little room for error in between. This of course does not address the question of why the EMT or constraint counting theory prediction for p^* is so accurate.

To properly understand the implications of our result for the critical behavior of the C_{11}/C_{44} ratio, one should recall that there are two different classes of problem whose elastic properties are being studied currently. Class 1 includes those problems where the elastic moduli go to zero only when the system becomes physically disconnected. This includes all percolation problems where enough microscopic forces have been specified so that geometrical connection implies elastic connection. Class 2 is the class of all rigidity percolation problems; that is, all problems in which geometrical connection does not necessarily imply elastic connection. As was stated in Chapter 1, all problems studied in this thesis are Class 2.

Our EMT predicts that C_{11}/C_{44} goes to a fixed point value at the rigidity threshold which does not depend on the initial value of the ratio but does depend on geometry, i.e., the track followed in phase space and thus the critical value of p_1 (see Figure 36). The numerical simulations confirmed this prediction quite well. This is the first and only such finding so far for a class 2 problem, analytical or numerical. Bergman and Kantor (1984) predicted, based on mean field theory and an exactly solvable fractal model for percolation backbones, that the critical value of C_{11}/C_{44} would go to a universal value dependent only on dimension. Our result clearly contradicts this; however, their prediction was really only for class 1 problems. Bergman (1984) showed for a honeycomb lattice class 1 problem that C_{11}/C_{44} did go to a critical value independent of the starting value. However he had no way of varying the geometry of his problem. Schwartz (1984) found the same type of behavior for the Born model, which gives a class 1 problem. Thorpe (1984) showed, using an EMT, for the class 1 problem of randomly punching elliptical holes in an elastic sheet, that the critical value of C_{11}/C_{44} depended on the ratio of the lengths of the semimajor and semiminor axes of the hole. This is the only indication thus far that Bergman and Kantor's prediction might be incorrect for a class 1 problem. There are no numerical results as of yet for different geometries of class 1 problems that would support or contradict their prediction. Feng et al. (1984) confirmed

Bergman's (1984) result for the critical exponent of C_{11} by doing simulations on a square net, but gave no results for C_{11}/C_{44} since they apparently did not compute C_{44}. Finally, the node-link picture developed by Kantor (1984) for class 1 problems assumes that the elastic properties of a lattice will become isotropic (i.e., $C_{11}-C_{12}=2C_{44}$) as the critical threshold is approached. There is no good numerical or analytical work for class 1 problems to support or deny this assertion thus far. For the class 2 problem studied in this chapter, the square net does <u>not</u> become isotropic at at $p^* = 0.5$ except perhaps at one isolated point along the critical line. The EMT would predict this point to be $p_1 = 0.6$, $p_2 = 0.4$, an isolated point of no apparent significance.

These questions of the universality of the ratios of critical amplitudes and of isotropy may turn out to be another area in which clear distinctions between ordinary connectivity percolation (class 1) and rigidity percolation (class 2) can be made.

APPENDICES

APPENDIX A

APPENDIX A

Trimming and Supertrimming Rules for Central Force Networks

The distinction between trimming and supertrimming is made clear by noting that trimming involves single sites only. Every other kind of removable unit (denoted a floppy unit) is classified under supertrimming.

The complete set of rules for determining whether a site is trimmable or not are summarized in the following statement:

> A single site in a central force network is trimmable if, in d dimensions, it is connected to the rest of the network by d or fewer bonds.

The justification is clear: any mass point has d degrees of freedom, so it can always satisfy d or fewer constraints, a bond being a single constraint in this case.

Units which are supertrimmable can be classified according to the type and number of their connections to the rest of the network. A connection by a single bond we call type 1, with the number of these given by r_1. A connection by a pin joint we call type 2, with the number of these given by r_2. Figure 44 shows an example of both types of connection for the triangular net.

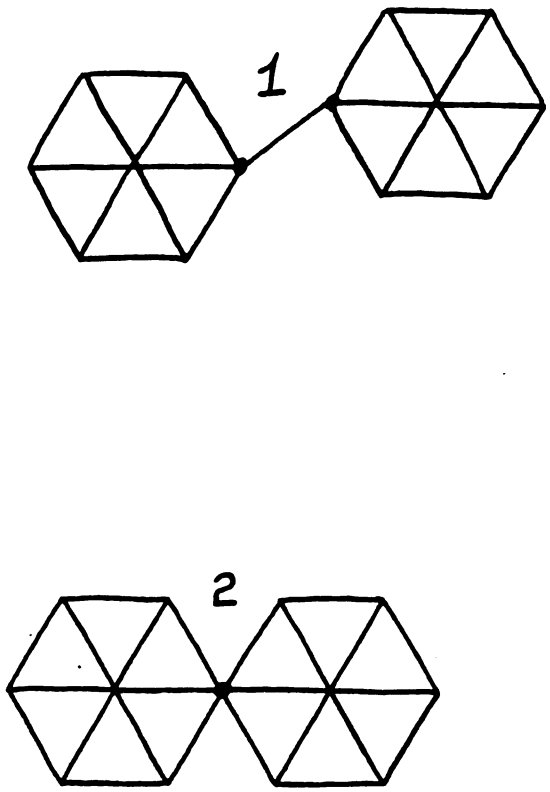

Figure 44. Two types of connections between floppy units and the rest of the network

It is important to realize that type 1 connections quench one degree of freedom of the attached floppy unit while type 2 connections quench two floppy degrees of freedom. Therefore in two dimensions, which is really the only case of interest as far as supertrimming goes, the rule to determine whether a given unit can be supertrimmed or not is:

if $r_1 + 2r_2 \leq 3$	supertrim
if $r_1 + 2r_2 > 3$	cannot supertrim

Three is the number of degrees of freedom of any extended body in two dimensions--two translational and one rotational. Note that $r_1 + 2r_2 > 3$ for a given unit does not necessarily mean that the unit is rigid. There can be internal floppy modes which still allow the unit to be removed. That is why trimming and supertrimming as formulated are incomplete. As these internal floppy modes can be extremely complicated, we have been unable to rigorously identify higher order rules.

APPENDIX B

APPENDIX B

Extrapolation Technique for Elastic Energy Relaxation

Empirically we found that as a network relaxed the elastic modulus $C^{(n)}$ near the final stages n of relaxation obeyed the asymptotic form

$$C^{(n)} = C^{(\infty)} + a\,b^{-n}$$

where $a > 0$, $b > 1$, and b itself was slowly decreasing with n but at a rate <u>much</u> slower than that of $C^{(n)}$. Each step in n really represents 50-100 actual relaxations per site. Call this a <u>large</u> relaxation step. If N of these large steps were used at a given value of p, then by fitting the exponential form above to $C^{(N-2)}$, $C^{(N-1)}$, and $C^{(N)}$, we can solve for $C^{(\infty)}$ to get

$$C^{(\infty)} = \frac{C^{(N)}C^{(N-2)} - \left(C^{(N-1)}\right)^2}{C^{(N)} - 2C^{(N-1)} + C^{(N-2)}}$$

$C^{(\infty)}$ will only be an upper bound, however, since the extrapolation technique assumes b constant while in fact the slow decrease in the value of b will result in a final

correctly relaxed value of the elastic modulus that is somewhat smaller than $C^{(\infty)}$. In effect the extrapolation technique is just a cheap way of getting several thousand more small relaxation steps. Table 4 gives an example where the extrapolated modulus can be compared with actual further relaxation steps. This data is taken from a BCC computation for the shear modulus, p=0.77.

Table 4. Extrapolation vs. relaxation

No. of small relaxation steps	Value of modulus before extrapolation	Value after
800	0.0745	0.0732
4800	0.0736	0.0702

APPENDIX C

APPENDIX C

EFFECTIVE MEDIUM THEORY OF PERCOLATION ON CENTRAL FORCE ELASTIC NETWORKS

SHECHAO FENG[*] *and M. F. THORPE*[**]

Schlumberger-Doll Research
P.O. Box 307
Ridgefield, CT 06877

E. GARBOCZI

Department of Physics and Astronomy
Michigan State University
East Lansing, MI 48824

Abstract

We show that effective medium theory gives an excellent description of regular lattices when nearest neighbor central force springs are present with probability p. Effective medium theory shows that all the elastic constants go to zero at $p_{cen} = d\ p_c$ where d is the dimension and p_c is the effective medium estimate of the ordinary percolation threshold.

[*] Present address: Department of Physics, Harvard University, Cambridge, MA 02138

[**] Permanent address: Department of Physics and Astronomy, Michigan State University, East Lansing, MI 48824

1. INTRODUCTION

There has been considerable interest in the elastic properties of random systems recently[1-4]. While much of this attention has focused on the critical properties of the random elastic network as it breaks up, it is of considerable interest to describe the overall behavior. We focus our attension in this paper on the central force elastic percolation model.[1] We show that the simplest effective medium theories give excellent agreement with numerical simulations for most values of p, the bond occupation probability, except for a very small range of values of p near p_{cen}, on both the triangular network and on the f.c.c. lattice.

Although it is unlikely that the present model will apply directly to any real physical system, it is an important one as it is the simplest member of a general class of models. These models are made up of units that can be connected but still transmit no elastic restoring forces. In the present case the units are bonds and a pair of two and just two connected bonds form a "free hinge" as there are no angular forces. The whole network has finite elasticity for high values of p because the high connectivity "locks" all the free hinges. As bonds are removed from the pure system, the local floppy regions are created which eventually prevent the rigid regions (i.e. the parts of the network that have finite elasticity) from percolating and the system loses its elasticity. Thus the breakup of the system is determined by rigidity percolation and not ordinary connectivity percolation.

The most important physical manifestation of this phenomenon is in the covalent random networks [5] where its local movement is not a free hinge but the dihedral angle associated with three connected bonds. The energy required to change the dihedral angle is small compared to that needed to change the bond lengths and bond angles, so it is reasonable to neglect it as a first approximation. This leads to a division of covalent random networks into low co-ordinated polymeric glasses and high co-ordinated amorphous solids.[5]

The other class of models for the elastic percolation phenomenon[2,3,4] involve specifying a sufficient number of microscopic forces so that all connected parts of the lattice are rigid by themselves and the elastic percolation transition occurs at the ordinary percolation threshold p_c, albeit with different exponents.[2,3,4]

The system under consideration is made up of Hooke springs connecting nearest neighbor sites i,j to give a potential

$$V = \frac{\alpha}{2} \sum_{<ij>} [(\bar{u}_i - \bar{u}_j)\cdot\hat{r}_{ij}]^2 p_{ij} \qquad (1)$$

where the angular brackets denote a sum over nearest neighbor pairs which are connected by springs with spring constant α and p_{ij} is a random variable that is associated with each bond and is 0, 1 with probability 1-p, p. The $\bar{u}_i$ are the displacements from equilibrium and $\hat{r}_{ij}$ is a unit vector connecting nearest neighbor

pairs in equilibrium.

In the next section we show how a constraints counting argument can be used to give an estimate of p_{cen} at which the elastic constants of the system vanish. In section 3 and 4 we develop effective medium theories for the elastic constants for $p > p_{cen}$ from two different viewpoints, both of which lead to the same result. The first one is a direct generalization of the method developed in the study of electrical condution near percolation threshold, and the second one applies the coherent potential approximation to the present problem.

2. CONSTRAINTS METHOD

The simplest way to estimate where the transition takes place is to use a constraints argument[5]. When p is small, the system consists of disconnected pieces and hence has many zero frequency modes whose number is given by the number of degrees of freedom (dN) minus the number of constraints ($\frac{1}{2}$zNp). Thus, the effective medium estimate of the fraction f of zero frequency modes is given by

$$f = (dN - \frac{1}{2}zNp)/dN$$

$$= 1 - \frac{zp}{2d} \qquad (2)$$

so that f goes to zero at $p_{cen} = 2d/z$.

Next consider comparison of this result in the numerical simulation. We have computed f numerically for a 168 atom triangular network (see inset in figure 1) and a 108 atom f.c.c lattice (see inset in figure 2). Both lattices had periodic boundary conditions and f was obtained by directly diagonalizing the dynamical matrix formed from (1) and counting the number of modes with eigenvalues of zero. It can be seen that equation (2) describes the results well except near p_{cen} where the very small deviations from (2) are due to a combination of finite size and critical effects.

A similar constraint counting argument for one, rather than d, degrees of freedom per site, which is the case for the electrical conduction problem, leads to the effective medium estimate for the ordinary percolation (i.e. the connectivity problem)[6] of $p_c = 2/z$ and hence

$$p_{cen} = d\, p_c \qquad (3)$$

The transition described here takes place well before ordinary percolation occurs because many connections in the network produce no elastic restoring force[1]. A simple example is shown in figure 3. Configurations like this correspond to one example of the floppy regions.[5]

3. STATIC METHOD

For $p > p_{con}$, it is of interest to develop a mean field theory for the elastic constants. We have done this in two ways; both of which lead to the same result. The one that is simpler conceptually is to adapt an argument used by Kirkpatrick[6] for the electrical resistor network. Suppose a uniform stress (uniaxial, hydrostatic, etc.) is applied to a lattice where all the springs are α_m and that the atoms labeled 1, 2 in figure 4 have a relative displacement, along $\hat{r}_{12}$ of δu_m. Now substitute a single "wrong bond" α as shown in figure 4 and imagine an extra external force f applied to 1 and 2 as shown to restore 1 and 2 to their positions before α was substituted for α_m. It is then easily seen that f should be:

$$f = \delta u_m(\alpha_m - \alpha) \tag{4}$$

From the superposition principle, the relative displacement δu between 1 and 2 induced by f when the system is unstressed is the same as the extra displacement between 1 and 2 when there is an applied uniform strain δu_m but no f. Then δu is the "fluctuation" in relative displacement of 1,2 due to the introduction of the wrong bond α. The relation between f and δu can be obtained in the following way. If the force f is applied to 1, 2 when all the springs are α_m, there will be an effective spring constant $\alpha_{eff} = \alpha_m/a^*$ where $0 < a^* < 1$ takes account of all the connections between 1, 2 including the direct one in this uniform system. We will calculate a^* later, but for now treat it as a known constant. If the α_m spring between 1 and 2 is removed, then the new effective spring constant α'_m between 1, 2 is

$$\alpha'_m = \alpha_m/a^* - \alpha_m \tag{5}$$

as shown in figure 4. If α is added in parallel to α'_m and the force f applied, then the relative displacement δu of 1 and 2 is given by

$$f = \delta u(\alpha'_m + \alpha) \tag{6}$$

or

$$\delta u = \delta u_m(\alpha_m - \alpha)/(\alpha_m/a^* - \alpha_m + \alpha) \tag{7}$$

The effective medium result is obtained by choosing α_m so that the average value $\langle \delta u \rangle$ of δu is zero to give

$$\left\langle \frac{\alpha_m - \alpha}{\alpha_m/a^* - \alpha_m + \alpha} \right\rangle = 0 \tag{8}$$

For a distribution $P(\alpha)$ of spring constants, this leads to

$$\int \frac{P(\alpha)d\alpha}{1 - a^*(1 - \alpha/\alpha_m)} = 1 \tag{9}$$

For the present case of interest $P(\alpha') = p\delta(\alpha - \alpha') + (1 - p)\,\delta(\alpha')$ gives

$$\frac{\alpha_m}{\alpha} = \frac{p - a^*}{1 - a^*} \tag{10}$$

which goes to zero when $p_{con} = a^*$.

The quantity a^* is obtained for the perfect lattice as follows. The force $\bar{F}_i$ on the atom i is given by

$$\bar{F}_i = -\frac{\partial V}{\partial \bar{u}_i} = -\sum_j \bar{D}_{ij}\cdot\bar{u}_j \tag{11}$$

where

$$\bar{D}_{ij} = \begin{cases} -\alpha_m \hat{r}_{ij}\hat{r}_{ij} & j \neq i \\ \alpha_m \sum_{j\neq i} \hat{r}_{ij}\hat{r}_{ij} & j = i \end{cases} \tag{12}$$

These equations can be inverted by Fourier transformation to give

$$\bar{u}_k = -\bar{D}^{-1}(\bar{k})\cdot\bar{F}_k \tag{13}$$

where $\bar{D}(\bar{k})$ is the dxd dynamical matrix for a Bravais lattice, and $\bar{F}_k$ and $\bar{u}_k$ are the Fourier transforms of the $\bar{F}_i$ and $\bar{u}_i$ respectively.

$$\bar{D}(\bar{k}) = \sum_{ij}\bar{D}_{ij}\exp[i\bar{k}(\bar{r}_j - \bar{r}_i)]$$

$$= \alpha_m \sum_{\delta}[1 - \exp(ia\bar{k}\cdot\hat{\delta})]\hat{\delta}\hat{\delta} \tag{14}$$

where $\hat{\delta}$ is a unit vector in the direction of one of the z nearest neighbors and a is the nearest neighbor separation. Putting $\bar{F}_j = f\,\hat{r}_{12}(\delta_{j1} - \delta_{j2})$, the negative of the

externally applied force as shown in figure 4, we find that

$$\bar{u}_2 - \bar{u}_1 = \frac{f}{N} \sum_{\bar{k}} [2 - \exp(ia\bar{k}\cdot\hat{r}_{12}) - \exp(-ia\bar{k}\cdot\hat{r}_{12})]\bar{D}^{-1}(\bar{k})\cdot\hat{r}_{12} \tag{15}$$

which defines

$$a^* = \frac{\alpha_m}{N} \sum_{\bar{k}} [2 - \exp(ia\bar{k}\cdot\hat{r}_{12}) - \exp(-ia\bar{k}\cdot\hat{r}_{12})]\hat{r}_{12}\cdot\bar{D}^{-1}(\bar{k})\cdot\hat{r}_{12} \tag{16}$$

As all bonds are equivalent, we can replace $\hat{r}_{12}$ by any of the nearest neighbor bonds $\hat{\delta}$, sum over all nearest neighbor bonds and divide by z to give

$$a^* = \frac{2\alpha_m}{Nz} \sum_{k\delta} \mathrm{Tr}[(1 - \exp(ia\bar{k}\cdot\hat{\delta}))(\hat{\delta}\hat{\delta})\cdot\bar{D}^{-1}(\bar{k})]$$

$$= \frac{2}{Nz} \sum_{\bar{k}} \mathrm{Tr}(1) = \frac{2d}{z} = p_{cen} \tag{17}$$

Thus, the result (11) can be written[7,8] as

$$\frac{\alpha_m}{\alpha} = \frac{p - p_{cen}}{1 - p_{cen}} \tag{18}$$

Since all the elastic constants C_{ij} of the network are linear functions of α_m only, we conclude that they all go to zero linearly at p_{cen}, and any ratio of two elastic constants is independent of p. In particular the ratio of the bulk modulus to the shear modulus of the triangular network is <u>always</u> 2.

Next consider comparison of this result with numerical simulation. The straight lines from eqation (18) are plotted in figures 1 and 2 for the triangular and the f.c.c. lattices and show excellent agreement with simulations except for a very small critical region near p_{cen}. Such close agreement between simulations and effective medium theories is rare although it does occur for the conductivity problem[6] in 2d. The deviations are larger in 3d for the conductivity problem[6] than in the results for springs in figures 1 and 2. Indeed 2d/z appears to be a <u>superior</u> estimate for p_{cen} than 2/z is for p_c. This is particularly apparent in comparing the results for the f.c.c. lattice in this paper and those in ref. 6. In general we would expect effective medium theories to do better in higher dimensons.

The numerical simulations were done by removing bonds at random in a lattice with

periodic boundary conditions, imposing an appropriate external small strain ϵ (which redefines the vectors that define the large periodic cell) and relaxing as fully as possible by moving atoms towards positions where there is no force on them. The elastic constants were obtained by computing the potential energy of the system via equation (1) and using $V = \frac{1}{2}C\epsilon^2$. This procedure has some advantages over that used previously[1] in that all atoms are treated equivalently and there are no "surface atoms". Typical strains used were $\epsilon = 10^{-5}$.

There are some subtle and important differences in the numerical simulations done in this work and those done previously[1]. In figure 3, the two bonds can be removed as they do not produce a restoring force. (Dangling bonds are also removed as in the conductivity problem[6]) However, when $\theta = 180°$ in figure 3, there are two ways to proceed. In ref. 1, it was assumed that there was a restoring force as given by the potential (1), whereas in the present work we assume there is none and remove such configurations. This has the effect of increasing p_{con} from ≈ 0.58 nearer to 2/3. We remove such configurations because "buckling" can occur in compression rendering the connection in figure 3 ineffective even if $\theta = 180°$. This model can be visualized as replacing all 180° bonds by $180° - \Delta$, evaluating the elastic properties for a small strain $\epsilon << \Delta$, and letting $\Delta \to 0$. Both models (i.e., ref. 1 and the present one) are equally valid and of course the effective medium theories cannot distinguish between them. In the numerical simulations to calculate f, as described previously, it was found that f was slightly larger for the $\Delta = 0$ case than for the small Δ one. However this was only appreciable around p_{con} and too small an effect to show on the scale of the inserts in figures 1 and 2.

4. COHERENT POTENTIAL APPROXIMATION

We now consider a multiple scattering approach in which all repeated scatterings from the same bond are summed to give a coherent potential approximation (C.P.A.)[9]. We find that same result (18) is obtained from this method. Writing the Hamiltonian for the system as

$$H = H_0 + V \tag{19}$$

where

$$H_0 = \sum_i \frac{\bar{p}_i^2}{2M} + \frac{\alpha_m}{2} \sum_{<ij>} [(\bar{u}_i - \bar{u}_j)\cdot\hat{r}_{ij}]^2 \tag{20}$$

and

$$V = \frac{\alpha - \alpha_m}{2}[(\bar{u}_1 - \bar{u}_2)\cdot\hat{r}_{12}]^2 \tag{21}$$

represents a single "defect" bond in an effective medium α_m as shown in the left hand part of figure 4. It is convenient to define Green's functions for the system described by H_0 as

$$\bar{P}_{ij} = \sum_n \left[\frac{<0|\bar{u}_i|n><n|\bar{u}_j|0>}{\omega - \omega_n + \omega_0} - \frac{<0|\bar{u}_j|n><n|\bar{u}_i|0>}{\omega + \omega_n - \omega_0}\right] \tag{22}$$

where $\bar{P}_{ij}$ is a d x d matrix. A similar quantity $\bar{G}_{ij}$ is defined for the system described by H. We rewrite (21) in matrix form with

$$\bar{V}_{ij} = (\alpha - \alpha_m)\hat{r}_{12}\hat{r}_{12}m_{ij} \tag{23}$$

where $m_{ij} = (\delta_{1i}\delta_{1j} + \delta_{2i}\delta_{2j} - \delta_{1i}\delta_{2j} - \delta_{2i}\delta_{1j})$ arises from the translational invariance of each bond. It is easy to show that the Dyson equation is satisfied, i.e.,

$$\bar{G} = \bar{P} + \bar{P}\cdot\bar{V}\cdot\bar{G} \tag{25}$$

where $\bar{P}$, $\bar{G}$ and $\bar{V}$ are considered as matrices in both site indices (i,j) and in a d dimensional vector space. Remembering that we are considering a single defect bond, Eq.(25) can be rewritten as

$$\bar{G} = \bar{P} + \bar{P}\cdot\bar{T}\cdot\bar{P} \tag{26}$$

where

$$\bar{T}_{ij} = \frac{\alpha - \alpha_m}{1 - 2(\alpha - \alpha_m)\hat{r}_{12}(P_{11} - P_{12})\cdot\hat{r}_{12}}\hat{r}_{12}\hat{r}_{12}m_{ij} \tag{27}$$

has the same <u>form</u> as $\bar{V}_{ij}$ but with a renormalized coefficient. Setting $<\bar{T}> = 0$, we find

$$<\frac{\alpha - \alpha_m}{1 - 2(\alpha - \alpha_m)\hat{r}_{12}\cdot(\bar{P}_{11} - \bar{P}_{12})\cdot\hat{r}_{12}}> = 0 \tag{28}$$

which is analogous to (8) except that it applies at all frequencies ω and $\alpha_m(\omega)$. Note that <u>all elements</u> of the T matrix are set equal to zero by (28) as all the T matrices

have the form of a scalar multiplying m_{ij}. The method of section 3 can also be easily generalized to finite frequencies.

The pure system Green functions $\bar{P}_{ij}$ obey the equation of motion (noting that $\bar{P}_{11} = \bar{P}_{22}$ and $\bar{P}_{12} = \bar{P}_{21}$)

$$M\omega^2 P_{11} = 1 + \frac{z\alpha_m}{d}\hat{r}_{12}\cdot(\bar{P}_{11} - \bar{P}_{12})\cdot\hat{r}_{12} \tag{29}$$

where P_{11} is the magnitude of the isotropic site diagonal Green function. As $\omega^2 \to 0$, equation (28) reduces to the previous result (8) with again $a^* = 2d/z$.

5. CONCLUSIONS

There is a slight difference between these two versions of effective medium theory for $p > p_{ces}$. In the first, the elastic constants C_{ij} are calculated, and the various masses are irrelevant. In the second, the sound velocities are calculated in the long wavelength limit. This leads to the elastic constants if it is assumed that the effective mass is independent of p. In reality, the effective mass will depend on p, but this dependence is expected to be much weaker than the dependence on p of the elastic constants near p_{ces}, analogous to the conductivity case. An account for such effects is obviously beyond the capabilities of effective medium theories.

To summarize, we have shown that simple effective medium theories give a remarkably good overall description of the dilute elastic systems with Hooke springs. The detailed behavior around p_{ces} is a subject still under study.

We should like to thank P. Sen for many useful conversations on this problem, and also R. J. Elliott, B. Halperin, B. Nickel and L. Schwartz for clarification on particular points. Two of us (S. F. and M.F.T.) would like to thank Schlumberger-Doll Research Center for their hospitality in the summer of 1984. The support of the O.N.R. and N.S.F. by M.F.T. and E.G. is gratefully acknowledged.

REFERENCES

1. S. Feng and P. N. Sen, Phys. Rev. Lett. 52, 216 (1984)
2. D. J. Bergman and Y. Kantor, Phys. Rev. Lett. 53, 511 (1984)
3. Y. Kantor and I. Webman, Phys. Rev. Lett. 52, 1891 (1984)
4. S. Alexander, preprint; S. Feng, P. N. Sen, B. I. Halperin, and C. J. Lobb, preprint; L. Benguigui, preprint;
5. M. F. Thorpe, J. Non Cryst. Solids 57, 355 (1983)
6. S. Kirkpatrick, Rev. Mod. Phys. 45, 574 (1973)
7. This result was first given, without proof, in G. R. Jerauld, L. E. Scriven and H. T. Davis, preprint and also by M. Sahimi, private communication.
8. M. Sahimi, B. D. Hughes, L. E. Scriven, and H. T. Davis, J. Chem. Phys. 78, 6849 (1983)
9. For a review, see R. J. Elliott, J. A. Krumhansl and P. L. Leath, Rev. Mod. Phys. 46, 465 (1974)

Figure Captions

Figure 1

The elastic constants C_{11} and C_{44} averaged over three configurations for a 440 atom triangular network. For the pure system (p=1), $C_{44} = C_{11}/3 = \alpha\sqrt{3}/4$. The inset shows the fraction of zero frequency modes f for a 168 atom triangular network averaged over three configurations. The straight lines are from the effective medium theories described in the text.

Figure 2

The elastic constants C_{11}, C_{44} and $B = (C_{11} + 2C_{12})/3$ averaged over three configurations for a 500 atom f.c.c. lattice. For the pure system (p=1), $C_{11} = 2C_{12} = 2C_{44} = \alpha\sqrt{2}/b$ where b is the nearest neighbor separation. The inset shows the fraction of zero frequency modes f for a 108 atom f.c.c. lattice averaged over three configurations. The straight lines are from the effective medium theories described in the text.

Figure 3

Showing a two coordinated bridge connecting two regions. This bridge is ineffective in transmitting any elastic restoring force and can be trimmed.

Figure 4

Showing the notation for constructing the effective medium theory. On the left a single bond between sites 1 and 2 is modified by having a spring constant α rather than α_m. the strain existing before the modification can be reestablished by applying a force f across the bond as shown. On the right, we show an equivalent circuit for the bond joining 1 and 2 as described in the text. The springs α'_m and α are connected in parallel.

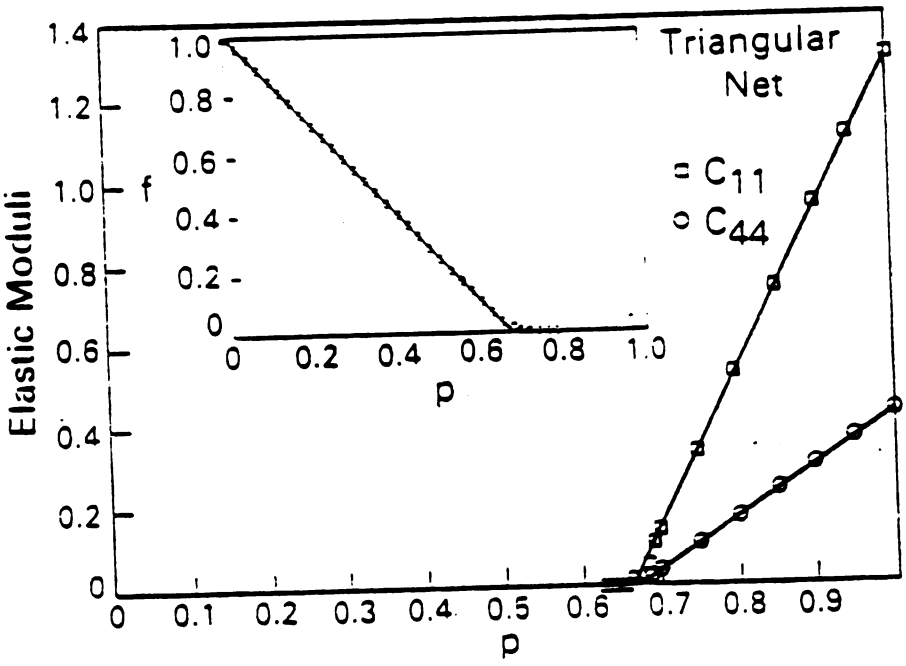
Elastic Moduli
1.4
1.2
1.0
0.8
0.6
0.4
0.2
0
0 0.1 0.2 0.3 0.4 0.5 0.6 0.7 0.8 0.9
p
f
1.0
0.8
0.6
0.4
0.2
0
0 0.2 0.4 0.6 0.8 1.0
p
Triangular
Net
= C_{11}
o C_{44}

Figure 1

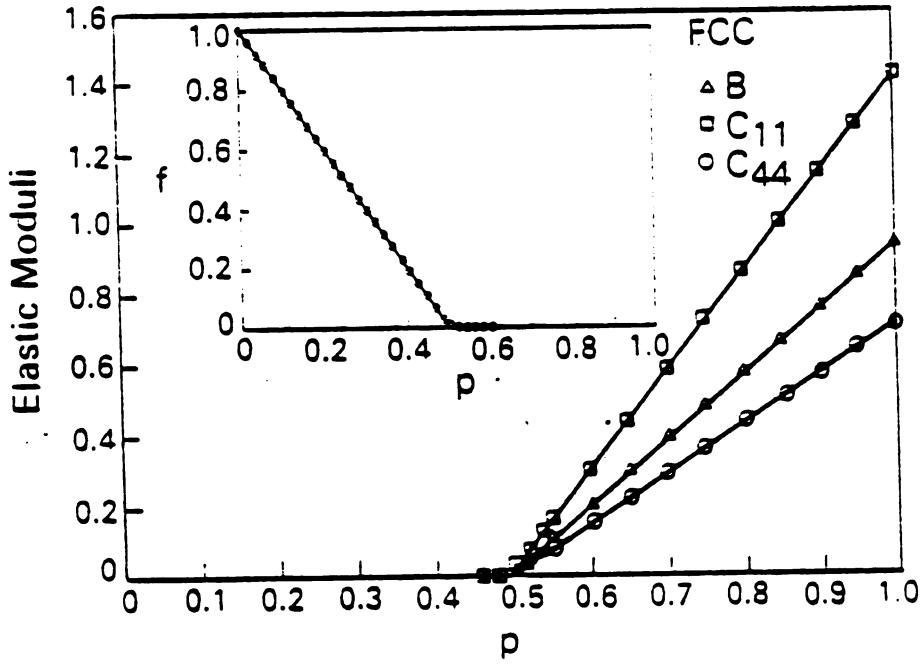

Figure 2

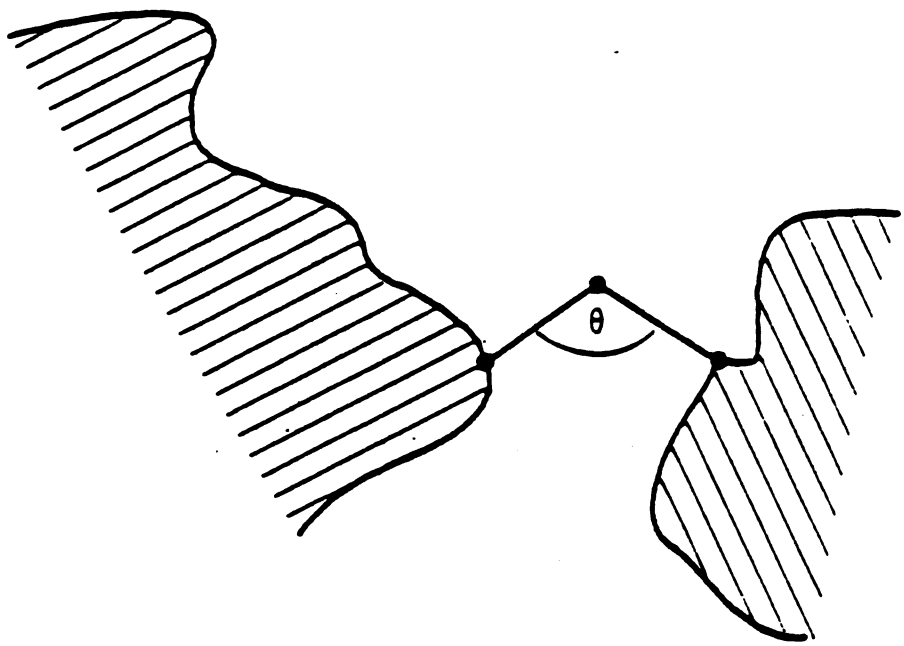

Figure 3

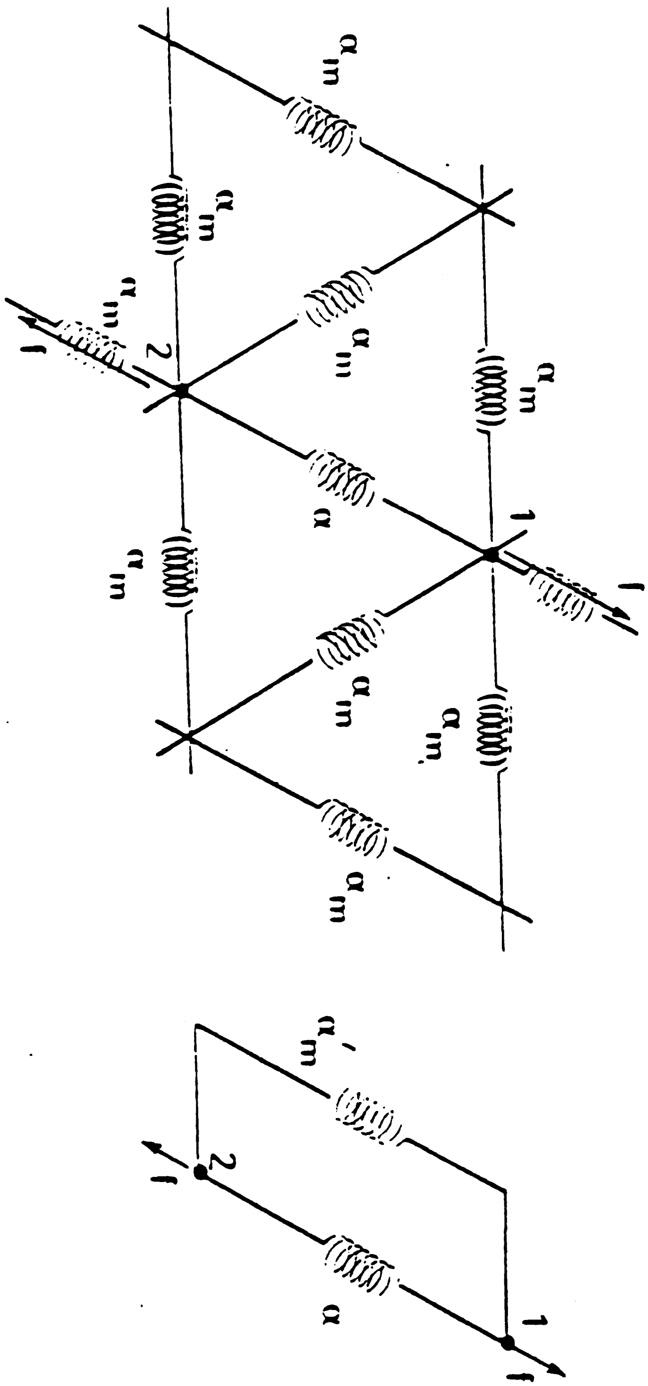

Figure 4

LIST OF REFERENCES

LIST OF REFERENCES

N. W. Ashcroft, N. D. Mermin, Solid State Physics, Holt Rinehart and Winston, Philadelphia (1976).

R. J. Bell, Reports on Progr. in Phys. 35, 1315 (1972).

R. J. Bell, Methods in Comp. Phys. 15, 215 (1976).

R. J. Bell, in Excitations in Disordered Systems, ed. by M. F. Thorpe, Plenum, New York (1982).

D. J. Bergman, to be published in January 1985 issue of Phys. Rev. B.

D. J. Bergman, Y. Kantor, Phys. Rev. Lett. 53, 511 (1984).

P. Dean, Rev. Mod. Phys. 44, 127 (1972).

R. J. Elliott, J. A. Krumhansl, P. L. Leath, Rev. Mod. Phys. 46, 465 (1974).

S. Feng, P. N. Sen, Phys. Rev. Lett. 52, 216 (1984).

S. Feng, P. N. Sen, B. I. Halperin, C. J. Lobb, Phys. Rev. B 30, 5386 (1984).

S. Feng, M. F. Thorpe, E. Garboczi, Phys. Rev. B 31, 276 (1985).

E. J. Garboczi, M. F. Thorpe, submitted to Phys. Rev. B (1985).

H. He, M. F. Thorpe, submitted to Phys. Rev. Lett. (1984).

Y. Kantor, I. Webman, Phys. Rev. Lett. 52, 1891 (1984).

S. Kirkpatrick, Rev. Mod. Phys. 45, 574 (1973).

C. Kittel, Introduction to Solid State Physics, 3rd ed., J. Wiley and Sons, New York (1967).

I. M. Lifshitz, Adv. Phys. 13, 483 (1964).

A. E. H. Love, A Treatise on the Mathematical Theory of Elasticity, Dover, New York (1944).

J.F. Nye, Physical Properties of Crystals, Clarendon Press, Oxford (1957).

L. Schwartz, P. Sen, S. Feng, M.F. Thorpe, to be published (1984).

M.F. Thorpe, J. Non-Crys. Sol. 57, 355 (1983).

R. Zallen, The Physics of Amorphous Solids, J. Wiley and Sons, New York (1983).